Sulfoxides as a New Reporting Element for Metal Ion Responsive Fluorescent Chemosensor Development

Dissertation

zur

Erlangung der naturwissenschaftlichen Doktorwürde

(Dr. sc. nat.)

vorgelegt der

Mathematisch-naturwissenschaftlichen Fakultät

der

Universität Zürich

von

Rahul Singh Kathayat

aus Indien

Promotionskomitee

Prof. Dr. Jay S. Siegel (Vorsitz)

PD Dr. Nathaniel S. Finney (Leitung der Dissertation)

Prof. Dr. Kim K. Baldridge

Dr. Henning J. Jessen

Zürich, 2014

Acknowledgement

I would like to begin my thesis, though mere words would not be enough, with a note of thanks to all those who helped me in my work as well as stay here in Zürich for last four and a half years. I am thankful to Prof. Dr. Nathaniel S. Finney, for not only giving me the interesting project but also a great supervision throughout my Ph.D. work. Discussions carried out with him in the last four and a half years were always motivating. I am also very grateful to Prof. Dr. Jay S. Siegel, Prof. Dr. Kim Baldridge and Dr. Henning J. Jessen of University of Zürich for being my committee members and providing me very valuable suggestions during my work.

My colleagues played an important role in my scientific growth over the last four and a half years. They provided a very friendly and helpful atmosphere for work as well as beyond the four walls of the laboratory. I would like to especially acknowledge Dr. Silvia V. Rocha and Dr. Mireille Vonlanthen, who helped me in learning fluorescence techniques which is the heart of my work.

I would like to take this opportunity to thank all my teachers and friends, since my childhood, who have contributed in shaping my life in one way or other. I would like to especially mention Amit K. Dutta, Biplab Dutta, Shiladitya Banerjee, Pradeep N. Reddy and Mahesh Vishe for the amazing time I spent with them here in Zürich. They gave me the memories which I am surely going to cherish forever.

My life is not complete without my loving wife, Anwesha, and my family. I thank them from the bottom of my heart for their immense support and unconditional love which provided me all the strength to reach my goals.

ABSTRACT OF THE DISSERTATION

Sulfoxides as a New Reporting Element for Metal Ion Responsive Fluorescent Chemosensor Development

by

Rahul Singh Kathayat

University of Zürich, 2014

Fluorescence spectroscopy is a powerful analytical tool for chemosensing. A fluorescent chemosensor consists of a receptor unit and a fluorophore to perform the functions of binding to analyte and reporting this binding event, respectively. The two units communicate through a signal transduction mechanism. Photoinduced electron transfer (PET) and photoinduced internal charge transfer (ICT) are most exploited signal transduction mechanisms for fluorescent chemosensing.

Nitrogen has been by far the most used reporting element in PET and ICT based fluorescent chemosensors for metal ions. Its limitations, like pH sensitivity and the required presence of N at anilinic or benzylic position for efficient functioning, have persuaded chemists to discover new reporting elements. Oxygen, phosphorus, arsenic have also been employed as reporting elements. Oxygen being very electronegative is not an appropriate reporting element for PET sensors. On the other hand, phosphorus is more readily oxidized than nitrogen, which suits it for PET sensors, but its susceptibility to aerial oxidation is a spoiler. PET from sulfur in thioethers has not yet been reported for metal ion detection.

Thiourea appended fluorescent chemosensors has been demonstrated for detecting metal ions. To further widen the range in which a sulfur based group can be exploited for chemosensing, our group used non-emissive aromatic sulfoxides for the detection of an explosive triacetone triperoxide (TATP). Following our curiosity to see what else we could use aromatic sulfoxides for, we

observed that metal ions like Li^+ and Zn^{2+} enhance fluorescence emission in phenyl pyrenyl sulfoxide.

Chapter 1 will provide a general introduction to chemosensors. Chapter 2 of the thesis will explore how we can use the observed behavior of phenyl pyrenyl sulfoxide to build metal ion responsive fluorescent chemosensors. The phenyl was replaced by methyl as our control (**Me**), exploiting versatility of the latter for further functionalization. Addition of metal ions like Li^+, Na^+, Mg^{2+}, Ca^{2+} and Zn^{2+} enhanced the quantum yield in acetonitrile (ACN) and obtained a maximum of 0.43 (*ca.* 36 fold enhancement) for Zn^{2+}. The binding affinities were low, but could be strengthened by exchanging methyl for an ethylamino group (**$EtNH_2$**). In Chapter 3, modifications of the **NH_2** end with strong chelator like picolyl amines or azacrown are discussed to address the issue of selectivity and binding affinities. We also looked at targets with no N-atom in the receptor unit and conclude that presence of N-atom is not required for strong binding or fluorescence response. To explore the potential of our sulfoxide-based sensor's functioning under physiological conditions, a fluorescence titration of sulfoxide with dipicolyl amine (**DiPic**) was carried out against $ZnCl_2$ in 1:9 ACN:aq. MOPS buffer (5 mM, pH 7.4). An exciting result observed was that the binding affinity (*ca.* log K_d = -5.3) remained unaffected on switching from ACN to buffer solution. Also, a net 13 fold enhancement in fluorescence was observed for **DiPic**.

To know how metal ion coordination raises fluorescence intensity and identify the appropriate structural parameters of a fluorophore for future fluorescent chemosensor development, efforts were made to acquire deeper understanding of sulfoxide excited states. Therefore, in Chapter 4, the role of substituent effect on the spectroscopic behavior of the sulfoxides was investigated. These results emphasize the formation of an ICT excited state with sulfoxide radical cation character. These results also indicate that electron deficient fluorophores with long excitation/emission wavelengths are the need of the hour for further sulfoxide-based metal ion responsive chemosensor development.

ABSTRACT OF THE DISSERTATION

Sulfoxide als eine Neue Melde-Einheit für Metall-Ionen Empfindliche, Fluoreszierende Chemosensor-Entwicklung

von
Rahul Singh Kathayat
Universität Zürich, 2014

Fluoreszenzspektroskopie ist ein starkes analytisches Werkzeug in der Chemosensorik. Ein fluoreszierender Chemosensor besteht aus einer Rezeptor-Einheit und einem Fluorophor, um die Funktion, an einen Analyten zu binden, und diesen Bindungsevent zu melden, entsprechend ausführen zu können. Die beiden Einheiten kommunizieren mit Signalübertragungs-mechanismen. Photoinduzierter Elektronen-transfer (PET) und photo-induzierter, interner Ladungstransfer (ILT) sind die am meisten verwendeten Signalübertragungsmechanismen in der fluoreszierenden Chemosensorik.

Stickstoff ist die am weitaus häufigsten verwendete Melde-Einheit in den auf PET und ILT basierenden Chemosensoren für Metall-Ionen. Dessen Einschränkungen, wie die pH-Empfindlichkeit und die benötigte Präsenz von Stickstoff in anilinischen oder benzylischen Positionen für effiziente Funktionsfähigkeit, haben Chemiker dazu bewogen, nach neuen Melde-Einheiten zu forschen. Sauerstoff, Phosphor und Arsen wurden ebenfalls als Melde-Einheit verwendet. Sauerstoff mit seiner ausgeprägten Elektronen-negativität ist kein geeignetes Element für PET Sensoren. Auf der anderen Seite wird Phosphor leichter oxidiert als Stickstoff, was es nützlich für PET Sensoren macht, aber seine Anfälligkeit gegenüber der Oxidation durch Luftsauerstoff vermindert seinen Wert. Die Benutzung von PET ausgehend von Schwefel in Thioether wurde bisher noch nicht für den Metall-Ionen Nachweis berichtet.

Der Nachweis von Metall-Ionen wurde für Thioharnstoff-haltige, fluoreszierende Chemosensoren demonstriert. Um den Anwendungsbereich

einer schwefelhaltigen Gruppe in der Chemosensorik zu vergrössern, hat unsere Forschungsgruppe nicht emittierende aromatische Sulfoxide für den Nachweis eines expolsiven Acetonperoxids (TATP) verwendet. Unserer Neugierde folgend, wozu aromatische Sulfoxide weiter verwendet werden könnten, haben wir bemerkt, dass Metall-Ionen wie Li^+ und Zn^{2+} die Fluoreszenzemission in Phenylpyrenylsulfoxiden verstärken.

Kapitel 1 wird eine allgemeine Einführung zu Chemosensoren beinhalten. Kapitel 2 der These wird darlegen, wie das beobachtete Verhalten von Phenylpyrenylsulfoxiden für den Aufbau von Metall-Ionen empfindlichen, fluoreszierenden Chemosensoren verwendet werden kann. Die Phenylgruppe wurde dazu durch eine Methylgruppe (**Me**) ersetzt, um die Vielseitigkeit der Letzteren für weitere Funktionalisierung nützen zu können. Die Zugabe von Metall-Ionen wie Li^+, Na^+, Mg^{2+}, Ca^{2+} und Zn^{2+} vergrösserte die Quantenausbeute in Acetonitril (ACN) und führte zu einem Maximum von 0.43 (ca. 36fache Vergrösserung) für Zn^{2+}. Die Bindungsaffinitäten waren tief, konnten aber erhöht werden, indem die Methylgruppe durch eine Ethylaminogruppe (**$EtNH_2$**) ersetzt wurde. In Kapitel 3 werden Modifikationen der **NH_2** Endgruppe mit starken Chelatoren wie Picolylaminen oder Aza-Kronen diskutiert, um die Problematik der Selektivität und der Bindungs-affinität zu adressieren. Des Weiteren wurden Zielmoleküle ohne N-Atom in der Rezeptor-Einheit studiert, woraus gefolgert werden konnte, dass die Anwesenheit eines N-Atoms weder für eine starke Bindung noch für die Fluoreszenz benötigt wird. Um das Potential des sulfoxidhaltigen Sensors in physiologischen Bedingungen zu erkunden, wurde eine Fluoreszenztitration des Sulfoxids mit Dipicolylamin (**DiPic**) gegen $ZnCl_2$ in 1:9 ACN:aq. MOPS Puffer (5nM, pH 7.4) durchgeführt. Ein begeisterndes Resultat war, dass die Bindungsaffinität (ca. log K_d = -5.3) beim Wechsel von ACN zur gepufferten Lösung unbeeinträchtigt blieb. Darüber hinaus wurde eine netto 13 fache Erhöhung der Fluoreszenz für **DiPic** beobachtet.

Ein tieferes Verständnis der angeregten Zustände von Sulfoxid wurde angestrebt, um zu verstehen, wie die Koordination von Metall-Ionen die Fluoreszenzintensität erhöht und um die geeigneten, strukturellen Parameter

eines Fluorophors für zukünftige, fluoreszierende Chemosensor-Entwicklungen zu identifizieren. Daher wird in Kapitel 4 die Rolle des Substituenteneffektes auf das spektroskopische Verhalten der Sulfoxide untersucht. Diese Resultate unterstreichen die Formation eines ILT angeregten Zustandes mit Sulfoxid radikalkationischen Charakters. Des Weiteren weisen sie darauf hin, dass elektronenarme Fluorophore mit langer Anregung/Emissionswellenlänge die aktuellen Zielmoleküle für weitere sulfoxidhaltige, Metall-Ionen empfindliche Chemosensor-Entwicklungen sind.

Contents

Chapter 1

Metal Ion Responsive Fluorescent Chemosensors

1.1 Introduction

Metal ions like Na^+, K^+, Ca^{2+}, Mg^{2+}, Zn^{2+} etc. play extremely important roles in biological processes.[1-5] Concentration of Na^+ and K^+ across the plasma membrane in neurons regulate transmission of the nerve impulse.[6] Mg^{2+} is an important constituent of chlorophyll, which is responsible for photosynthesis.[7] Fe^{2+} plays an important role in the transport of oxygen in the body.[8] Both the excess and deficiency of these essential metal ions impact our health. There are many metal ions which have hazardous effect on human beings, other biological species and the environment too. Therefore, detection of metal ions draws a great interest of chemists, biologists and environmental scientists.

Many techniques are being pursued to analyze metal ions *e.g.*, atomic absorption spectrometry, flame photometry and ion-selective electrodes.[9-11] All of these techniques suffer from disadvantages like large sample size, destructiveness and high expense. Fluorescence spectroscopy, as an analytical technique, has many advantages over the aforesaid techniques.[12,13]

Fluorescence is a very sensitive technique, therefore its usage scales down to as small as molecular level.[14,15] It is a very versatile technique and therefore can be performed in all the phases (solid, liquid or gas). Fluorescence is also the fastest technique because of its short lifetime, generally in the range of *ca.* 10^{-8}-10^{-10} s.[16] In fluorescence spectroscopy, one has to measure the emission from a source, which makes it also a non-invasive technique. Last but not the least, fluorescence technique requires, in principle, only cheap and hence economical instrumentation.[17,18]

Having recognized all the benefits of fluorescence spectroscopy over other techniques, the difficult part is that it cannot be applied directly for metal ion detection, since the latter are non-fluorescent in character. However, the fundamental drawback could be resolved by employing a fluorescent chemosensor - a molecule, small or large, which transforms chemical information

into an analytically useful signal.[19-24] The deeper understanding of a fluorescent chemosensor demands knowledge of its photophysical properties, and interaction between the chemosensor and the analyte (*i.e.*, metal ion) which is the subject of supramolecular chemistry.

Before we explore the fluorescent chemosensors and work presented in the thesis in great details, a quick recap of fluorescence is required, in order to get acquainted with all the photophysical processes occurring from the excited state of a molecule.

1.2 Fluorescence

The emission of a photon by a molecule from its excited electronic state is called luminescence. Depending on the nature of the excited state, luminescence can be described as fluorescence or phosphorescence. Moreover, a molecule participates in many other processes in the excited state. All these various processes occurring from the excited state of a molecule can be illustrated with the Jablonski diagram shown in ***Figure 1.1***.[16] S_0 represents the ground electronic state of the molecule. A molecule can have two different sets of excited electronic states which are following: Singlet states (S_1, S_2...S_n), if the electrons have paired spins or Triplet states (T_1, T_2...T_n), if the electrons have the same spin. Each electronic state is associated with vibrational levels marked as (0,1,2...). When a molecule absorbs a photon (**blue arrow**; ***Figure 1.1***), it is promoted to the vibrational levels of higher excited state. Absorption of photon is taken to be a fast process (~10^{15} s^{-1}) such that no displacement of nuclei occurs. This postulate is called the Franck-Condon principle.[16,25-27] In the excited state molecule can lose its energy by collision with neighboring molecules and vibrationally relax to the lowest vibrational level of S_1 state. This process is termed internal conversion (**IC**; **curvy arrows**; ***Figure 1.1***).

Figure 1.1: *Jablonski diagram.*

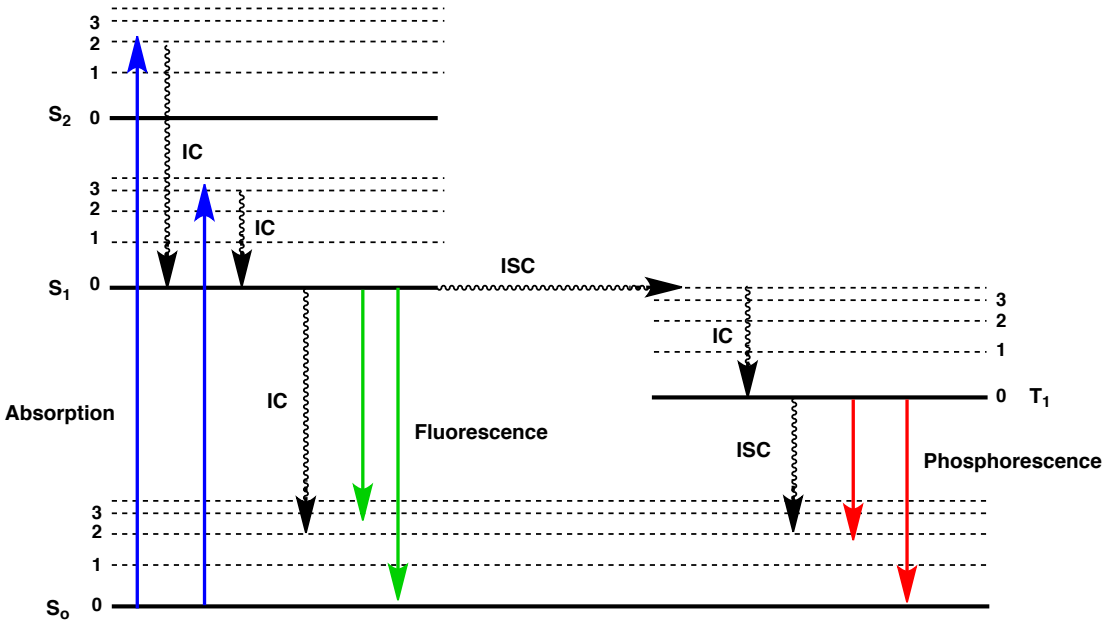

From the lowest vibrational level of S_1, molecule can return to the higher vibrational levels of S_0 state either by IC or emitting a photon. The latter process is called fluorescence (**green arrow**; ***Figure 1.1***). The phenomenon of fluorescence was first observed from quinine solution under sunlight by Sir John Frederick William Herschel.[28] The speed of IC is ~10^{12} s^{-1} which is higher than that of fluorescence, ~10^{8}-10^{10} s^{-1}. Therefore, with rare exceptions only, molecule promoted to higher excited states also reaches to the lowest vibrational level of S_1 state by IC. In other words fluorescence occurs from the lowest vibrational level of S_1 state and the nature of fluorescence spectra does not change with excitation wavelength. This principle is called Kasha's rule.[29] From the S_1 state a molecule can also change its state to T_1. This process is called intersystem crossing (**ISC**; **curvy arrows**; ***Figure 1.1***). The emission of photon from lowest vibrational level of T_1 to S_0 is called phosphorescence (**red curve**; ***Figure 1.1***). This process is spin forbidden and occurs very slowly, > 10^{3} s^{-1}. The loss of energy in the excited state of a molecule by processes like IC, ISC etc., is reflected as difference between excitation and emission maxima wavelength. This shift is termed Stokes Shift, after Sir G. G. Stokes.[30]

In the excited state molecule can undergo various kinds of photochemical reactions, energy transfer, etc., which are not explained above. Since all the processes like IC, ISC, photochemical reactions and energy transfer, do not involve emission of photon, they are together termed as non-radiative processes and provide deactivation pathways for excited states. Fluorescence and phosphorescence are together called radiative processes.

The quantum yield of molecule is defined as the ratio of number of photons emitted to the absorbed photons. It is represented by Φ_F. Lifetime of fluorescence is defined as the average time a molecule spends in the excited state S_1 before returning to the ground state S_0 and is represented by τ.

1.3 Fluorescent chemosensor

An analyte is a substance which needs to be detected. It can vary from any size to any complexity. A sensor is a device which detects the analyte. A sensor of biotic origin is called a biosensor whereas, of abiotic origin is called chemosensor. A chemosensor which exploits phenomenon of fluorescence for analyte detection is termed as fluorescent chemosensor.[19-24,31]

A fluorescence-based chemosensor is comprised of two parts that are as follows:

- Receptor unit - This part is responsible for the recognition of the analyte by the sensor under investigation. The recognition occurs when an interaction between the receptor unit of sensor and an analyte takes place. This interaction is of supramolecular nature *i.e.*, H-bonding, coordination, etc.

- Fluorophore - This part is responsible for the reporting of recognition of the analyte by the receptor. The fluorophore performs this by undergoing photophysical modifications like change in intensity,[32] Stokes Shift,[33,34] or change in life time,[35] which can be conveniently analyzed.

Figure 1.2 provides a cartoon representation of a type of fluorescent chemosensor in which selective binding of analyte alters the emission intensity. The terminology 'off/on' state describes switching from non-emissive to emissive state of fluorescence on binding to analyte.

Figure 1.2: *Cartoon of fluorescent chemosensor showing change in emission on analyte binding.*

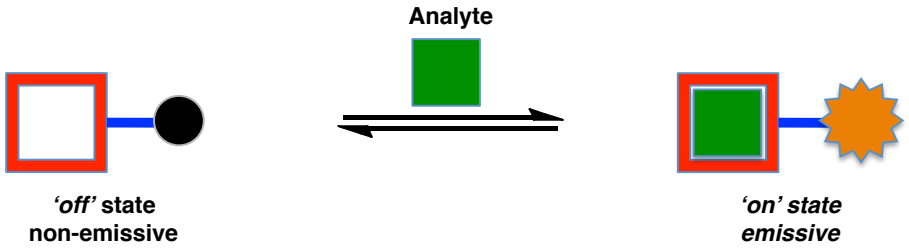

1.4 Signal transduction mechanisms

As discussed above, a fluorescent chemosensor performs two functions - analyte detection and reporting. Recognition of an analyte is an event which occurs in the ground state S_0 of a fluorophore, whereas the reporting of that (*i.e.*, photophysical changes) occurs from the excited state S_1 of the fluorophore. Therefore, in fluorescent chemosensor, coordination between recognition of an analyte and photophysical response requires a signal transduction mechanism.[19-24] Analyte binding in S_0 state can modulate the electronic structure of fluorophore or rotational ability or distance between two fluorophores, etc. Based on these modulations, various types of signal transduction mechanisms are possible, such as:

- Photoinduced Electron Transfer (PET)
- Photoinduced Internal Charge Transfer (ICT)
- Forster Resonance Energy Transfer (FRET)
- Excited State Proton Transfer
- Monomer-Excimer formation
- Conformational restriction

The next two sections will specifically discuss the background of the PET and ICT signal transduction mechanisms and provide some examples of their application in fluorescent chemosensors.

1.4.1 Photoinduced Electron Transfer (PET)

1.4.1.1 Background

The transfer of electrons upon absorption of light plays an important role in photosynthesis. Hence, photoinduced electron transfer has been extensively studied.[36,37] This process relies on the enhanced ability of one species in the excited state to accept/donate electron from/to a nearby donor/acceptor. This process can be well explained by a general representation of frontier molecular orbitals as illustrated in ***Figure 1.3***.

Figure 1.3: *Frontier molecular orbital representation of* ***PET****.* ***Case 1:*** *Excited fluorophore is reduced.* ***Case 2:*** *Excited fluorophore is oxidized.*

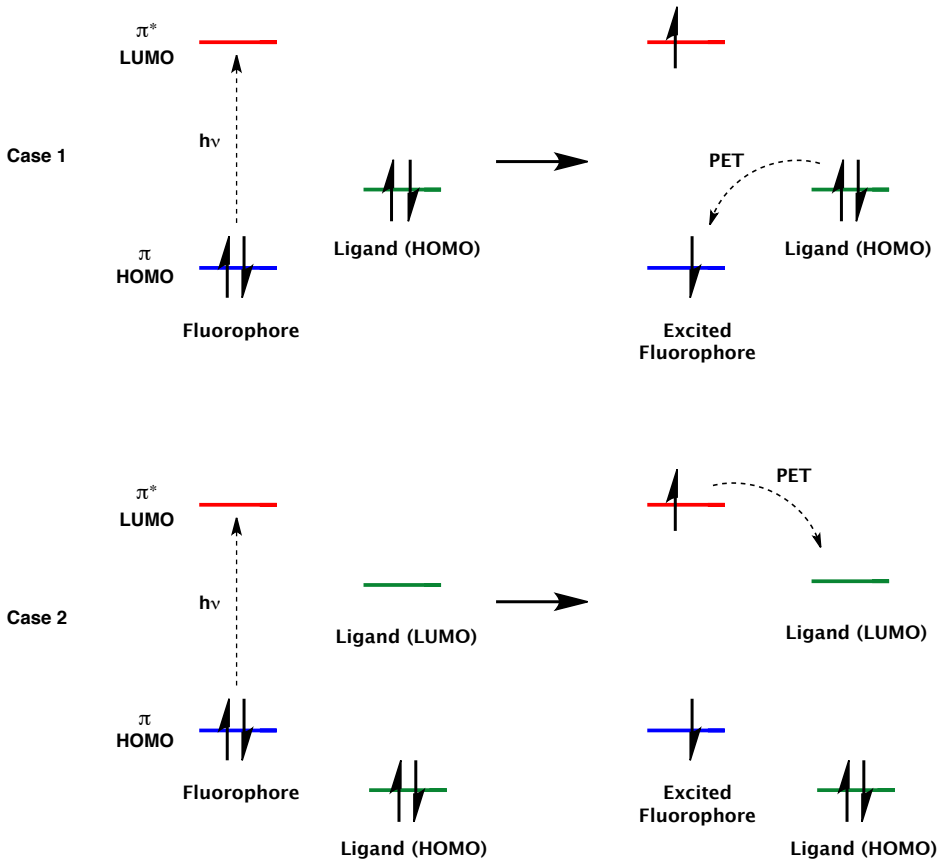

For laying foundation of PET in fluorescent chemosensors, we will use terms fluorophore and ligand in place of electron acceptor/donor and donor/acceptor respectively, at our convenience. In the case 1 (***Figure 1.3***), the highest occupied molecular orbital (HOMO) on the ligand is higher in energy than π orbital of the excited fluorophore and thus electron transfer occurs from the ligand to the excited fluorophore. On the contrary in the case 2 (***Figure 1.3***), the lowest unoccupied molecular orbital (LUMO) on the ligand is lower in energy than $\pi*$ orbital of the fluorophore and hence electron transfer takes place from excited fluorophore to the ligand.

The feasibility of the electron transfer process is dependent on two factors. The first is the thermodynamic factor *i.e.*, matching of the redox potentials of the fluorophore and ligand. The pioneering work of Rehm and Weller established the relation between PET and the thermodynamic factors.[38,39] The second factor is the structural factor. The two sites *i.e.*, fluorophore and the ligand, should be closely placed to each other in space for efficient overlap of the electronic wavefunctions. The rate of electron transfer has been presumed to exponentially decrease with increasing distance between fluorophore and ligand.[40]

1.4.1.2 PET based metal ion responsive fluorescent chemosensors

The phenomenon of PET has been intensively used for the development of fluorescent chemosensors in the last two and half decades.[19,20,24,41] The PET based chemosensor comprises a fluorophore, where transitions like excitation and emission occur, and a receptor/ligand, which plays the role of fluorescence quencher as well as binder of foreign species/guests. The appropriate fluorophore and ligand pair can be selected from the knowledge of their redox potentials.[24,20] The two sites (fluorophore and ligand) are connected through a spacer, which precludes through bond electronic communication.[18] The working of fluorescence 'off-on' chemosensor is illustrated by frontier molecular orbitals in ***Figure 1.4***.[19]

Figure 1.4: *Frontier molecular orbital representation of working in PET based fluorescence 'off-on' chemosensor.*

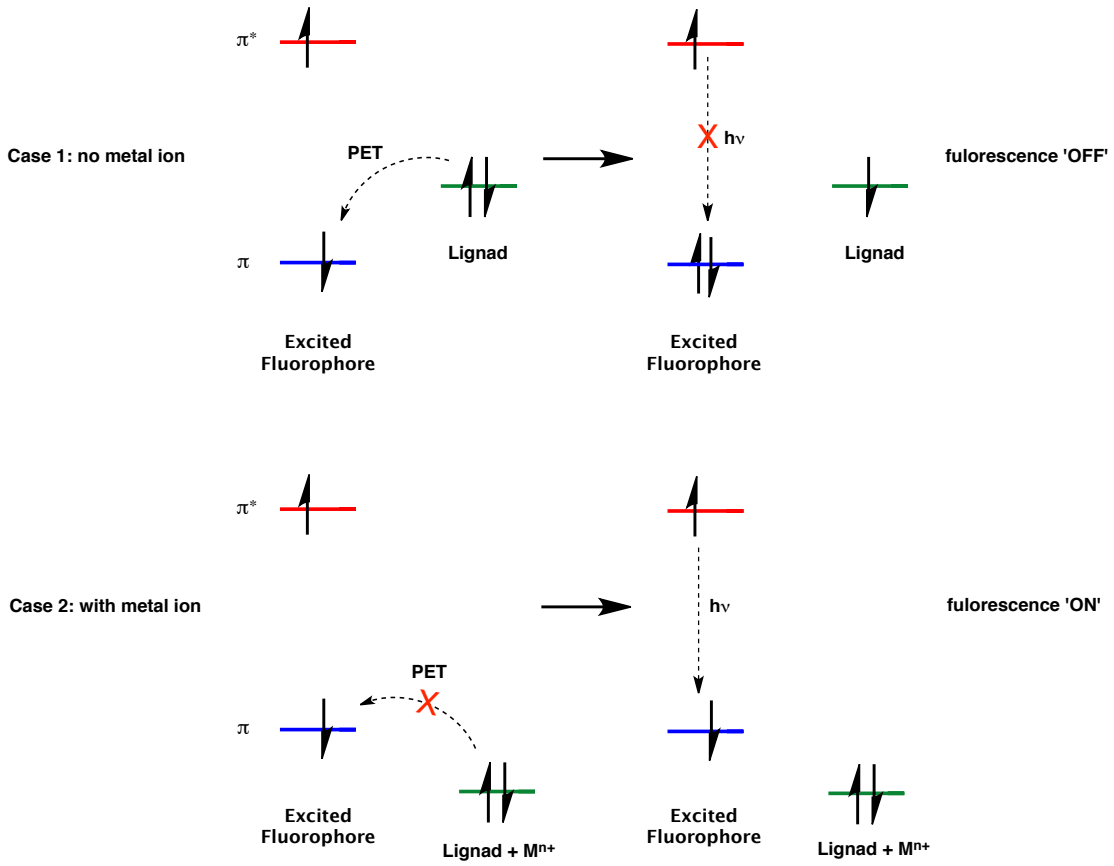

In the absence of metal ion (**case 1**; ***Figure 1.4***), the transfer of an electron from the ligand to the π orbital of excited fluorophore is thermodynamically favorable. Hence, the π orbital will be fully occupied and the electron in $\pi*$ orbital of fluorophore would not be able to return to the π orbital. Consequently, no emission will be observed. Metal ion coordination with ligand drags down its HOMO (**case 2**; ***Figure 1.4***), which makes the electron transfer to the π orbital of excited fluorophore thermodynamically unfavorable. This leads to the circumstance where the electron in $\pi*$ orbital of fluorophore can return to the partially filled π orbital. Hence, the fluorescence is regained.

The first example of a designed PET-based sensor for metal ions was reported by de Silva *et al.*, which was based on coronand receptor unit (**1**; ***Figure 1.5***). Binding of K^+ in methanol was observed to raise the quantum yield from 0.003 to 0.14.[42]

Figure 1.5: *PET based coronand appended sensor for K^+.*

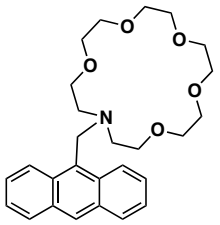

1

Czarnik *et al.* reported a series of chemosensors **2** (***Figure 1.6***) based on varying size of polyazamacrocycle receptor unit.[43] Chemosensors **2** provide *ca.* 25-190 fold enhancement in fluorescence intensity on binding with soft metal ions like Zn^{2+} and Cd^{2+} in aqueous solution.

Figure 1.6: *Series of polyazamacrocycle based PET sensor.*

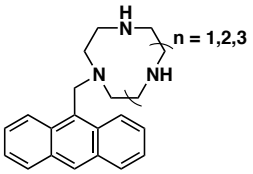

2

Cryptands are known to be strong chelators for alkali metal ions. A cryptand appended PET sensor **3** (***Figure 1.7***) has been reported by Golchini *et al.*[44] Sensor **3** has been used for monitoring the K^+ ions level in blood and biological membrane; however, it is very pH sensitive. This problem was appropriately overcome in benzoannelated sensor **4** (***Figure 1.7***), in which the basicity of the aliphatic N-atom of cryptand is greatly reduced.[45]

Figure 1.7: *Storngly binding cryptands based PET sensor for K^+.*

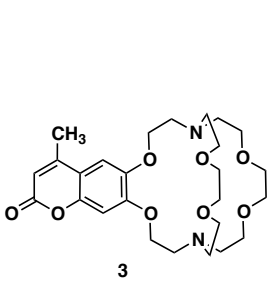

3

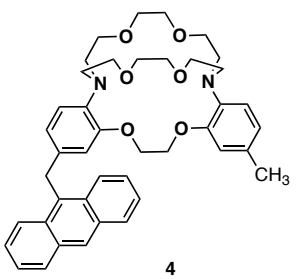

4

Lippard *et al.* designed two fluorescent chemosensor **5a-b** (***Figure 1.8***) for Zn^{2+} based on fluorescein.[46] The advantages associated with these sensors are excitation and emission wavelengths in visible range (~ 500 nm), strong binding (K_d ~ 1 nM) and 3-5 fold fluorescent enhancements. This allows monitoring of high level of Zn^{2+} in neurons associated with neurological disorders *e.g.*, Alzheimer's disease.

Figure 1.8: *Zinpyr sensors for* Zn^{2+}.

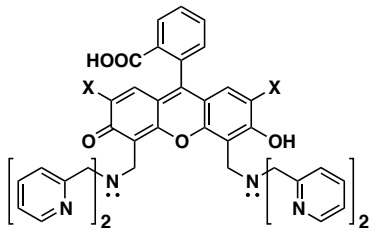

5a; X = Cl Zinpyr-1
5b; X = H Zinpyr-2

All the sensors discussed so far were based on fluorescence 'off-on' principle. One could also develop sensors where the guest induces the PET quenching *i.e.*, 'on-off' of fluorescence. A series of 1,3-diaryl-5-pyridyl-4,5-dihydropyrazoles based sensors **6a-c** (***Figure 1.9***) were reported by de Silva *et al.* in which protonation of pyridyl ring induces switching off of fluorescence.[47]

Figure 1.9: *Proton-induced fluorescence 'on-off' sensor.*

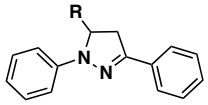

6a; R = 2-Pyridyl
6b; R = 3-Pyridyl
6c; R = 4-Pyridyl

1.4.2 Photoinduced Internal Charge Transfer (ICT)

1.4.2.1 Background

Photoinduced internal charge transfer (ICT) relies on the enhanced polarization of heteroatom-containing π-electron systems in the excited state.[48]

Due to difference in extent of polarization, a molecule has different dipole moments in the S_0 and S_1 states. The excited state generated is also called ICT state. Molecules showing ICT are susceptible to the electric effects of the surroundings. For instance, the influence of solvent polarity on the spectroscopic properties is illustrated in ***Figure 1.10***.[19,20]

Figure 1.10: *Effect of solvent polarity on spectroscopic properties of a chromophore. (D = electron donor end and A = electron acceptor end)*

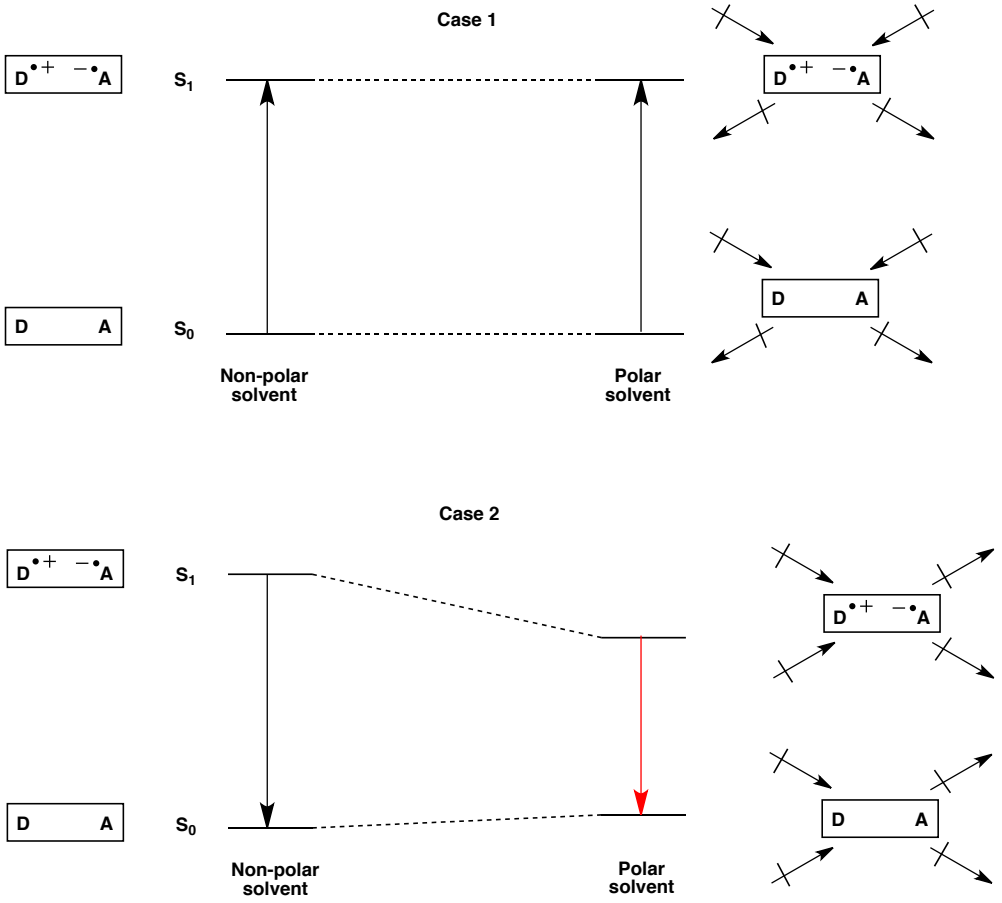

For convenience, an extreme situation is considered, where chromophore is assumed to have little or no dipole moment in the S_0 state. Absorption of a photon by a chromophore is a very fast process (~ 10^{15} s^{-1}). Therefore, the dipoles of neighboring solvent molecules, like in the S_0 state, are randomly oriented around chromophore in the ICT/dipolar S_1 state (**case 1**; ***Figure 1.10***). Consequently, no significant effect of solvent polarity on the S_1 state is observed. On the contrary, lifetime for emission from the S_1 state is in the range of 10^8-10^{10}

s^{-1}. Such a long lifetime of chromophore in the S_1 state is adequate for the neighboring solvent molecules to reorient their dipole along the chromophore's dipole (**case 2**; ***Figure 1.10***). The reorientation of dipole in polar solvent stabilizes the S_1 state, whereas, S_0 state is destabilized. As a result, a bathochromic shift is observed in the fluorescence emission, on switching from non-polar to polar solvent.

Chromophores **7**[49] and **8**[50] are some of the well known examples of molecules exhibiting photoinduced ICT (***Figure 1.11*****)**. The key feature of these molecules is the presence of strong electron donating and withdrawing groups.

Figure 1.11: *ICT based Chromophores.*

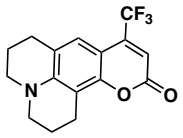

7

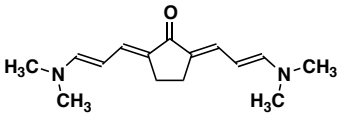

8

1.4.2.2 ICT based metal ion responsive fluorescent chemosensors.

As discussed in the ***Section 1.4.2.1***, electric effects from the surroundings alter the photophysical behavior of ICT based chromophores and this feature can be exploited for the detection of metal ions.[19,20,24] ***Figure 1.12*** demonstrates how coordination of the metal ions with fluorophore induces the photophysical changes. Based on metal ion coordination to either the donor end or the acceptor end, two different kinds of ICT systems can be built. Metal ion coordination at the donor end destabilizes the S_1 state more than the S_0 state (***i***; ***Figure 1.12***) and results in blue shift of the UV-Vis and fluorescence spectra. However, metal ion coordination at the acceptor end stabilizes the S_1 state more than the S_0 state (***iii***; ***Figure 1.12***) and results in red shift of the UV-Vis and fluorescence spectra.

Figure 1.12: *Influence of metal ion coordination on ICT based sensors.*

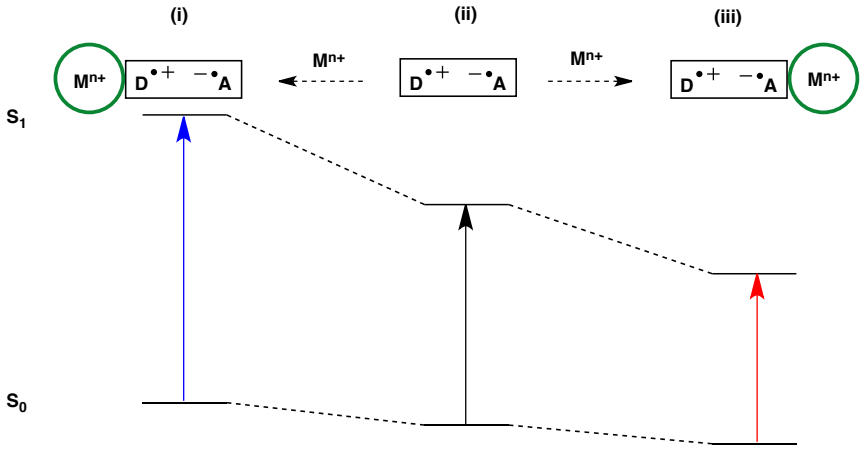

In general, the effect of metal coordination is observed more in UV-Vis than in fluorescence spectra. Since fluorescence emission has longer lifetime than absorption, ligand:metal complex can break due to the photogenerated repulsion between metal ions and the donor end. This interpretation was demonstrated by steady state and kinetic studies on coronand based chromophores, **9** and **10** (***Figure 1.13***), and their Li^+ and Ca^{2+} complexes, performed by Valeur[51,52] and Lapouyade *et al.*[53,54]

Figure 1.13: *Lumophores studied by Valeur and Lapouyade et al.*

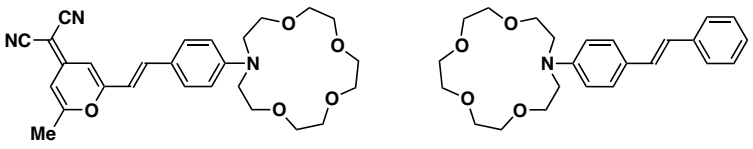

9 **10**

Fura-2 (**11**; ***Figure 1.14***) is a very popular fluorescent chemosensor reported by Tsien *et al.*[55], which is based on the principle of ICT. It has been widely used for Ca^{2+} imaging in cells. The tetraacetate facilitated chelation of Ca^{2+} decouples the N-atom from the π-electron system of the fluorophore and inhibits ICT. The Ca^{2+} binding induces 30 nm and 7 nm of blue shift in the absorption and emission spectra respectively.

Figure 1.14: *Fura-2 developed by Tsien et al.*

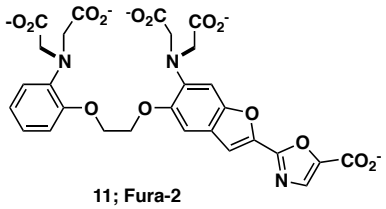

11; Fura-2

Lapouyade *et at.*[56] reported a coronand based fluorophore **12** (***Figure 1.15***) in which coordination occurs at the electron acceptor end. As discussed before for this type of ICT based fluorophore (***iii***; ***Figure 1.12***), a red shift in fluorescence emission was observed on Ca^{2+} coordination.

Figure 1.15: *Example of metal ion coordination at acceptor end of ICT sensor.*

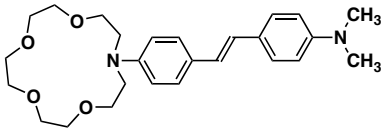

12

1.5 Summary and Objective

The phenomenon of fluorescence has been proved to be a powerful analytical tool for chemosensing of metal ions in biological and environmental assays. Fluorescent chemosensors can be built based on employing various kind of signal transduction mechanisms. The most widely used signal transduction mechanism for fluorescent chemosensors are photoinduced electron transfer (PET) and photoinduced internal charge transfer (ICT). These signaling mechanisms and hence fluorescent chemosensors show widespread use of nitrogen as the reporting element. However, these florescent chemosensors suffer many limitations, for instance that nitrogen should be present preferably at an anilinic or benzylic position. The presence of nitrogen further complicates the functioning as basicity of the nitrogen lone pair makes chemosensors pH sensitive.

Efforts have been made to explore other elements to widen the scope of fluorescent chemosensor development. Among these are oxygen, phosphorus and arsenic, whereas sulfur is unexplored. Oxygen is very electronegative and hence unwilling to participate in the PET process. The high oxidizability of phosphorus than nitrogen can be used to develop PET based sensor. Indeed, it has been shown that oxidation of P(III) in phosphines to P(V) switches on the fluorescence emission.[57,58] This feature has been used to detect H_2O_2.[57] However, high oxidizability of P(III) in phosphines make them prone to aerial oxidation and hence cumbersome to work with. Arsenic has not found much use for chemosensing except for the system reported by Tsien *et al.* where fluorescein based dye was used to label recombinant protein molecules in live cells.[59] As the use of sulfur as reporting element for fluorescent chemosensor has seen only a few mentions, our group fell in love with it and has accomplished many advances in this area.

The objective of the thesis is to demonstrate the immense opportunity which lies in exploiting a sulfur based moiety (*i.e.*, sulfoxide) as the reporting element for the development of metal ion responsive fluorescent chemosensors. The next chapter will specifically concentrate on how sulfoxides evolved as an interesting choice for the aforementioned purpose.

Chapter 2

Sulfoxide as Reporting element for Metal Ion responsive Fluorescent Chemosensors

2.1 Introduction

2.1.1 Sulfur based fluorescent chemosensors

The salient features of sulfur, like low electronegativity, high polarizability, ready oxidizability, etc., render it a soft base. This disparate nature of sulfur (*i.e.*, soft base) as compared to nitrogen and oxygen (*i.e.*, hard bases) lead it to display different types of coordination chemistry.[60,61] Sulfur can therefore be exploited in chemosensing of metal ions which are typically soft acids - those with large size, high polarizability and low positive charge.

2.1.2 Sulfur in thioethers

The ease of oxidizability of the sulfur atom in thioethers would seem to be an inspiration to the community to develop fluorescent chemosensors based on sulfur as the reporting element, which would work by the PET signal transduction mechanism. However, only a single instance of PET in a weakly-emissive sulfide (**13a**; ***Figure 2.1***) has been reported, which turns to more emissive sulfoxide **13b** on oxidation.[62]

Figure 2.1: *Griesbeck's naphthalimide based thioether involving PET.*

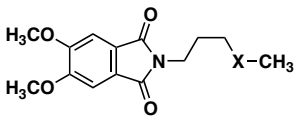

13a; X = S

13b; X = SO

To our surprise, according to the best of our knowledge, no report has been published so far in the literature benefiting from suppressing PET quenching in thioether on metal coordination. The efforts from our group towards exploiting PET in thioether for development of metal ion responsive fluorescent chemosensor met limited success.[63]

2.1.3 Sulfur in thioureas

Sulfur as recognition element has been used for chemosensing in thiourea based receptor units. The strength of the thiourea moiety lies in its dual nature of interaction with cations as well as anions. The soft sulfur part can coordinate to the soft metal ions, whereas the NH group interacts with the anions through H-bonding.[64,65] Sticking to theme of sulfur as the recognition moiety we will discuss only the utility of thiourea unit for metal ion responsive fluorescent chemosensing.

There are only few reports of metal ion responsive fluorescent chemosensor based on the thiourea moiety. In early report by Bren *et al.* investigation of luminescent properties of a series of mono and bisthioureas, based on N-(9-anthrylmethyl) alkyl amines, was carried out with heavy transition metal ions.[66] Compound **14** (***Figure 2.2***) was determined to be a highly effective chemosensor for Hg^{2+} with *ca.* 34 fold enhancement in the fluorescence intensity. Notably, it was not shown that PET was the signaling mechanism operating in these chemosensors, and there is reason to suspect that the fluorescence enhancements have another origin.[67]

Figure 2.2: *Bren's bisthiourea derivative for Hg^{2+} chemosensing.*

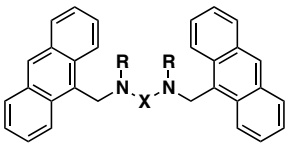

14

X = $(CH_2)_6$

R = C(S)NHPh

Motivated by these scarce reports, our group recently developed a series of thiourea-appended naphthalimides **15a-d** (***Figure 2.3***) in which coordination of metal ion inhibits the PET quenching and thus restores the fluorescence emission.[68] The salient features of these chemosensors were selective and strong binding for Hg^{2+} (*i.e.,* log K_d ~ -5.9 to -7.8) in aqueous media and pH tolerance.

Figure 2.3: *Finney's thiourea based chemosensor for Hg^{2+}.*

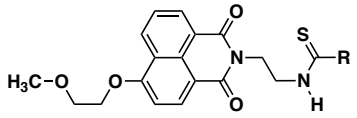

R

15a = $N(CH_3)CH_2Py$

15b = $N(CH_2)_2Py$

15c = $N(CH_2Py)_2$

Py = 2-pyridyl

15d =

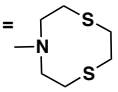

Our group has reported another example of a thiourea appended chemosensor **16** (***Figure 2.4***) which show fluorescence 'turn-on' in presence of Hg^{2+}.[69] The signal transduction mechanism, in this case, relies on the reduction in conformation changes of flanking biaryl rings occurring in the excited state, which was triggered by complexation of thioureas and Hg^{2+} ions.[69,70]

Figure 2.4: *Thiourea appended biarylpyridine based chemosenor.*

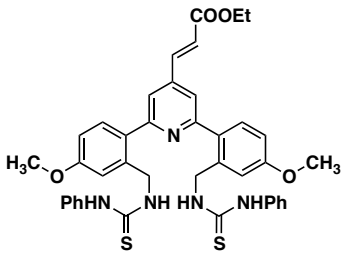

16

2.1.4 Oxidation of sulfur for chemosensing

In general, in the series of an aromatic sulfide/sulfoxide/sulfone, sulfoxides have been found to be anomalously non-emissive.[71,72] For instance, in the naphthalene-based sulfide/sulfoxide/sulfone (**17a-c**; ***Figure 2.5***), sulfoxide **17b** has a fluorescence quantum yield (Φ_F) of 0.02, far less than corresponding sulfide **17a** (0.12) and sulfone **17c** (0.36).[71] The less fluorescent nature of aromatic sulfoxides will be discussed in greater details in ***Section 2.2***.

Figure 2.5: *Naphthalene based sulfide/sulfoxide/sulfone series studied by Jenks et al.*[71]

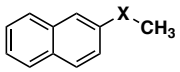

17a; X = S

17b; X = S(O)

17c; X = $S(O)_2$

To cash on the less emissive nature of sulfoxide, our group reported pyrene based sulfoxides (**18a-c**; ***Figure 2.6***) in developing the first visual fluorescent assay for the detection of an explosive triacetone triperoxide (**TATP**; ***Figure 2.6***) in nmol-quantities.[73] The method relies on the oxidation of the less emissive sulfoxides profluorophores **18a-c** to the respective brightly fluorescent sulfones.

Figure 2.6: *Sulfoxide based profluorescent probes for **TATP** detection.*

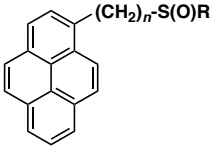

18a; n = 0, R = Ph

18b; n = 1, R = Ph

18c; n = 1, R = (*p*-OMe)Ph

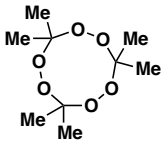

TATP

2.1.5 Exploiting sulfoxide for metal ion detection

Sulfoxide are known, albeit weak, metal ion chelators.[74,75] They exhibit O and/or S coordination depending on the characteristics of metal ion centre, *e.g.*, hardness/softness, steric bulk and π-accepting ability of ligand.[74,75]

In light of the well established metal ion coordination chemistry of sulfoxides, our group was interested in the correlation between fluorescent emission of aromatic sulfoxides and metal ion binding. Following our curiosity, we observed that addition of $ZnCl_2$ and $LiClO_4$ enhanced the fluorescence intensity of phenyl pyrenyl sulfoxide (**18a; PyS(O)Ph**) as illustrated in ***Figure 2.7***.[76] These

observations point out the great potential of exploiting less emissive aromatic sulfoxides for metal ion-responsive fluorescent chemosensor development.

Figure 2.7: *Fluorescence emission response of* ***18a*** *with metal ions in DCM.*

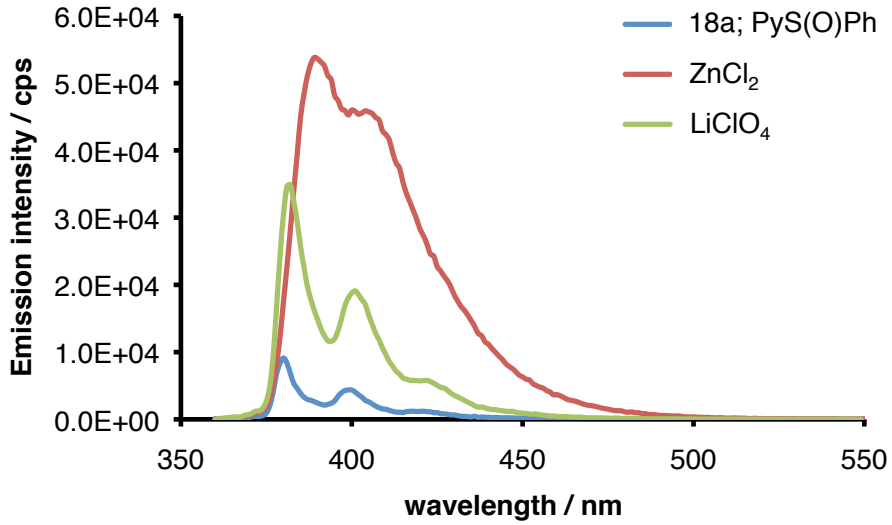

Before illustrating how we exploited this enormous potential in less emissive aromatic sulfoxide for metal ion detection, it would be appropriate now to understand the reason for low emission in aromatic sulfoxides.

2.2 Photophysical properties of alkyl aryl and diaryl sulfoxides

2.2.1 Weak luminescence in aromatic sulfoxides

Aromatic sulfoxides are observed to be less fluorescent than their parent unsubstituted arenes. A series of benzene ring based aromatic sulfides/sulfoxides/sulfones, outlined in ***Figure 2.8***, were investigated by Jenks *et al.*[77] Fluorescence emission was not observed at room temperature for any sulfoxide, and only selectively appeared at 77 K for chromophores **21**, **27** and **28**.

Fluorescence emission could only be acquired at room temperature for aromatic chromophores larger and more fluorescent than benzene. Some of

Figure 2.8: *Benzene based sulfide/sulfoxide/sulfone studied by Jenks et al.*

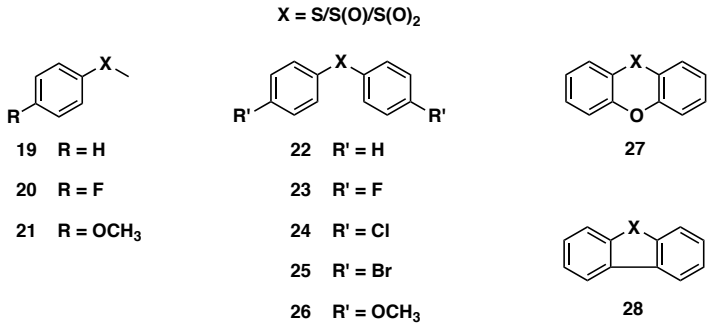

those sulfoxides are shown in ***Figure 2.9***.[71] In most of these sulfoxides, at room temperature, there was a similarity in the fluorescence spectra to those of the corresponding parent arenes. These sulfoxides were found to have singlet energies (E_S) within 4 kcal·mol^{-1} of those of the parent arenes. Differences of only few kcal·mol^{-1} was determined between spectroscopic singlet energies of the corresponding sulfides and sulfones of **29-30**, and the corresponding parent arenes. These observations suggest that heavy atom or symmetry breaking effects of sulfur atom are not responsible for less fluorescence emission in sulfoxides.

Figure 2.9: *Large aromatic ring based sulfoxides studied by Jenks et al.*

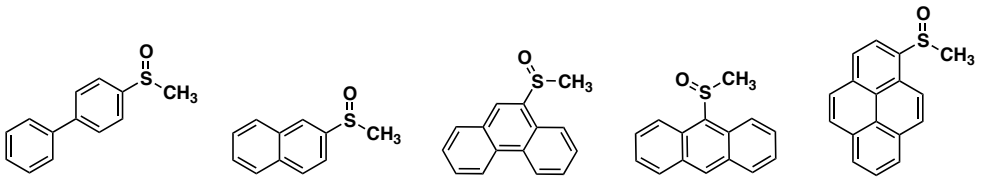

The fluorescence quantum yields (Φ_F) of **29-33** are in the range of 0.005-0.090 at room temperature, and increased at 77 K. The quantum yields of triplet formation (Φ_T) were found to be reduced by a factor of two or more in sulfoxides **29-32** relative to the parent arenes. However, sulfoxide **33** stood out as an exception with Φ_T (0.35) similar to that of pyrene (0.38) in acetonitrile. The considerably lower sum of Φ_F and Φ_T than unity, and fluorescence enhancement

in frozen glass matrix, suggested that there is an important nonradiative deactivation pathway available for sulfoxides **29-33** from the electronic singlet excited state.

2.2.2 Stereomutation† at sulfur center

A very important property of A non-symmetrical sulfoxide is that it contains a stereogenic centre at sulfur. Sulfoxides, in general, are thermally very stable. Sulfoxides undergo stereomutation under drastic conditions like elevated temperatures or acidic media.[78] The extraordinary thermal stability of chiral sulfoxides render them useful as chiral auxiliaries for asymmetric synthesis.[79,80]

Mislow *et at.* investigated thermal racemization of a series of chiral aryl *p*-tolyl sulfoxides and found it to be a high energy barrier process (*ca.* $E_a \sim 40$ kcal·mol^{-1}).[81] The stereomutation in these sulfoxides is established to exclude any bond breaking/forming but rather pass through a transition state comprising a planar geometry. This process is also called pyramidal inversion.[82]

2.2.3 Photochemical stereomutation of sulfoxides

The photochemistry of aromatic sulfoxides is quite rich, and involves numerous possible deactivation pathways for the excited states. Sulfoxides are known to undergo reactions like photochemical rearrangements, desulfurization, α-cleavage, photosensitized oxidation.[83-87] In complement to thermal racemization, sulfoxides are known to undergo photochemical racemization at sulfur.[71,88]

First ever report of photoracemization came in 1965 from Mislow *et al.*[88] They investigated a series of chiral aryl *p*-tolyl sulfoxides (**34a-b**; ***Figure 2.10***) and termed the light induced pyramidal inversion. Addition of naphthalene to **34a**

† *Stereomutation means interconversion of enantiomers (racemization) or diastereomers (epimerization).*

enhanced the quantum efficiency of inversion, and with intramolecular naphthalene in **34b** further improvement in quantum efficiency of inversion was observed. No racemization, even in the presence of added naphthalene, was observed in methyl *n*-butyl sulfoxide **35**.[88] This result emphasized that a minimum of arene sulfinyl group is required for photoracemization. Based on quenching experiments with piperylene in **34a-b**, transfer of excitation energy from naphthalene to *p*-toluene sulfinyl was inferred.[89]

Figure 2.10: *Sulfoxides investigated by Mislow et al.*

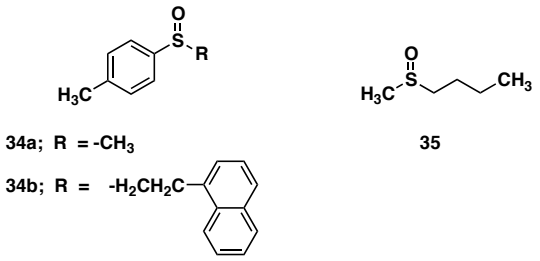

34a; R = -CH_3 **35**

34b; R = -H_2CH_2C

In order to understand the underlying mechanism of naphthalene sensitized photostereomutation, Cooke and Hammond investigated chiral sulfoxides **36a-f** (***Figure 2.11***).[90,91] Measurement of singlet and triplet energies in

Figure 2.11: *Sulfoxide studied by Cooke and Hammond.*

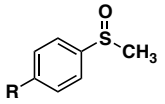

36a; R = CH_3 **36d; R = OH**

36b; R = Br **36e; R = H**

36c; R = Cl **36e; R = $C(CH_3)_3$**

36a and **36b** suggested that excitation energy transfer from naphthalene to sulfoxides would be endothermic and unlikely to proceed. Based on the effect of sulfoxide concentration on naphthalene fluorescence and quantum yield of inversion, involvement of exciplex between excited naphthalene and ground state sulfoxide was proposed. The absence of a significant substituent effect on the rate of naphthalene fluorescence quenching in **36a-f** precludes the involvement of charge transfer in the exciplex.[90]

The pioneering work of Jenks *et al.* addressed problems related to the mechanism for photostereomutation in alkyl aryl and diaryl sulfoxides. The next sections will deal with various mechanistic pathways that could account for the photostereomutation of sulfoxides.

2.2.3.1 Radical fragmentation as a mechanism for photostereomutation

α-Cleavage, or C-S bond scission had been extensively studied for many sulfoxides and reported in the literature.[85] The mechanism of photolysis of aryl benzyl sulfoxides **37** had been rigorously established as outlined in ***Figure 2.12***.[92] The primary and secondary photolytic processes of sulfoxide and

Figure 2.12: *A general sequence of reactions following α-cleavage in aromatic sulfoxides on irradiation.*

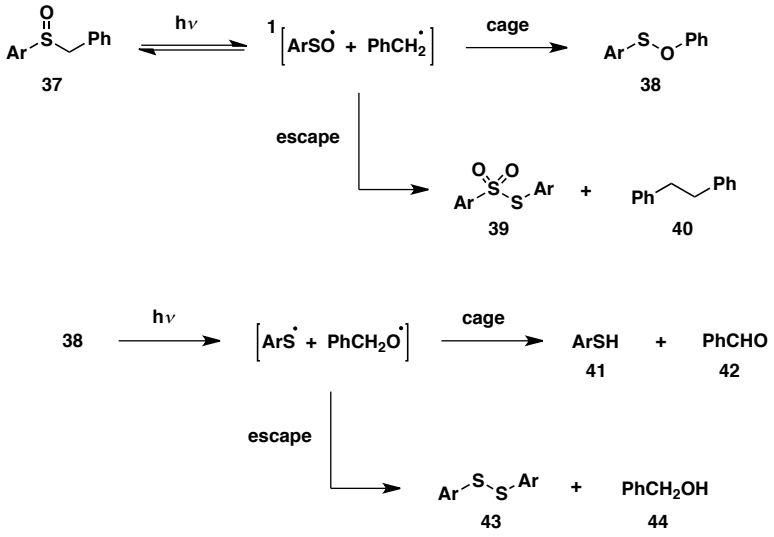

sulfenate, respectively, gave a variety of products. The product distribution was dependent on excitation wavelength, viscosity of the solvent and irradiation time. Low viscosity solvents were found to favor radical “escape” products rather than radical “cage” products. The contrary is true for high viscosity solvents.

The sulfinyl radical, generated by α-cleavage, is achiral. Recombination of the achiral geminate radical pair with randomization of stereochemistry provides

an opportunity for photostereomutation. The quantum efficiency of photolytic conversion in various alkyl aryl sulfoxides, with varying nature of alkyl substituent, was studied.[93] The structure of the alkyl radical involved increases the efficiency of photolytic conversion in the order as follows:

$$\text{aryl} < 1^{o} < 2^{o} < 3^{o} < \text{benzyl}$$

The presence of sulfinyl radical **49** was established by transient absorption spectroscopy after nanosecond laser photolysis of various aryl sulfoxides **45-48** (***Figure 2.13***) in variety of solvents.[94,95] The extinction coefficients (ε) of 1.1×10^4 and 1.3×10^3 $M^{-1}cm^{-1}$ were determined from the absorption spectrum of **49** at wavelengths (λ_{max}) of 300 and 450 nm respectively. This result gave the substantial evidence for the intermediacy of sulfinyl radicals in photoassisted cleavage of C-S bond in sulfoxides.

Figure 2.13: *A series of sulfoxides studied by Jenks et al. for establishing intermediacy of sulfinyl radical in α-cleavage.*

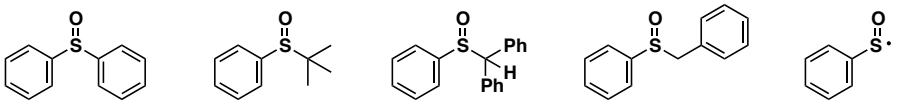

45 **46** **47** **48** **49**

The aryl benzyl sulfoxides **48** are expected to have the triplet energies (E_T) of ~ 80 kcal·mol^{-1}.[77] In the presence acetone as triplet sensitizer (E_T = 79 kcal·mol^{-1}), the product distribution dramatically changed relative to direct photolysis. The triplet sensitization experiment suggested that the multiplicity of the reactive state is a singlet under "normal" photolysis conditions.[92,96]

2.2.3.2 Non-homolytic/non-radical pathway as mechanism for photostereomutation‡

The quantum yield of photochemical inversion (Φ_{inv}) was measured for optically resolved sulfoxides **30** and **33 (*Figure 2.14*)**. In these two sulfoxides, at room temperature, the sum of $\Phi_{F,}$ Φ_T and $2\Phi_{inv}$ is approximately equal to sum of Φ_F and Φ_T for corresponding parent arenes. As, described in ***Section 2.2.3.1*** the aryl or 1^o alkyl substituent disfavors the homolysis of aromatic sulfoxides. This observation suggested the prime significance of direct inversion at the sulfur center as a non-radiative pathway for excited state deactivation.

Figure 2.14: *Sulfoxides studied by Jenks et al.*

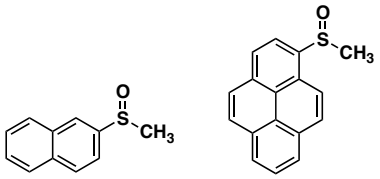

30 **33**

Using benzophenone (E_T = 69 kcal·mol^{-1}), triplet sensitized photoracemization of optically resolved sulfoxide **30** (E_T = 61 kcal·mol^{-1}) was studied for the time period which had enabled complete photoracemization in absence of any sensitizer. No stereomutation in **30** was observed with benzophenone. Photoracemization in **30** was also observed to remain unaffected by the presence of triplet quenchers like piperylene or isoprene even at concentrations up to 25 mM. These facts provide evidence against a role for a triplet state in photoracemization.

‡ *It was assumed that during photostereomutation, like pyramidal inversion, the sulfoxide achieves a trigonal planar transition state. The resulting sulfoxide would then have an equal probability to either invert or not, to either of the enantiomers. So, Φ_{inv} is ideally half of the "racemization" process. (This is in analogy to the photochemical cis-trans isomerization of simple olefins from transition a state with twisted olefin character.)*

2.2.3.3 Direct evidence for non-radical/non-homolytic pathway

Investigation was done on the photolysis of a substrate with two adjacent stereogenic centers, (R_S,S_C)-1-deuterio-2,2-dimethylpropyl *p*-tolyl sulfoxide **(R_S,S_C)-50** (*i.e.*, R-configuration at sulfur and S at the adjacent carbon) as illustrated in ***Scheme 2.1***.[97] The direct inversion at sulfur center was expected to provide S_S,S_C as the only diastereomeric product. In contrast, following α-cleavage pathway**,** the recombination of achiral radical pair without any selectivity should lead to formation of all three new stereoisomers (S_S,S_C, S_S,R_C and R_S,R_C). In 1° alkyl aryl sulfoxides like **50**, it was observed that the quantum yield for α-cleavage is reduced because it leads to the formation of relatively unstable phenyl or primary alkyl radicals.[93] A very high overall Φ_F of 0.45 was measured for inversion of sulfur center.[98] Dominance of stereomutation at the sulfur centre only, in comparison with adjacent stereogenic centre, strongly substantiated the availability of the nonradical pathway for photochemical stereomutation.

Scheme 2.1: *Photolysis of (R_S,S_C)-1-deuterio-2,2-dimethylpropyl p-tolyl sulfoxide* ***(R_S,S_C)-50*** *studied by Jenks et al.*

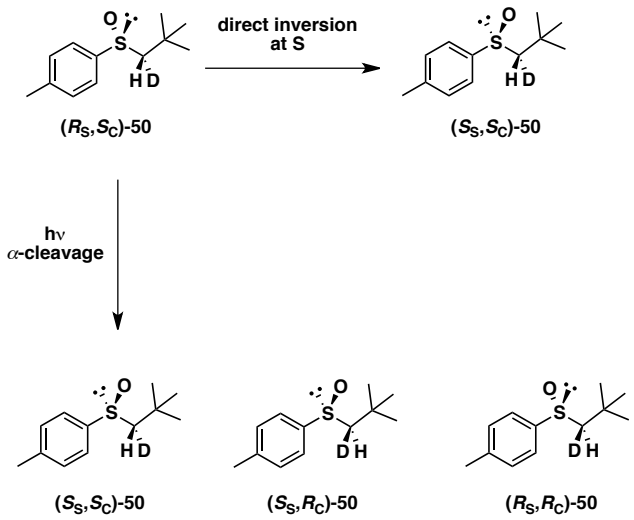

2.2.3.4 Photoracemization of sulfoxide: Non-cleavage pathway

To demonstrate that the non-radiative pathway is available for the photoracemization from the excited state without involving radicals,

multireference *ab initio* calculations were performed on ground and excited states of dimethyl sulfoxide (DMSO) and the hypothetical molecule H_2SO.[99] Based on these calculations, a model for direct photoracemization was proposed. The various processes leading to photoracemization without involving radical formation are illustrated in ***Figure 2.15***. For DMSO, a value of 41.5 kcal·mol^{-1} was obtained for the ground state pyramidal inversion at sulfur. In the absence of any directly comparable experimental value for DMSO, it is consistent with experimental data for alkyl aryl sulfoxides.[81]

Figure 2.15: *A simplified model for direct photoracemization.*

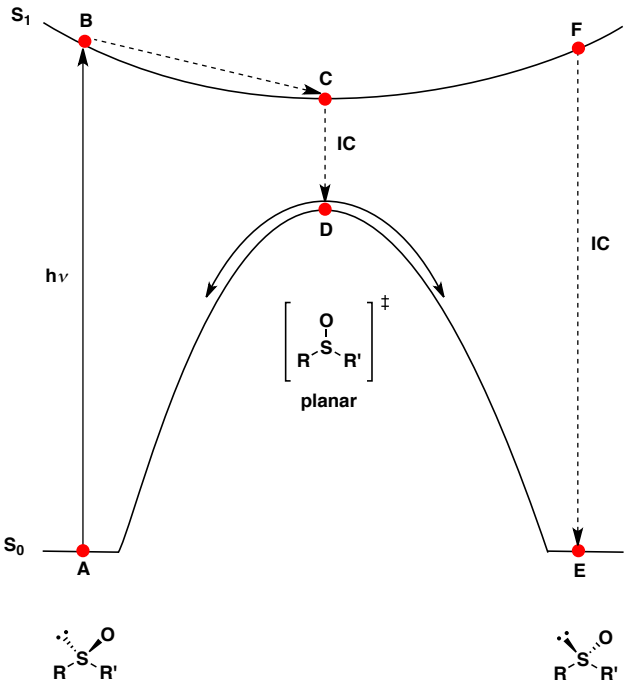

For both H_2SO and DMSO, stationary points with C_{2v} symmetry (**C; *Figure 2.15***), lower in energy than any C_s symmetry stationary point, were found on the excited state energy surfaces. The vertical excitation of the sulfoxide from equilibrium ground state S_0 to S_1 (*i.e.*, A to B) would preferably be followed by geometrical relaxation of vertical geometry to the lowest energy stationary point (*i.e.*, B to C). In the case of DMSO, this lowest energy relaxed excited state geometry was calculated to be just 6 kcal·mol^{-1} above the ground state with same geometry (*e.g.*, D). As the energy gap (CD *vs.* BA) is small, according to the energy gap rule the rate of internal conversion (k_{IC}) between the relaxed excited

state geometry and ground state (*i.e.*, C to D) is expected to be very fast. From the top of the ground state the sulfoxide can randomly slide down to either side (A or E) to result in racemization.

2.3 Simplest alkyl pyrenyl sulfoxide - first control target

The objective of this work is to develop chemosensor based on our early observation that metal ion coordination led to fluorescence enhancement in phenyl pyrenyl sulfoxide (**PyS(O)Ph**; ***Section 2.1.5***). Further development requires appropriate alterations of this fluorophore. However, the phenyl group does not provide versatility for further modifications. We could overcome this problem by replacing phenyl with a 1^{o} alkyl group, in which appropriate alterations would be more facile. In order to follow this approach we chose the target with methyl group (**Me**; ***Figure 2.16***) in exchange for phenyl as our simplest alkyl pyrenyl sulfoxide control target.

Figure 2.16: Me *as a control compound.*

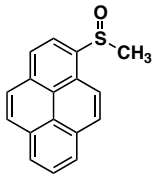

Me

2.3.1 Synthesis of Me

The target compound **Me** was synthesized from commercially available pyrene **51** by the synthetic pathway outlined in ***Scheme 2.2***. Pyrene underwent selective bromination by NBS under electrophilic substitution condition to give 1-bromopyrene **52** in 95% yield.[100] 1-Bromopyrene **52** was treated with the *n*-BuLi in dry THF at -78 ^{o}C to generate a nucleophile *in situ* by lithium-halogen exchange. The nucleophile thus generated was quenched by an electrophile, dimethylsulfide, to give **53** in 70% yield.[73] The sulfide **53** was then partially

oxidized by 0.9 equivalents of meta-chloroperbenzoic acid (mCPBA) to the first target, **Me**, in 92% yield.

Scheme 2.2: *Synthesis of* ***Me****.*

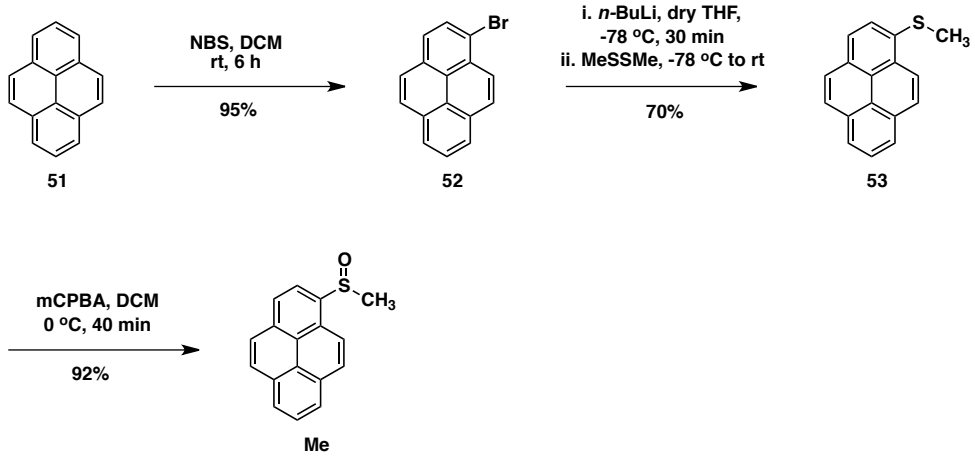

2.3.2 Photophysical properties of Me

The typical UV-Vis and emission spectra of **Me** and other target molecules discussed in following sections consist of very well structured peaks (***Figure 2.17***). The longest excitation and emission wavelength maxima for **Me** were observed to be at 349 and 377 nm respectively (***Table 2.1***). The longest excitation wavelength was used for excitation of fluorophores in all metal ion titration experiments.

Table 2.1: *Spectroscopic data for* ***Me****.*

$\lambda_{ex}^{a,b}$	$\lambda_{em}^{a,b}$	ε / 10^3 M^{-1} cm^{-1}	Φ_F^c	τ^d / ns
349	377	34.7	0.012	1.18

Measurements done in ACN. [a]Excitation/emission spectra acquired for 10^{-5} M ***Me****. [b]Longest wavelength excitation/emission maxima. [c]Absolute quantum yield. [d]χ^2 = 1.3.*

Figure 2.17: *10^{-5} M **Me** in acetonitrile (ACN). a) UV-Vis spectra and b) emission spectra.*

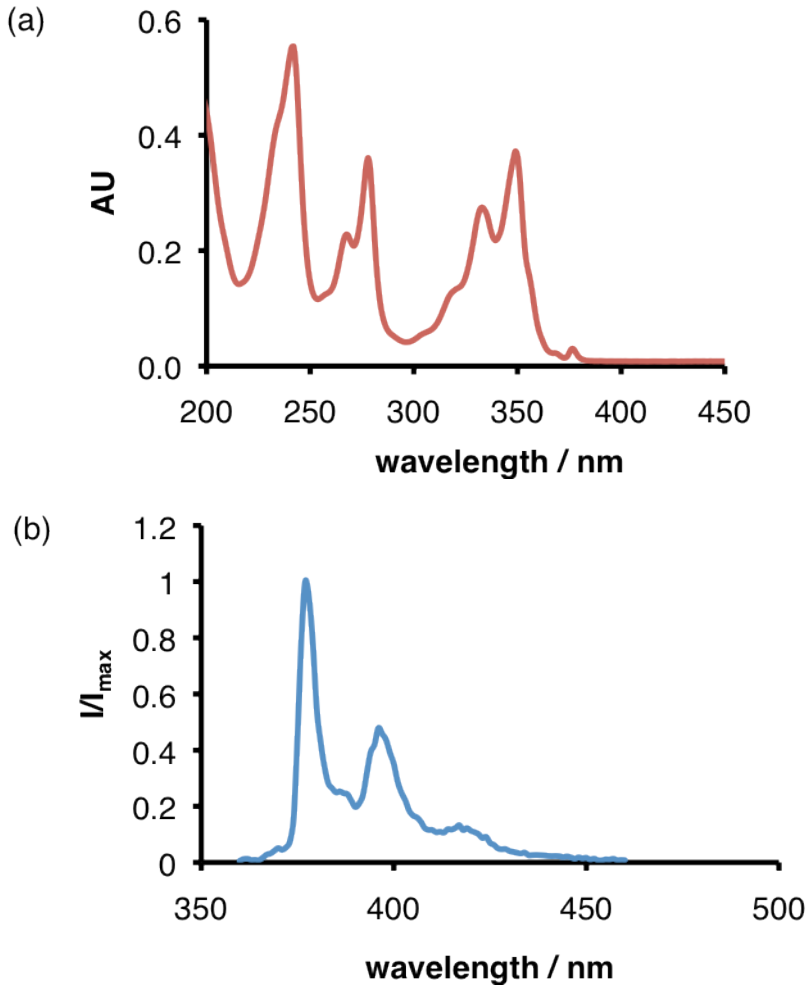

2.3.3 Fluorescence titration of Me with metal ions

All titrations were performed in acetonitrile (ACN) as solvent. Metal salts were chosen on the basis of their solubility in ACN. Li^+, Na^+, Mg^{2+} and Ca^{2+} ions were added as perchlorates while Zn^{2+} ion was added as the chloride. A representative fluorescence titration of **Me** with $ZnCl_2$ is demonstrated in ***Figure 2.18***.

Figure 2.18: *Representative fluorescence titration: 10^{-5} M* ***Me*** *with $ZnCl_2$ in ACN.*

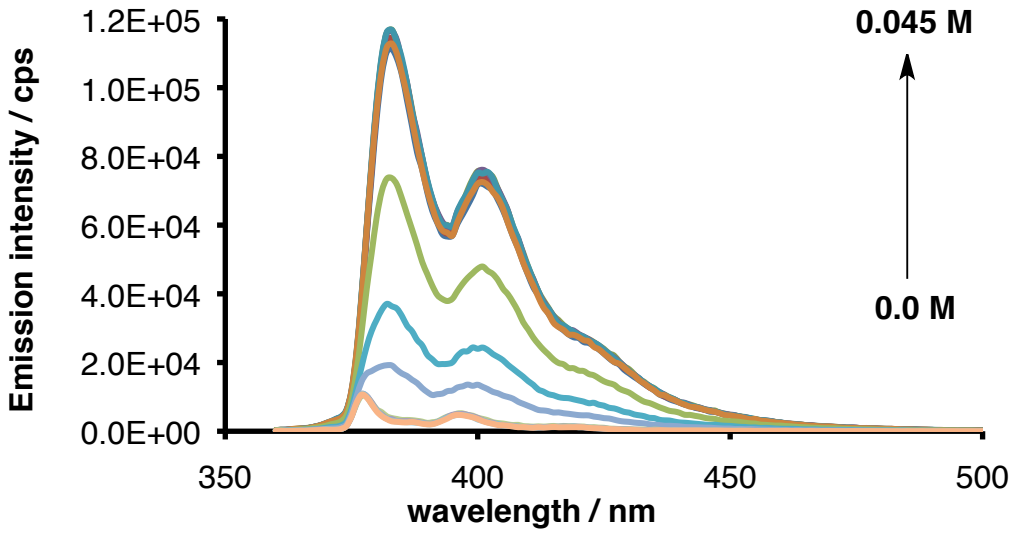

Addition of $ZnCl_2$ increases the fluorescence intensity of **Me** by 36 fold. However, the UV-Vis spectra remain unperturbed by changing the concentration of $ZnCl_2$ (***Figure 2.19***). This observation substantiates that enhancement in fluorescence of **Me** caused by the Zn^{2+} ions is only due to the increase in the Φ_F *i.e.*, inhibition of some deactivation pathway available to **Me** from the excited state.

Figure 2.19: *UV-Vis titration: 10^{-5} M* ***Me*** *with $ZnCl_2$ in ACN.*

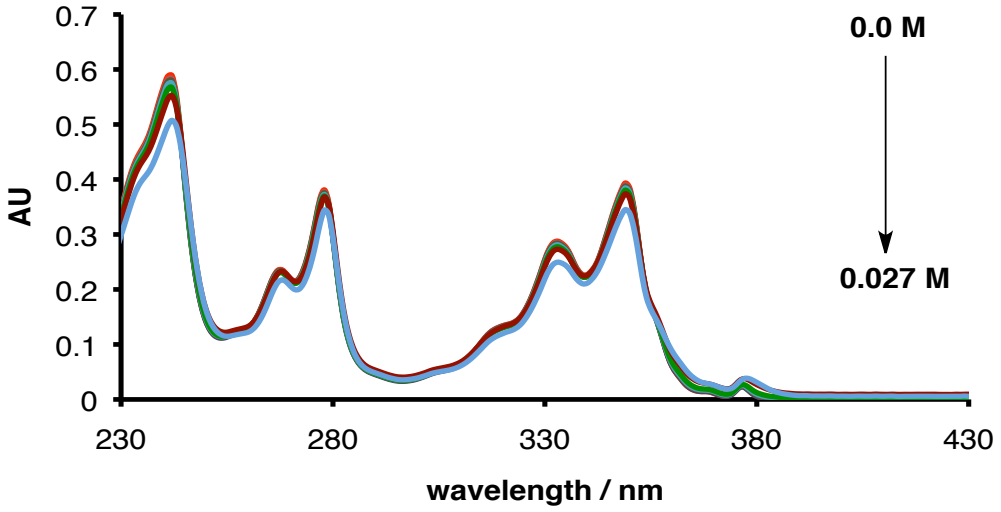

From analysis of dissociation constant, represented as log K_d, (***Table 2.2***) it can be estimated that all these ions are only weakly bound to the **Me**. The binding affinity of **Me** for both Mg^{2+} and Ca^{2+} ions is similar, and nearly one order of magnitude larger than for Zn^{2+} ion. The binding affinity of **Me** with Li^+ is the least among the ions analyzed, whereas, for Na^+ no response could be observed. In all of these titrations mere ≤ 5 nm of bathochromic shift was observed in the longest wavelength emission maximum, at maximum fluorescence enhancement. The Li^+ ion enhances the fluorescence intensity only by 13 fold whereas Mg^{2+} and Ca^{2+} increase by 33 and 26 fold respectively. It has been a general observation that the monovalent cations enhance the fluorescence intensity less than the divalent cations.

Table 2.2: *Dissociation constant (log K_d) and relative enhancement in fluorescence (I/I_o) for* ***Me****.*[a]

M^{n+}	log K_d	I/I_o
Li^+	-0.8	13
Na^+	–	–
Mg^{2+}	-2.6	33
Ca^{2+}	-2.5	26
Zn^{2+}	-1.4	36

Measurements done in 10^{-5} M ACN solution (for details see ***Section 2.6.2****). [a]Entries marked – indicate binding too weak to allow log K_d determination.*

2.4 Introduction of N-atom

After success with the **Me** control, we aspired to strengthen chelation of various metal ions. Appropriate modifications were contemplated by introducing N-atom at the α and β-positions to the sulfoxide moiety. In order to achieve our objectives, two molecules were designed by exchanging methyl substituent in **Me** with 2-pyridyl and ethyl amino group as illustrated in ***Figure 2.20***.

Figure 2.20: *Targets with N-atom at α and β position to S(O).*

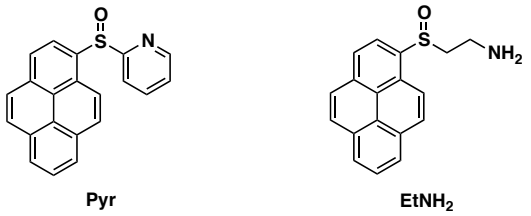

2.4.1 Synthesis of Pyr

The target **Pyr** was synthesized (***Scheme 2.3***) by similar methodology to that described for the synthesis of **Me**. After lithium-halogen exchange on **52**, the *in situ* generated nucleophile was quenched by 2,2'-dipyridyl disulfide as an electrophile to give sulfide intermediate **4** in 78% yield. Compound **54** was oxidized to the corresponding sulfoxide target **Pyr** in 87% yield.

Scheme 2.3: *Synthesis of **Pyr**.*

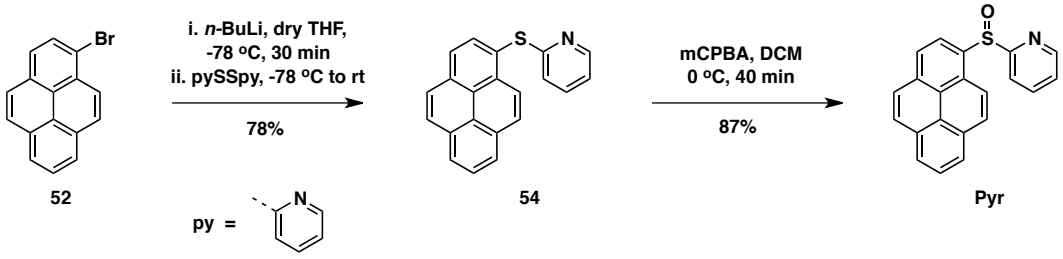

2.4.2 Synthesis of $EtNH_2$

The synthesis of target **$EtNH_2$** was achieved from 1-bromopyrene **52** as outlined in ***Scheme 2.4***. The thiolate generated from reacting cysteamine hydrochloride with KOH in dry DMF, under continuous flow of N_2, was treated with 1-bromopyrene **52** at 110 ^oC. After 1 hr of heating, the reaction mixture was cooled to room temperature. Subsequent reaction with Boc_2O at room temperature gave **55** in overall yield of 96%. Oxidation of **55** with mCPBA furnished Boc-protected sulfoxide **56** in a yield of 97%. Deprotection of the Boc-group in intermediate **56** with 10% TFA:DCM provided **$EtNH_2$** in 79% yield.

Scheme 2.4: *Synthesis of* ***EtNH$_2$***.

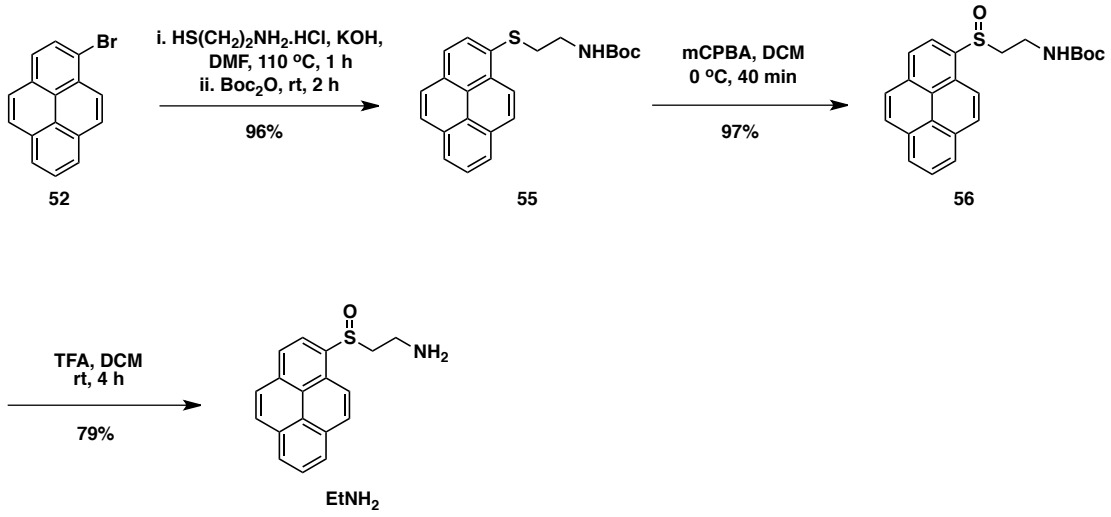

2.4.3 Photophysical properties of Pyr and EtNH$_2$

The longest wavelength excitation and emission maximum were observed to be slightly red shifted in these targets in comparison to **Me** (***Table 2.3***). However, a major variation was observed in the Φ_F. **Pyr** is ~ 5 times more fluorescent than **Me** whereas, for **EtNH$_2$**, Φ_F is not very different than that for **Me.**

Table 2.3: *Spectroscopic data for* ***Pyr*** *and* ***EtNH$_2$****.*

Compound	λ_{ex}[a,b]	λ_{em}[a,b]	ε / 10^3 M^{-1} cm^{-1}	Φ_F[c]
Pyr	352	380	35.3	0.059
EtNH$_2$	349	378	31.1	0.009

Measurements done in ACN. [a]Excitation/emission spectra acquired at 10^{-5} M. [b]Longest wavelength excitation/emission maxima. [c]Absolute quantum yield.

2.4.4 Fluorescence titration of Pyr with metal ions

Binding affinities of **Pyr** with various ions, Li^+, Mg^{2+} and Ca^{2+}, remained similar to that for **Me** (***Table 2.4***). The binding of these metal ions with **Pyr** was associated with enhancement of fluorescence intensity, but only to a lesser extent than **Me**. These observations could be rationalized by taking into account the inherent high Φ_F of **Pyr** relative to **Me**.

Table 2.4: *Dissociation constant (log K_d) and relative enhancement in fluorescence (I/I_o) for* ***Pyr****; Measurements done in ACN.*[a]

M^{n+}	log K_d	I/I_o
Li^+	-0.4	3.5
Na^+	–	–
Mg^{2+}	-2.3	3.0
Ca^{2+}	-2.5	5.0
Zn^{2+}	-2.2	0.4

Measurements done in 10^{-5} M ACN solution (for details see ***Section 2.6.2****). [a]Entries marked – indicate binding too weak to allow log K_d determination.*

Figure 2.21: *Fluorescence titration of 10^{-5} M* ***Pyr*** *with $ZnCl_2$ in ACN.*

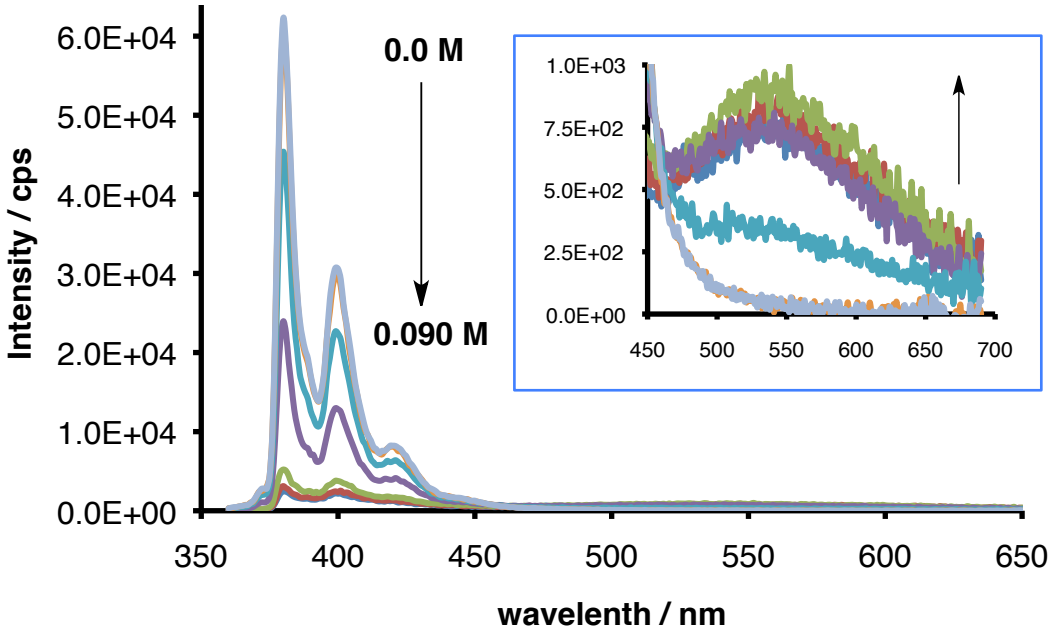

An anomalous response of **Pyr** was observed with Zn^{2+}. Though binding affinity of **Pyr** for Zn^{2+} ion increased by one order of magnitude relative to **Me**, binding suppresses the fluorescence intensity. This peculiar observation intrigued us to look at the fluorescence titration of **Pyr** with $ZnCl_2$ in more detail (***Figure 2.21***). Reduction in fluorescence intensity in 360-450 nm was accompanied by enhancement of fluorescence intensity in 470-670 nm region.

Significant changes were also observed in UV-Vis spectra in terms of bathochromic shift in longest absorption wavelength maximum (***Figure 2.22***). These changes in fluorescence and UV-Vis spectra are specifically present in case of titration with $ZnCl_2$. Therefore, it can be concluded that the new Ligand:Metal (**L:M**) complex has very different spectroscopic properties than observed with other metal ions, which is reflected in the quenching of overall fluorescence intensity for **Pyr** with $ZnCl_2$.

Figure 2.22: *UV-Vis titration of 10^{-5} M* ***Pyr*** *with $ZnCl_2$ in ACN.*

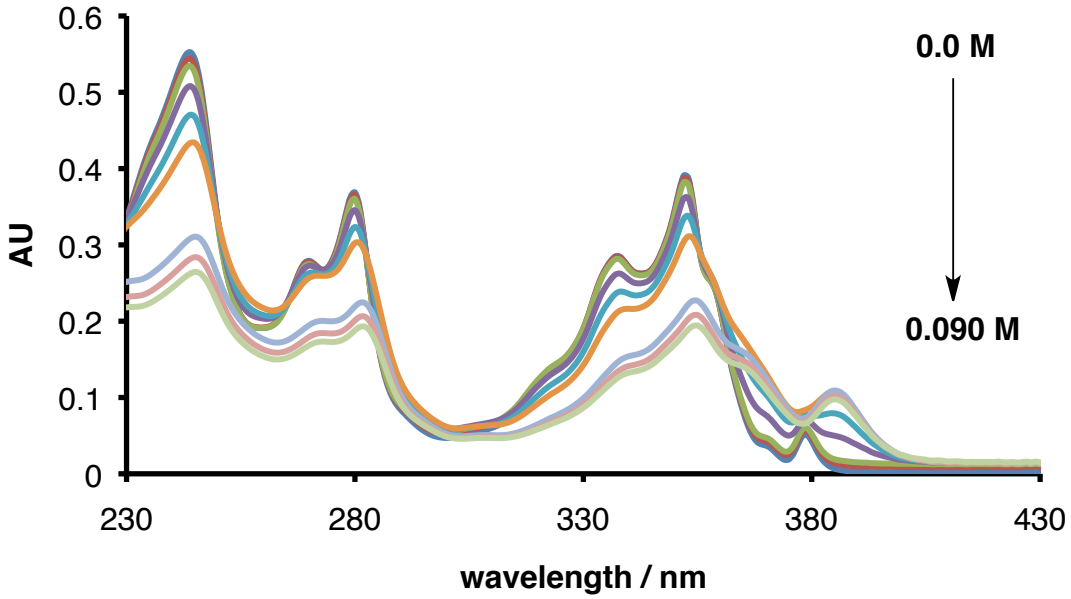

1:1 **$ZnCl_2$:Pyr** was stirred in 5% MeOH:DCM solution for 3 hours. After evaporation of solvent, the residue was dissolved in minimum amount of 5% MeOH:DCM. Crystallization was achieved with slow evaporation of the solution. The crystal structure (***Figure 2.23***; ***Appendix I***) clearly shows that the -S(O)- group coordinates to the Zn^{2+} ion through its O-atom and that the N-atom of pyridine moiety participates in the cooperative binding.

Figure 2.23: *Crystal structure of* ***Pyr-ZnCl$_2$****.*

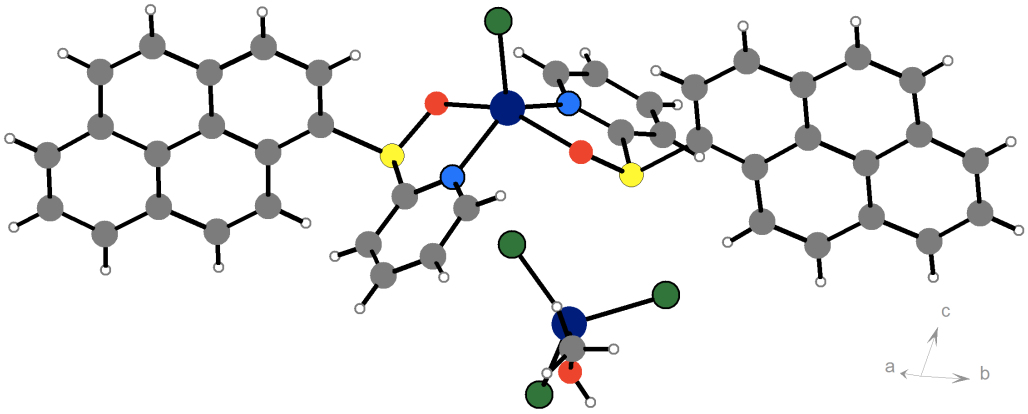

It would not be appropriate to predict, at this point in time, the stoichiometry of the L:M complex in solution just from the knowledge of the crystal structure. But, these observations that formal 1:1 L:M stoichiometry could exhibit 2:1 complex for transition metal ion (*e.g.*, Zn^{2+}), make us cautious in interpreting Job plots. We note that the formation of such 2:1 L:M complex could account for the diminished fluorescence via excimer deactivation of the pyrene excited state.

Table 2.5: *Dissociation constant (log K_d) and enhancement in fluorescence (I/I_o) of* ***EtNH$_2$****.*[a]

M^{n+}	log K_d	I/I_o
Li^+	-2.0	33
Na^+	–	–
Mg^{2+}	-5.7	44
Ca^{2+}	-5.7	42
Zn^{2+}	-5.3	48

Measurements done in 5x10^{-7} M ACN solution (for details see ***Section 2.6.2****).* [a]*Entries marked – indicate binding too weak to allow log K_d determination.*

2.4.5 Fluorescence titration of $EtNH_2$ with metal ions

Strong binding affinity was observed for **$EtNH_2$** with various metal ions, as illustrated in ***Table 2.5***. In comparison to **Me**, the binding affinities for Mg^{2+} and Ca^{2+} ions increased nearly by 1000 fold. In the case of Zn^{2+}, binding affinities were enhanced by a full four orders of magnitude. For Li^+ ion the binding affinity did not increase by much (*ca.* 10 fold). Along with the increases in binding affinities with various metal ions, fluorescence enhancements are also slightly higher than that with **Me**. The maximum quantum yield ($\Phi_F^{max} = \Phi_F * I/I_o$) of 0.44 was achieved with $ZnCl_2$.

All efforts to crystallize a $EtNH_2$:$ZnCl_2$ complex were futile. The stoichiometry of $EtNH_2$:$ZnCl_2$ complex was thus determined by Job plot[101] as shown in ***Figure 2.24***. It could be estimated from the plot that maximum change in fluorescence intensity was achieved with equimolar **$EtNH_2$** and $ZnCl_2$, which suggests formation of 1:1 L:M complex.

Figure 2.24: *Job plot* ***$EtNH_2$*** *with* *$ZnCl_2$.*

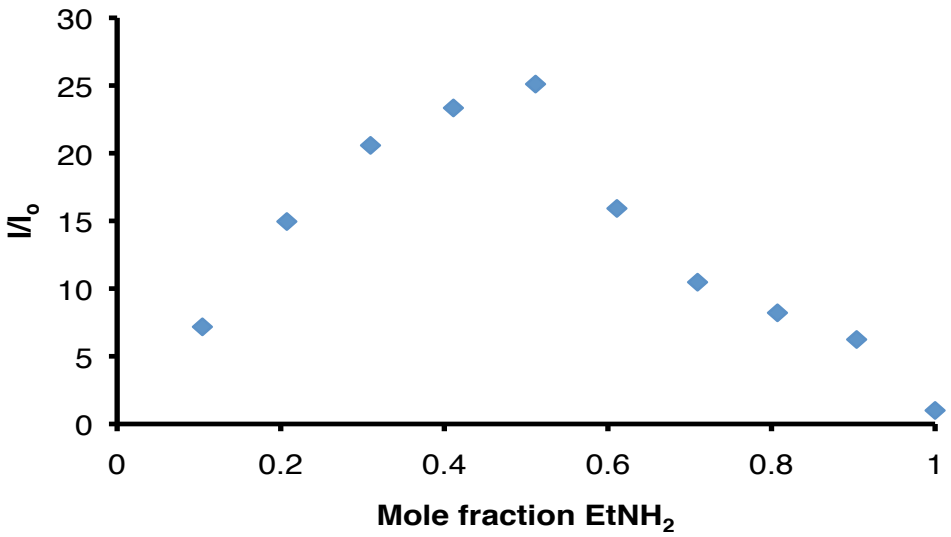

2.5 Conclusion

The background of low fluorescence in aromatic sulfoxides has been discussed in great detail. We envisioned that the weakly-emissive nature of sulfoxides could be exploited for fluorescent chemosensor development. Following our curiosity in fluorescence response of phenyl pyrenyl sulfoxide against metal ions, we observed enhancement in fluorescence intensity with Li^+ and Zn^{2+}.

In order to generalize and develop metal ion responsive chemosensors based on these observations, a control target **Me** was first synthesized. The control target **Me**, successfully, exhibited gain in Φ_F in presence of $LiClO_4$, $Mg(ClO_4)_2$, $Ca(ClO_4)_2$ and $ZnCl_2$, though the binding affinities were very low (log $K_d \geq -2.6$).

Efforts were made to strengthen the binding affinities by modifying the control target **Me**. An N-atom was introduced at the α and β positions from S(O) by replacing methyl with the 2-pyridyl (**Pyr**) and ethylamino (**$EtNH_2$**) groups respectively. **$EtNH_2$** had Φ_F similar to that for **Me** and *ca.* 1000 fold fluorescence enhancement was observed for divalent cations. Moreover, the success with **$EtNH_2$** and the naked **NH_2** terminal lays down a foundation for further modification to address the issue of selectivities against various metal ions in the next generation targets.

2.6 Experimental part

2.6.1 General notes

All reagents and solvents used for reactions were reagent grade and used without further purification unless otherwise noted.

Column chromatographic purification was performed with Merck silica gel gel 60 (particle size 0.040-0-063 mm) or deactivated alumina (5% w/w water), neutral, Brockmann Grade 1, 58 angstroms, -60 Mesh Powder. Solvent for elution was determined by thin layer chromatography (TLC). Analytical TLC was performed with Merck TLC Silica gel gel 60 F_{254} or Macherey-Nagel pre-coated TLC-sheets Polygram Alox N/UV_{254}.

^{1}H-NMR chemical shifts are reported in parts per million (ppm) relative to the solvent peaks ($CDCl_3$ 7.26 ppm, CD_2Cl_2 5.30 ppm or Acetone-d_6 2.05 ppm). Multiplicities are given as: s (singlet), d (doublet), t (triplet), q (quartet), dd (doublet of doublets), m (multiplet).

^{13}C-NMR chemical shifts are reported in parts per million (ppm) relative to the solvent peaks ($CDCl_3$ 77.23 ppm, CD_2Cl_2 54.0 ppm or Acetone-d_6 29.90 ppm).

IR frequencies are given in cm^{-1}. Signal intensities are presented as weak (w), medium (m), strong (s) and very strong (vs).

All optical measurements were performed in spectroscopic grade acetonitrile (ACN). Fluorescence excitation/emission measurements were carried on Edinburgh FLS920 spectrophotometer, using 450W Xenon arc lamp, with excitation and emission slit widths at 1 nm. Emission spectra were obtained by exciting at the longest wavelength excitation maximum. Fluorescence lifetimes were measured using nanosecond flash lamp with computer controlled power supply, for solutions with O.D ~ 0.1. Absolute quantum yields were measured using an integrating sphere accessory. For each compound, three independent solutions (O.D ~ 0.1) were analyzed.

UV-Vis measurements were carried out on a Agilent 8453 UV-Vis spectrophotometer. For each comopund, four independent solutions of varying concentration were analyzed and the extinction coefficient was calculated by

linear least-squares fitting of plots of A *vs.* concentration. All fits gave R^2 values of ≥ 0.999.

2.6.2 Metal ion titrations

2.6.2.1 Protocol for metal ion titrations

For **Me and Pyr,** and **$EtNH_2$** 2 mL of 10^{-5} M and $5x10^{-7}$ M solutions respectively, in ACN were placed in quartz cuvette. Initial fluorescence emission spectra were recorded. Metal salts were added as 5 μL solutions of molar concentrations $2x10^{-5}$ to $2x10^{-2}$ M, until fluorescence emission reached a maximum value.

2.6.2.2 Binding constant determination

For each metal ion titration, I/I_o (emission with metal salt/ emission without metal salt) was plotted against log $[M^{n+}]$. Binding constant was calculated by non-linear least-squares fitting of these plots using the program Prism3 (Graphpad, Inc., San Diego, CA). All fits gave R^2 values of ≥ 0.99.

2.6.2.3. Stoichiometry determination by Job plot

Job plots were obtained by varying mole fraction of the target compound in the mixture with the relevant metal ion and measuring the fluorescence intensity. The mixtures were prepared by taking appropriate volumes of ~10^{-5} M stock solutions of compound and metal ion, both in ACN, to keep the final volume to 2 mL.

2.6.3 Synthetic details and tabulated spectroscopic data.

DCM: Dichloromethane
EtOAc: Ethyl acetate

Fmoc-Cl: Fluorenylmethyloxycarbonyl chloride

mCPBA: *m*-chloroperbenzoic acid

MeOH: Methanol

NBS: N-bromosuccinamide

rt: Room temperature

TEA: Triethylamine

TFA: Trifluoroacetic acid

THF: Tetrahydrofuran

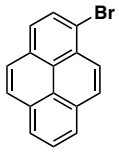

1-Bromopyrene (52):[100] To a solution of pyrene (**51**, 507.3 mg, 2.508 mmol, 1 eq) in DCM (8.5 mL), NBS (467.1 mg, 2.624 mmol, 1.05 eq) was added and the resulting solution stirred for 6 h at rt. The reaction mixture was diluted with DCM (20 mL) and washed with brine (2x15 mL). The aq. layer was washed with DCM (10 mL) and the combined organic layers were dried over $MgSO_4$ and evaporated. Purification by column chromatography (silica gel; hexane) gave 1-bromopyrene (**52**, 673.0 mg, 95%).

R_f: 0.36 (silica gel TLC; hexane).

^{1}H-NMR (400 MHz; $CDCl_3$), δ: 8.45 (d, *J* = 9.2 Hz, 1H), 8.25-8.18 (m, 4H), 8.12-8.02 (m, 4H).

IR(neat), cm^{-1}: 3034 (w), 1587 (w), 1481(w), 1014 (w), 835 (vs).

EI-MS(+): Calculated for $C_{16}H_9Br$ $[M]^+$ 279.99; found 280.00.

^{1}H-NMR data were in accord with those previously reported.[100]

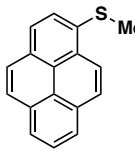

53:[102] *n*-BuLi (2.5 mL, 1.6 M in hexane, 4.0 mmol, 1.1 eq) was added dropwise to a solution of **52** (1.011 g, 3.594 mmol, 1 eq) in dry THF (50 mL) at -78 ^oC under N_2. The resulting solution was stirred for 30 min and methyl disulfide (392.9 mg, 4.171 mmol, 1.15 eq) was added. After 15 min of stirring, the dry ice-acetone bath was removed and the reaction mixture was allowed to reach rt**.** The solvent was then evaporated and the crude residue was dissolved in DCM (50 mL) and washed with brine (50 mL). The aq. layer was washed with DCM (50 mL) and the combined organic layers

were dried over $MgSO_4$ and evaporated. Purification by column chromatography (silica gel; 10% DCM:hexane) gave **53** (630.1 g, 70%).

R_f: 0.36 (silica gel TLC; 30% DCM:hexane).

^{1}H-NMR (400 MHz; $CDCl_3$), δ: 8.57 (d, *J* = 9.2 Hz, 1H), 8.15 (dt, *J* = 17.6, 8.5 Hz, 4H), 8.02-7.99 (m, 4H), 2.71 (s, 3H).

^{13}C-NMR (125 MHz; $CDCl_3$), δ: 133.3, 131.7, 131.2, 129.6, 129.5, 127.8, 127.5, 127.1, 126.3, 125.5, 125.3, 125.2, 124.7, 123.9, 17.5.

IR(neat), cm^{-1} 3038 (m), 2917 (m), 1593 (m), 1482 (m), 1429 (m), 1178 (m), 1030 (m), 838 (vs).

HRMS-EI(+):Calculated for $C_{17}H_{12}S$ $[M]^+$ 248.0660; found 248.0659.

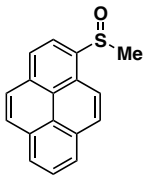

Me:[71] To a solution of **53** (37.3 mg, 0.150 mmol, 1 eq) in DCM (1.5 mL), mCPBA (37.9 mg, 55% assay, 0.120 mmol, 0.9 eq) was added at 0 °C. The solution was stirred for 40 min. The resulting reaction mixture was diluted with DCM (10 mL) and washed with saturated aq. $NaHCO_3$ (10 mL). The organic layer was dried over $MgSO_4$ and evaporated. Purification by column chromatography (silica gel; 50% EtOAc:DCM) gave **Me** (29.3 mg, 92%).

R_f: 0.17 (silica gel TLC; 50% EtOAc:DCM).

^{1}H-NMR (400 MHz; CD_2Cl_2), δ: 8.68 (d, *J* = 8.1 Hz, 1H), 8.39 (d, *J* = 8.1 Hz, 1H), 8.30-8.26 (m, 2H), 8.24-8.07 (m, 5H), 2.91 (s, 3H).

^{13}C-NMR (100 MHz; $CDCl_3$), δ: 138.2, 133.2, 131.3, 130.5,129.4, 129.1, 127.4, 127.2, 126.8, 126.6, 126.5, 125.7, 124.5, 124.5, 120.7, 120.4, 43.6.

IR(neat), cm^{-1}: 3045 (w), 2913 (w), 1591 (m), 1415 (m), 1190 (s), 1056 (vs), 952 (s), 847 (vs).

HRMS-EI(+): Calculated for $C_{17}H_{12}OS$ $[M]^+$ 264.0609; found 264.0608

^{1}H-NMR data were in accord with those previously reported.[71]

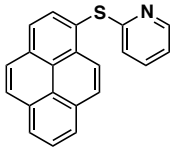

54: *n*-BuLi (0.74 mL, 1.6 M in hexane, 1.18 mmol, 1.2 eq) was added dropwise to a solution of **52** (0.277 g, 0.987 mmol, 1 eq) in dry THF (9 mL) at -78 °C under N_2. The resulting solution was stirred for 30 min and 2,2'-dipyridyldisulfide (0.260 g, 1.18 mmol, 1.2 eq) was

added. After 15 min of stirring, the dry ice-acetone bath was removed and the reaction mixture was allowed to reach rt. The solvent was then evaporated and the crude residue was dissolved in DCM (30 mL) and washed with brine (30 mL). The aq. layer was washed with DCM (20 mL) and the combined organic layers were dried over $MgSO_4$ and evaporated. Purification by column chromatography (5% deactivated alumina; 50% DCM:Hexane) gave **E** (0.242 g, 78%).

R_f: 0.18 (silica gel TLC; 50% DCM:hexane)

^{1}H-NMR (400 MHz; $CDCl_3$), δ: 8.66 (d, *J* = 9.2 Hz, 1H), 8.44 (ddd, *J* = 4.9, 1.8, 0.9 Hz, 1H), 8.35 (d, *J* = 7.9 Hz, 1H), 8.25-8.03 (m, 7H), 7.25 (ddd, *J* = 8.1, 7.5, 1.9 Hz, 1H), 6.94 (ddd, *J* = 7.4, 4.9, 1.0 Hz, 1H), 6.49 (d, *J* = 8.2 Hz, 1H).

^{13}C-NMR (101 MHz; $CDCl_3$), δ: 162.36, 149.74, 136.86, 134.73, 133.92, 132.94, 131.29, 131.09, 129.21, 128.98, 127.4, 126.6, 126.15, 126.08, 125.76, 125.57, 125.32, 124.78, 124.55, 120.9, 119.78.

IR(neat), cm^{-1}: 3040 (m), 1572 (vs), 1557 (m), 1446 (s), 1416 (vs), 1118 (s), 845 (vs) 756 (s).

HRMS-ESI(+): Calculated for $C_{21}H_{14}NS$ $[M+H]^+$ 312.08415; found 312.08376.

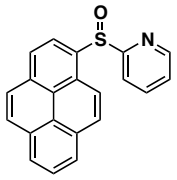

Pyr: To a solution of **54** (89.0 mg, 0.285 mmol, 1 eq) in DCM (3 mL), mCPBA (63.3 mg, 70% assay, 0.257 mmol, 0.9 eq) was added at 0 °C. The solution was stirred for 40 min. The resulting reaction mixture was diluted with DCM (15 mL) and washed with saturated aq. $NaHCO_3$ (15 mL). The organic layer was dried over $MgSO_4$ and evaporated. Purification by column chromatography (5% deactivated alumina; 5% EtOAc:DCM) gave **Pyr** (73.2 mg, 87%).

R_f: 0.40 (Silica gel TLC; 5% EtoAc:DCM).

^{1}H-NMR (400 MHz; CD_2Cl_2), δ: 8.88 (d, *J* = 9.2 Hz, 1H), 8.49 (d, *J* = 8.2 Hz, 1H), 8.36 (ddd, *J* = 4.7, 1.7, 0.8 Hz, 1H), 8.27-8.22 (m, 4H), 8.18 (dt, *J* = 8.0, 0.9 Hz, 1H), 8.14-8.03 (m, 3H), 7.88 (td, *J* = 7.8, 1.8 Hz, 1H), 7.20 (ddd, *J* = 7.6, 4.7, 1.1 Hz, 1H).

^{13}C-NMR (126 MHz; CD_2Cl_2), δ: 167.0, 149.8, 138.5, 137.6, 133.6, 131.4, 130.8, 129.6, 129.6, 129.2, 127.4, 126.9, 126.6, 126.6, 125.6, 124.8, 124.3, 122.9, 122.3, 119.1.

IR(neat), cm^{-1}: 3044 (s), 1589 (m), 1578 (s), 1560 (s), 1450 (s), 1419 (s), 1190 (m), 1050 (vs), 1037 (s), 846 (vs), 770 (m).

HRMS-ESI(+): Calculated for $C_{21}H_{13}NNaOS$ $[M+Na]^+$ 350.06104; found 350.06101.

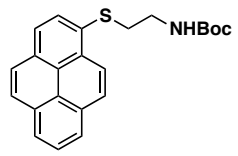

55:[103] To KOH (143.2 mg, 2.552 mmol, 3.0 eq) in dry DMF (4 mL) under N_2, cysteamine hydrochloride (144.0 mg, 1.268 mmol, 1.5 eq) was added. The resulting mixture was stirred at rt until KOH disappeared and a solution of **52** (236.4 mg, 840.8 μmol, 1 eq) in dry DMF (4 mL) was added dropwise. The resulting reaction mixture was heated at 110 °C for 1 h. After cooling to rt Boc_2O (311.9 mg, 1.429 mmol, 1.7 eq) was added and stirred for 2 h at rt. The reaction mixture was diluted with DCM (25 mL) and washed with brine (2x20 mL). The combined aq. layers were washed with DCM (25 mL) and the combined organic layers were dried over $MgSO_4$ and evaporated. Purification by column chromatography (silica gel; DCM) gave **55** (304.7 mg, 96%).

R_f: 0.17 (silica gel TLC; DCM).

^{1}H-NMR (500 MHz; $CDCl_3$), δ: 8.71 (d, *J* = 9.2 Hz, 1H), 8.23-8.01 (m, 8H), 4.88 (s, 1H), 3.33-3.32 (m, 2H), 3.21 (t, *J* = 5.7 Hz, 2H), 1.38 (s, 9H).

^{13}C-NMR (125 MHz; $CDCl_3$), δ: 155.9, 132.0, 131.6, 131.2, 131.1, 130.4, 129.6, 128.5, 128.0, 127.5, 126.5, 125.7, 125.7, 125.5, 125.9, 124.7, 124.7, 79.7, 40.19, 36.1, 28.5.

IR(neat), cm^{-1}: 3333 (w), 3040 (w), 2967 (m), 1700 (vs), 1505 (s), 1366 (s), 1168 (vs), 949 (w), 843 (s).

HRMS-ESI(+):Calculated for $C_{23}H_{23}NNaO_2S$ $[M+Na]^+$ 400.13417; found 400.13367.

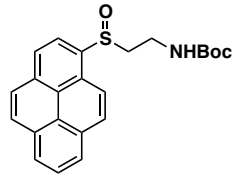

56: To a solution of **55** (75.4 mg, 0.200 mmol, 1 eq) in DCM (8 mL), mCPBA (44.3 mg, 70% assay, 0.180 mmol, 0.9 eq) was added at 0 °C and stirred for 40 min. The reaction mixture was diluted with DCM (10 mL) and washed with saturated aq. $NaHCO_3$ (10 mL). The organic layer was dried over $MgSO_4$ and evaporated.

Purification by column chromatography (silica gel; 30% EtOAc:DCM) gave **56** (68.9 mg, 97%).

R_f: 0.16 (silica gel TLC: 30% EtOAc:DCM).

^{1}H-NMR (300 MHz; $CDCl_3$), δ: 8.60 (d, *J* = 8.1 Hz, 1H), 8.34 (d, *J* = 8.1 Hz, 1H), 8.25 (dd, *J* = 7.0, 5.8 Hz, 2H), 8.16-8.03 (m, 5H), 5.29-5.26 (m, 1H), 3.62 (d, *J* = 0.3 Hz, 2H), 3.45-3.36 (m, 1H), 3.02 (dt, *J* = 13.5, 5.1 Hz, 1H), 1.39 (s, 9H).

^{13}C-NMR (125 MHz; $CDCl_3$), δ: 155.9, 135.3, 133.4, 131.3, 130.5, 129.6, 129.3, 127.5, 127.4, 126.9, 126.8, 126.6, 125.5, 124.7, 124.5, 121.4, 120.3, 79.8, 55.3, 35.5, 28.5.

IR(neat), cm^{-1}: 3313 (m), 3046 (w), 2977 (m), 1709 (vs), 1516 (s), 1365 (m), 1168 (vs), 1052 (s), 848 (s).

HRMS-ESI(+):Calculated for $C_{23}H_{23}NNaO_3S$ $[M+Na]^+$ 416.12909; found 416.12946.

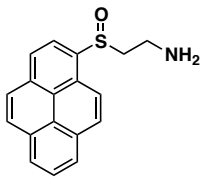

EtNH$_2$: To a solution of **56** (32.1 mg, 81.6 μmol, 1 eq) in DCM (1.2 mL), TFA (0.12 mL, 1.6 mmol, 20.0 eq) was added at rt and stirred for 4 h. The reaction mixture was diluted with DCM (10 mL) and washed with aq. NaOH (pH 12; 10 mL). The aq. layer was washed DCM (2x10 mL) and the combined organic layers were dried over Na_2SO_4 and evaporated. Purification by column chromatography (silica gel; 93:5:2 DCM:MeOH:Et_3N) gave **EtNH$_2$** (19.0 mg, 79%).

R_f: 0.26 (silica gel TLC; 93:5:2 DCM:MeOH:Et_3N).

^{1}H-NMR (400 MHz; CD_2Cl_2), δ: 8.58 (d, *J* = 8.1 Hz, 1H), 8.37 (d, *J* = 8.1 Hz, 1H), 8.29 (d, *J* = 2.6 Hz, 1H), 8.27-8.06 (m, 6H), 3.30-3.22 (m, 1H), 3.15-3.04 (m, 2H), 3.01-2.94 (m, 1H).

^{13}C-NMR (125 MHz; CD_2Cl_2), δ: 137.5, 133.5, 131.7, 131.0, 129.6, 129.4, 127.8, 127.8, 127.2, 126.9, 126.8, 128.9, 124.9, 124.8, 121.7, 121.1, 60.8, 37.0.

IR(neat), cm^{-1}: 3365 (s), 3043 (m), 2920 (w), 1591 (s), 1190 (s), 1041 (vs), 1018 (vs), 848 (vs).

HRMS-ESI(+):Calculated for $C_{18}H_{15}NNaOS$ $[M+Na]^+$ 316.07666; found 316.07644.

Chapter 3

Elaboration of β-Amino Sulfoxide Chemosensors

3.1 Introduction

In the previous chapter, exceptionally low fluorescence in aromatic sulfoxides and their metal chelating ability was introduced, which made them good candidates for developing 'turn-on' based fluorescent chemosensors for detecting metal ions. Following our observations that the metal ion coordination enhances the fluorescence emission of **PyS(O)Ph**,[73] a fluorophore control **Me** was designed. The very fragile binding affinity in **Me** was shown to be intensified by the introduction of N-atom at β position as in the case of chemosensor **EtNH$_2$**.

3.2 Modification of NH_2 terminal in $EtNH_2$

The success with **EtNH$_2$**, in the form of higher binding affinities and similar extent of fluorescence enhancements as compared to **Me** for various metal ions analyzed, provides a fertile ground for further strengthening the binding affinities by modifying the NH_2-terminal. The primary amino group can be derivatized to well established aggressive receptor units like picolyl amine (**57a**; **MePic** and **57b**; **DiPic**) and azacrown ethers (**57c**; **AC-NO$_3$** and **57d**; **AC-NO$_4$**) as depicted in ***Figure 3.1***.[104,105]

Figure 3.1: *Modified* ***EtNH$_2$; 57a-d****.*

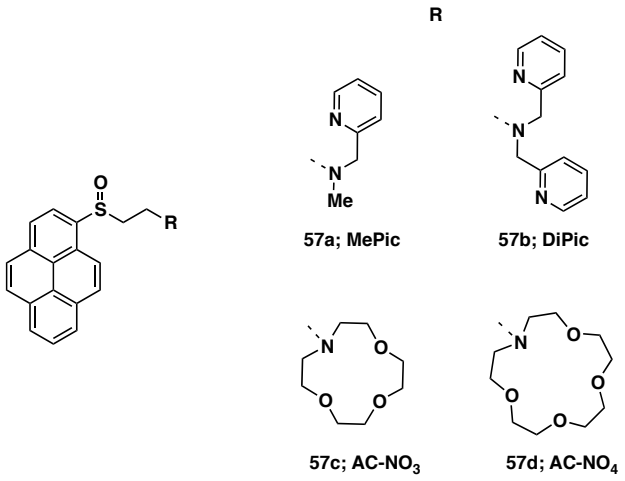

3.2.1 Retrosynthetic analysis of 57a-d

The four derivatives of $EtNH_2$ (**57a-d; *Figure 3.1***) could be synthesized by nucleophilic conjugate addition based chemistry on α,β-unsaturated sulfoxide **58** (***Scheme 3.1***).[106] Access to intermediate **58** can be fulfilled in four transformations from the already synthesized 1-bromopyrene **52**.

Scheme 3.1: *Retrosynthesis for* ***57a-d****.*

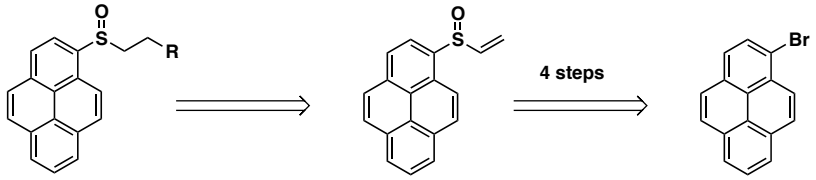

3.2.2 Synthesis of intermediate 58

The synthesis of intermediate **58** was accomplished as outlined in ***Scheme 3.2***. 1-Bromopyrene **52** was treated with the thiolate generated in situ from 2-mercaptoethanol and KOH in DMF at 110 °C for 1 h.[103] The sulfide **59** was isolated in 90% yield after purification by chromatography.

Scheme 3.2: *Synthesis of intermediate* ***58****.*

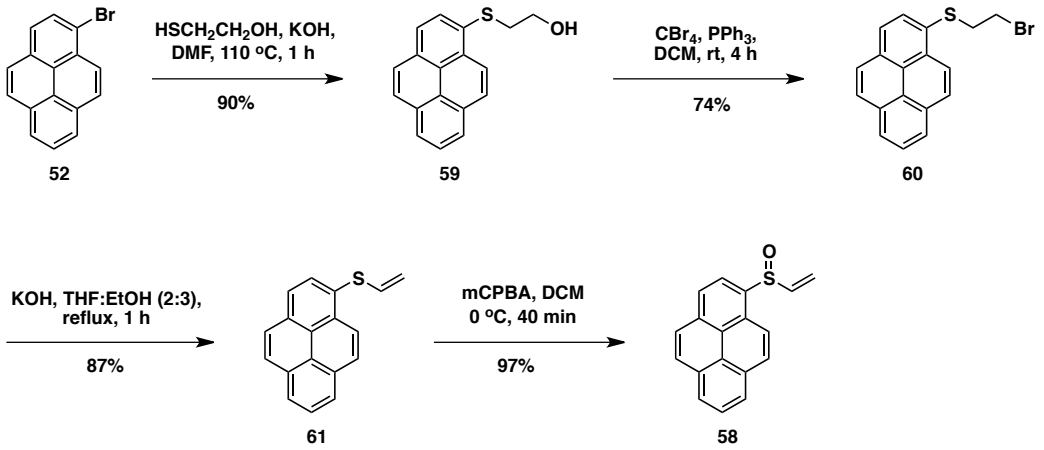

The hydroxyl group in the sulfide **59** was transformed to the bromide **60** by Appel reaction in 74% yield.[107] In the presence of the base, at reflux condition in

THF:EtOH (2:3), sulfide **60** underwent dehydrobromination to furnish pyrenyl vinyl sulfide **61** in good yield (*ca.* 87%).[108] The oxidation of pyrenyl vinyl sulfide **61** with 0.9 equiv. mCPBA gave the corresponding sulfoxide intermediate **58** in 97% yield.

3.2.3 Synthesis of 57a-d

After gaining access to pyrenyl vinyl sulfoxide **58**, it was subjected to Michael addition with appropriate 2° amines to obtain various $EtNH_2$ functionalized targets (**57a-d; *Scheme 3.3***). Fluorophores **57a-d** were isolated in moderate to very good yields (74-92%).

Scheme 3.3: *Synthesis of* ***57a-d****.*

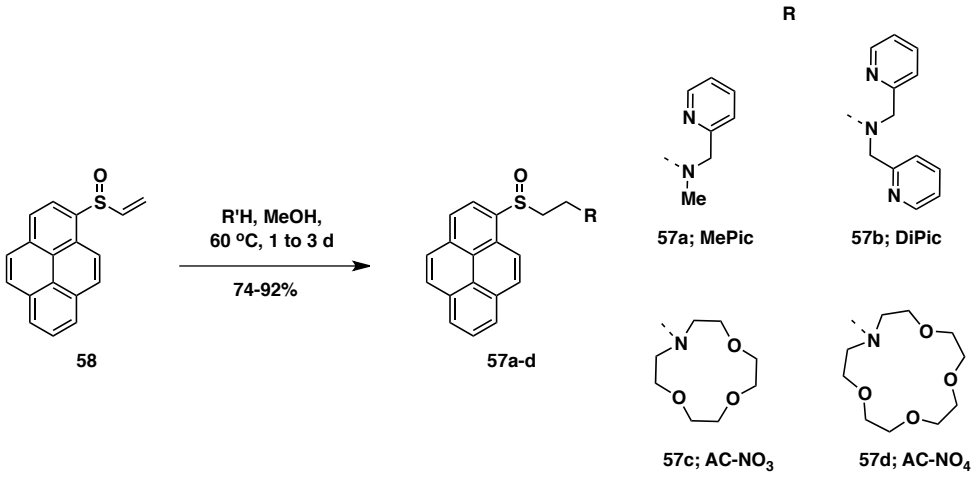

3.2.4 Photophysical properties of 57a-d

Spectroscopic properties of **57a-d**, like the longest excitation and emission wavelengths, extinction coefficients and absolute quantum yields, were measured in acetonitrile (ACN). Any difference from that of **$EtNH_2$** could barely be observed in their longest excitation and emission wavelengths (***Table 3.1***). Extinction coefficients were also found to be similar. However, variations were observed in Φ_F with reduction in **57a-c** (*ca.* 3 fold) and increment in **57d** (*ca.* 4 fold) than that of **$EtNH_2$**.

Table 3.1: *Spectroscopic properties of* ***57a-d****.*

Compound	λ_{ex} [a,b]	λ_{em} [a,b]	ε [c]	Φ_F [d]
$EtNH_2$	349	378	31.1	0.009
57a; MePic	350	378	30.6	0.003
57b; DiPic	350	378	27.6	0.004
57c; AC-NO_3	350	378	28.5	0.003
57d; AC-NO_4	350	378	27.2	0.041

Measurements done in ACN. [a]Excitation/emission spectra acquired at 10^{-5} M. [b]Longest λ excitation/emission maxima. [c]10^3 M^{-1} cm^{-1}. [d]Absolute quantum yields.

3.2.5 Fluorescence titrations of 57a-d with metal ions

Interesting manifestations of variation in receptor unit were observed (***Table 3.2***). In general, target molecules with azacrown ether unit have more powerful binding affinities with I and II group metal ions. Modification of the NH_2 terminal with picolyl and azacrown leads to emergence of binding to Na^+.

Table 3.2: *log K_d of* ***$EtNH_2$*** *and* ***1a-d*** *vs. metal ions.*[a]

M^{n+}	$EtNH_2$	57a; MePic	57b; DiPic	57c; AC-NO_3	57d; AC-NO_4
Li^+	-2.0	-2.8	-5.2	-5.9	-6.2
Na^+	–	-1.0	-2.5	-4.0	-5.1
Mg^{2+}	-5.7	-5.8	-5.7	-6.6	-5.9
Ca^{2+}	-5.7	-5.4	-5.9	-6.4	-6.5
Zn^{2+}	-5.3	-4.65	-5.3	-5.5	-4.5

Measurements done with 5 x 10^{-7} M in ACN (for details see ***Section 2.6.2****). [a]Entries marked – indicate binding too weak to allow log K_d determination.*

In the case of Li^+, binding affinity grows from very weak in **$EtNH_2$** to many orders of magnitude higher. However, the response to divalent ions remains stronger: log K_d -6.6 between **AC-NO_3** and Mg^{2+} indicates sub-nM detection limit (the maximum for our current analytical system). The various Job plots examined

between **AC-NO$_4$** and Li^+, Mg^{2+} and Ca^{2+} establish the stoichiometry of Metal:Ligand to be 1:1 (***Appendix II***).

Figure 3.2: *Fluorescent enhancement of 5 x 10^{-7} M* ***57a-d*** *with various M^{n+} in ACN.*

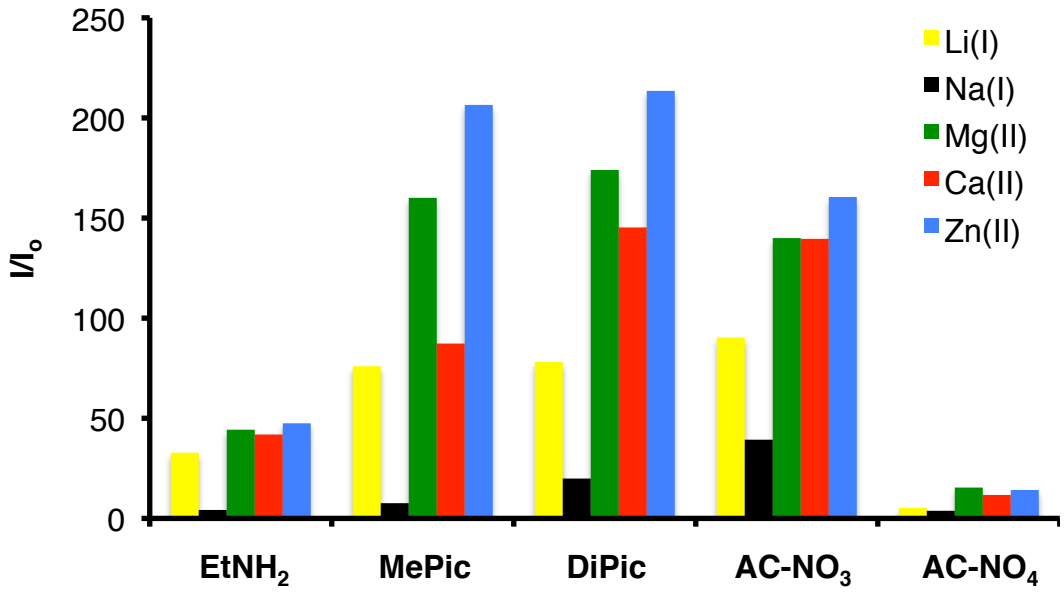

The various ions examined show enhancement in fluorescence of target molecules **57a-d**, as illustrated in ***Figure 3.2***. A maximum Φ_F of *ca.* 0.80 was observed for picolyl receptors with Zn^{2+}. In general, as pointed out earlier, divalent ions bring about greater change in the fluorescence intensity on coordination.

The enormous enhancements in fluorescence intensity for **57a-c** with various metal ions are very impressive. But, attention should be paid to the intrinsic Φ_F of **57a-c** (0.003-0.004) versus that for **EtNH$_2$** (0.009). On account of the lower initial emission in **57a-c** than **EtNH$_2$**, the former can show higher gain in fluorescence intensity on metal ion coordination. The low intrinsic Φ_F of **57a-c** implies the presence of a concurrent deactivation pathway besides the sulfoxide's deactivation process. The next section deals with understanding this additional deactivation pathway.

3.3 Determination of additional pathway in 57a-c

The Φ_F of **57a-c** are lower than that of $EtNH_2$. These observations justify that deactivation pathway other than sulfoxide's deactivation is also present in these molecules. The very first proposition is that effective photoinduced electron transfer (PET) occurring from the N-atom, at the β position from the sulfoxide group, as illustrated in ***Figure 3.3***.

Figure 3.3 *PET from N-atom.*

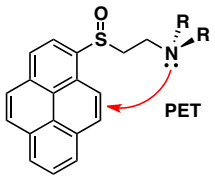

3.3.1 Validation of PET

In order to establish the occurrence of PET from the N-atom, two different approaches were pursued. The first approach was to compare the Φ_F of **$EtNH_2$** and it's diethyl derivative **$EtNEt_2$** as shown in ***Figure 3.4***. It has been reported that in the series of *n*-propylamines, difficulty of electrochemical oxidation follows

Figure 3.4: $EtNH_2$ *and diethyl derivative* ***$EtNEt_2$****.*

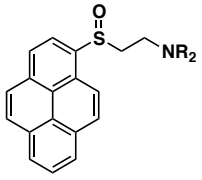

$EtNH_2$; R = H

$EtNEt_2$; R = Et

the trend outlined in ***Scheme 3.4***.[109] On the same lines, in diethyl derivative **$EtNEt_2$** the electron removal or oxidation of the N-atom and, hence, PET to the excited fluorophore should be more efficient than in case of **$EtNH_2$**. Magnification of PET efficiency, as a consequence, should drop the Φ_F in **$EtNEt_2$**.

Scheme 3.4: *Peak potential (E_p) as 1.02, 1.26 and 1.63 (**left to right**); Conditions: 10 Vs^{-1}, 25 ^oC, 0.1 M $NaClO_4$ in ACN and 2-7 mM amine.*

$$(n\text{-}C_3H_7)_3N \;<\; (n\text{-}C_3H_7)_2NH \;<\; (n\text{-}C_3H_7)NH_2$$

Another approach to figure out existence of PET from β N-atom was to carry out titration of **$EtNH_2$** with an acid.[110] The protonation of N-atom would block the lone pair for PET and thus fluorescence emission should be retrieved.

3.3.2 Synthesis of $EtNEt_2$

The diethyl derivative **$EtNEt_2$** *(**Scheme 3.5**)* of ethyl amino pyrenyl sulfoxide was prepared by nucleophilic conjugate addition on pyrenyl vinyl sulfoxide **58** with diethylamine. Sulfoxide **$EtNEt_2$** was obtained in a moderate yield of 84% after the purification.

Scheme 3.5: *Synthesis of **$EtNEt_2$**.*

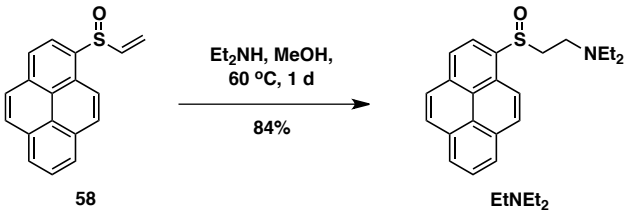

3.3.3 Spectroscopic properties of $EtNEt_2$

The Φ_F of **$EtNEt_2$** was found to be *ca.* 10 times less than that of **$EtNH_2$** *(**Table 3.3**)*. Thus, strong fluorescence quenching in diethyl derivative **$EtNEt_2$** validates the PET quenching in our fluorophores.

Table 3.3 : *Absolute quantum yield in ACN.*

Compound	Φ_F
$EtNH_2$	0.009
$EtNEt_2$	<0.001

3.3.4 Trifluoroacetic acid (TFA) titration of $EtNH_2$

It can be learnt from ***Figure 3.5*** that addition of 1 eq. TFA raises the emission for **$EtNH_2$**. Enhancement in fluorescence emission demonstrates involvement of PET quenching by N-atom.

Figure 3.5: *Titration of* ***$EtNH_2$*** *(10 μM in ACN) with TFA.*

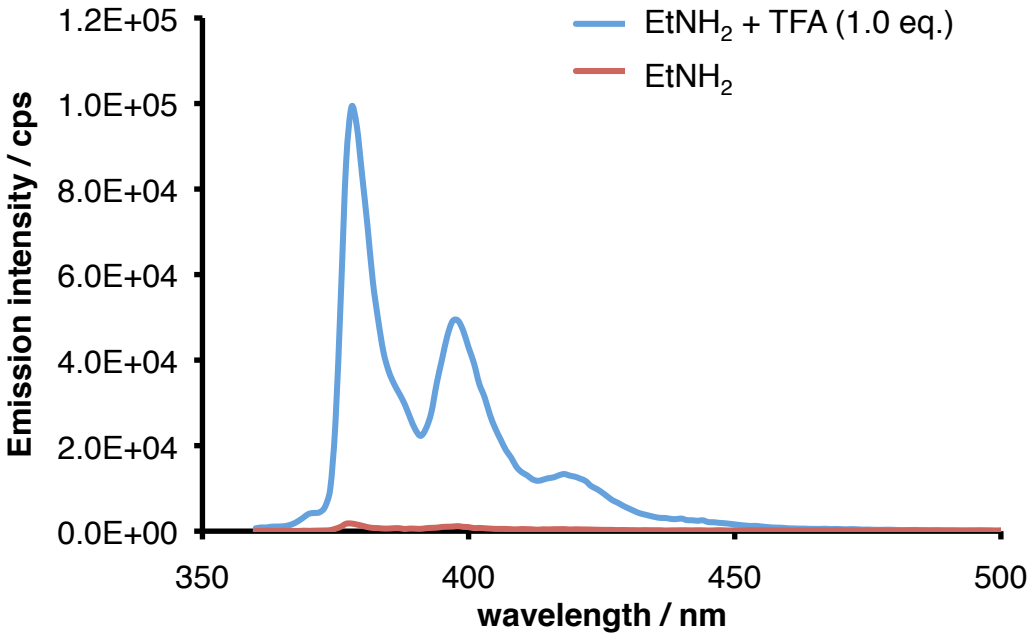

3.4 Contribution of PET and sulfoxide deactivation pathways

Existence of PET quenching by N-atom at the β position from sulfoxide group has been established in the ***Sections 3.3.3 and 3.3.4***. It is, therefore, noteworthy to figure out how much enhancement in fluorescence is contributed by the suppression of PET quenching upon metal ion binding. In the following section we will try to figure that out by segregating the two deactivation pathways - PET and sulfoxide - in our target molecules.

3.4.1 Sulfone *vs.* sulfoxide TFA titrations

Sulfones are known to be more fluorescent and do not deactivate as their sulfoxide counterparts do. Therefore, the sulfone derivative of **$EtNH_2$** would point out the influence of PET deactivation only and split two deactivation pathways. To understand the contribution of the two deactivation pathways, TFA titrations on the following sulfoxides and sulfones *(**Figure 3.6**)* were carried out which will be discussed in ***Section 3.4.3***.

***Figure 3.6: Me** and **$EtNH_2$** and sulfone derivatives.*

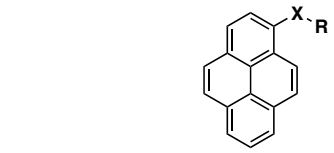

Me; X = SO, R = $-CH_3$ **$EtNH_2$; X = SO, R = $-(CH_2)_2NH_2$**

Me-SO_2; X = SO_2, R = $-CH_3$ **$EtNH_2$-SO_2; X = SO_2, R = $-(CH_2)_2NH_2$**

3.4.2 Synthesis of sulfones

The synthesis of sulfones was achieved as outlined in ***Scheme 3.6***. The complete oxidation of the sulfide **53** to the corresponding sulfone **Me-SO_2** was carried out with 2.2 eq. of mCPBA. This oxidation furnished **Me-SO_2** in 86% yield.

***Scheme 3.6:** Synthesis of **Me-SO_2** and **$EtNH_2$-SO_2**.*

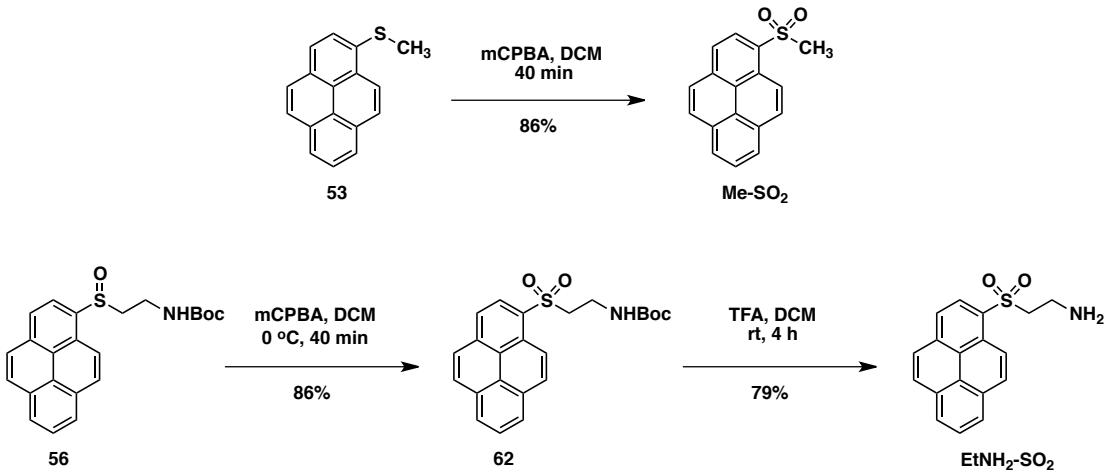

Ethylaminopyrenyl sulfone **$EtNH_2$-SO_2** was synthesized in two steps from sulfoxide **56**. **56** was oxidized using mCPBA to the Boc-protected sulfone intermediate **62** in 86% yield. Deprotecting Boc group in intermediate **62**, with the commonly used 10% TFA:DCM mixture, gave the final sulfone **$EtNH_2$-SO_2** in 79% yield.

3.4.3 TFA titrations of Me, $EtNH_2$ and corresponding sulfones

In the case of **Me** and its sulfone derivative **Me-SO_2**, no change in Φ_F was observed in the presence of TFA (*i.e.,* $\Phi_F^{max} = \Phi_F$), as PET quenching is not plausible (***Table 3.4***). Whereas, $\Phi_F^{max} \neq \Phi_F$ in the case of **$EtNH_2$** and its sulfone **$EtNH_2$-SO_2**. For **Me-SO_2** and **$EtNH_2$-SO_2**, the Φ_F^{max} is nearly similar which suggests that in **$EtNH_2$-SO_2**, PET quenching by N-atom is the only deactivation pathway available and which on being suppressed by TFA, results into Φ_F^{max} similar to that of **Me-SO_2**. If the argument that only PET quenching is present had been extended to **$EtNH_2$**, Φ_F^{max} of 0.01 would have been expected after the addition of TFA. However, Φ_F^{max} is 18 fold more than the expected.

Table 3.4: *TFA titrations of **Me**, **$EtNH_2$** and sulfone derivatives in ACN.*

Compound	Φ_F[a]	$\Phi_F^{max} = \Phi_F * (I/I_o)_{TFA}$
Me	0.01	0.01
Me-SO_2	0.41	0.41
$EtNH_2$	0.006	0.18
$EtNH_2$-SO_2	0.10	0.49

[a] *Absolute quantum yield (without degassing).*

This result strongly demonstrates that suppression of deactivation pathway associated with sulfoxide is the prevalent factor for the fluorescence enhancement upon TFA titration. In an analogy, it should be equally implied for the fluorescence enhancement of targets **1a-d** with various metal ions.

3.5 Targets with no N-atom

Previously, in **Section 3.3** we encountered PET as an additional deactivation pathway present along with the one associated with sulfoxides, in our target molecules containing N-atom at β position to the sulfoxide. We demonstrated in **Section 3.4** that the large enhancements in fluorescence emission on metal ion coordination could only be achieved by suppressing the sulfoxide deactivation pathway. However, PET, though only to a small extent, acts as a disturbance to the response from sulfoxide against various metal ions. In order to eliminate the PET deactivation pathway, targets without any N-atom in the receptor units were designed as illustrated in ***Figure 3.7***.

Figure 3.7: *Targets with crown ether.*

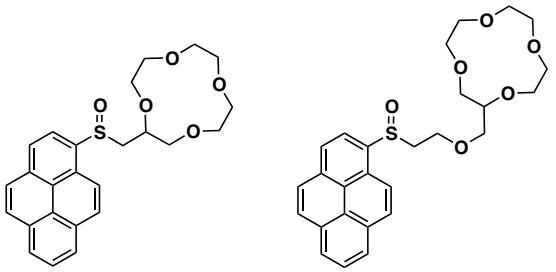

3.5.1 Synthesis of targets with crown receptors

Synthesis of both targets containing crown receptors (***Figure 3.7***) required tosylated crown ether **64** as a precursor. 2-Hydroxymethyl-12-crown-4 (**63**) was treated with tosyl chloride and transformed to the required tosylate derivative **64** in 78% yield *(**Scheme 3.7**)*.[111]

Scheme 3.7: *Synthesis of crown precursor **64**.*

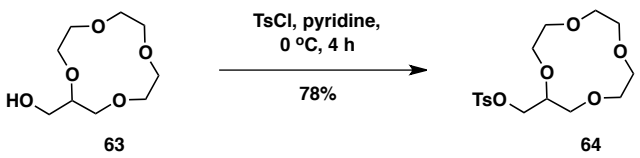

The crown ether appended sulfoxide **Crown-O_4** was synthesized from 1-bromopyrene in two steps as outlined in ***Scheme 3.8***. Lithium-halogen exchange on 1-bromopyrene **52** followed by quenching with S_8 resulted *insitu* generation of the corresponding pyrenyl thiolate.[100] Addition of the crown ether tosylate **64** gave sulfide **65** in an overall yield of 67%. **65** was oxidized using mCPBA, as described in previous sections. The sulfoxide **Crown-O_4** was obtained in 87% yield from sulfide **65** as diastereomeric mixture.

Scheme 3.8: *Synthesis of* ***Crown-O_4.***

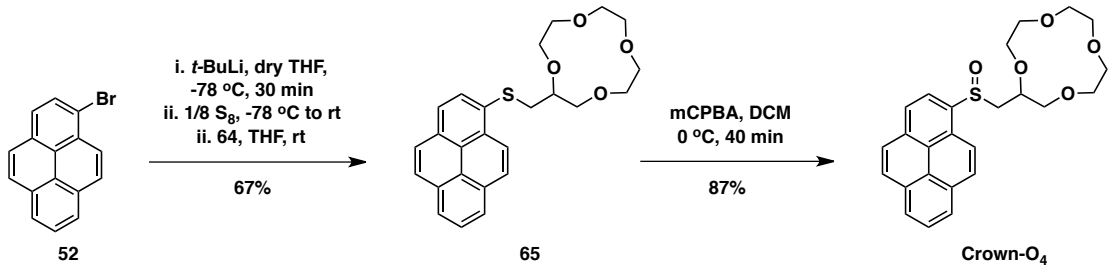

The synthesis of fluorophore **Crown-O_5** was achieved from the already synthesized precursor, 2-hydroxyethylpyrenyl sulfide **59,** in two steps as illustrated in ***Scheme 3.9***. The hydroxyl group in **59** was deprotonated with NaH under dry conditions. The nucleophile, thus generated, was reacted with the electrophilic tosylate crown ether **64** to furnish sulfide **66** in 40% yield.[112]

Scheme 3.9: *Synthesis of* ***Crown-O_5.***

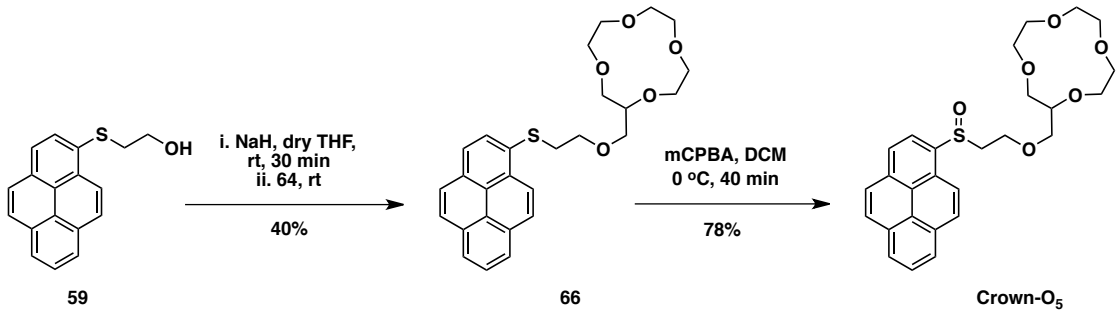

The competing elimination reaction in crown tosylate **64** resulted in very low yield of the sulfide **66**. The *m/z* peak for corresponding alkene product was observed in LCMS. The sulfide **66** was finally oxidized in 78% yield to the diastereomeric mixture of sulfoxide **Crown-O_5**.

3.5.2 Photophysical properties of targets with crown receptors

The longest excitation and emission wavelength for both targets remain similar. No big changes were observed in the extinction coefficients as well. A surprisingly high Φ_F was obtained for **Crown-O$_5$**, which is difficult to explain.

Table 3.5: *Spectroscopic data of crown appended targets.*

Compound	λ_{ex} [a,b]	λ_{em} [a,b]	ε [c]	Φ_F [d]
Crown-O$_4$	349	378	27.5	0.015
Crown-O$_5$	350	378	28.3	0.035

Measurements done in ACN. [a]Excitation/emission spectra acquired at 10^{-5} M. [b]Longest λ excitation/emission maxima. [c]10^3 M^{-1} cm^{-1}. [d]Absolute quantum yields.

3.5.3 Metal ion titrations of targets with crown receptors

In general the binding affinity for Zn^{2+} was found to be much weaker than that for any other target appended with N-atom containing receptor unit. Ca^{2+} ion shows a very selective and high affinity binding among all the I and II group metal ions (***Table 3.6***). The persistence of high binding affinity of these molecules for

Table: 3.6: *log K_d (I/I_o); 5 x 10^{-7} M Crown targets in ACN (for details see* ***Section 2.6.2****).*

M^{n+}	Crown-O$_4$	Crown-O$_5$
Li^+	-2.1 (5)	-4.0 (9)
Na^+	-2.5 (3)	-3.0 (4)
Mg^{2+}	-3.6 (27)	-4.6 (19)
Ca^{2+}	-5.7 (27)	-5.9 (20)
Zn^{2+}	-1.9 (26)	-2.3 (20)

Ca^{2+} ions (log K_d = -5.7 to -5.9) as with DiPic (log K_d = -5.9) suggests that N-atom is not the prerequisite for developing fluorescent chemosensor based on

sulfoxide as reporting element. No fluorescence response was observed on treating 0.5 μM **Crown-O$_4$** in 90% ACN:H_2O with up to 10^5 equivalents of TFA. This aspect of these molecules shows extremely high tolerance against pH sensitivity and promises excellent prospects for functioning under physiological conditions. Introduction of an extra O-atom (*i.e.*, **Crown-O$_5$** *vs.* **Crown-O$_4$**), primarily, raises the binding affinity for all the metal ions, however, impact is greater for Li^+ and Mg^{2+}. Job's plot of **Crown-O$_4$** with Ca^{2+} demonstrates the Metal:Ligand stoichiometery to be 1:1 (***Appendix III***).

3.6 Functioning of sulfoxide based fluorescent chemosensor under physiological conditions

In order to have a potential application of sulfoxide based fluorescent chemosensor system, their ability to function under physiological conditions is essential. To determine how our sulfoxide based system copes under these conditions, the response of **DiPic** target against $ZnCl_2$ was analyzed in 10% ACN: aq. MOPS Buffer (5 mM, pH 7.4).

***Figure 3.8: DiPic** vs $ZnCl_2$ in 10% ACN: aq. MOPS buffer.*

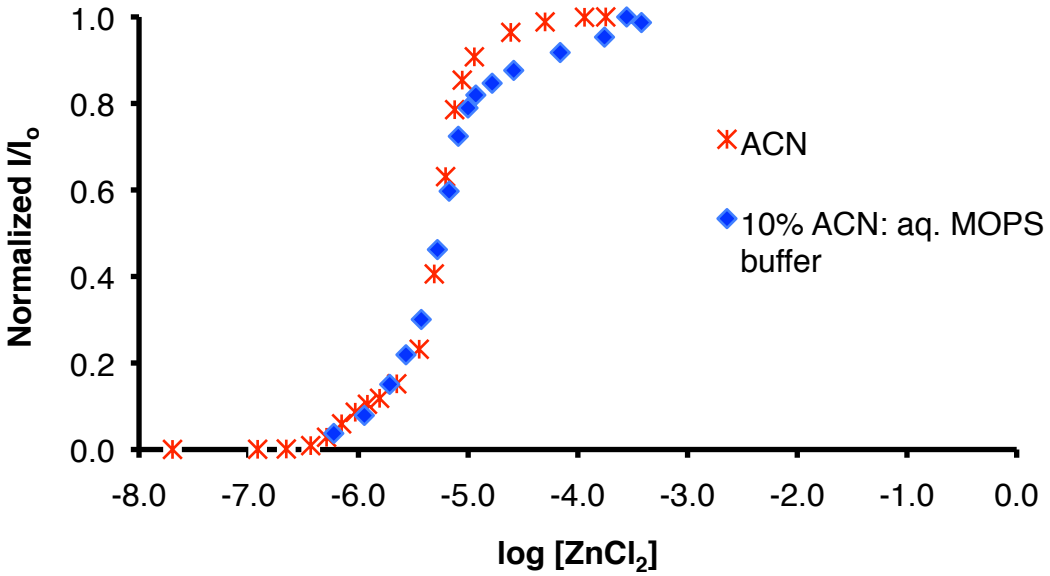

It can be learnt from ***Figure 3.8*** that not much change in the binding affinity (*ca.* log K_d = -5.3) was observed on switching from organic solvent to the

aq. buffer system. 13 fold gain in the fluorescence emission (intrinsic Φ_F = 0.025) was observed with the addition of 1.5 eq. $ZnCl_2$.[113] This result shows the viability of exploiting sulfoxide as the novel response element for further fluorescent chemosensor development for metal ions in the years to come.

3.7 Conclusion

Variation of recognition moiety by modifying **NH_2** end in **$EtNH_2$** with picolyl and azacrown were shown to increase the binding affinity for Li^+ and Na^+ ions. In one case, **AC-NO_3** *vs.* Mg^{2+}, binding in the sub-nM range was established as the maximum for our current system. The N-atom at the β position from sulfoxide of the targets are involved in PET and, therefore, suppression of PET and sulfoxide deactivation, in conjunction, results in large fluorescence enhancements. However, it was established that suppression of sulfoxide deactivation was the prevalent mechanism for the high gains in the fluorescence emission.

Analysis of targets with no N-atom, stressed the fact that acid tolerant and yet stronger binding responsive chemosensor could be afforded with such an approach. Titration of **DiPic** with $ZnCl_2$ in 10% ACN: aq. MOPS buffer unfolds the remarkable potential of sulfoxide as response element for further advancement of fluorescent chemosensor for metal ions under physiological conditions.

Discovery of any practical application of sulfoxide as response element for fluorescent chemosensing will strongly rely on fluorophores with longer excitation and emission wavelengths. Moreover, the selection of an appropriate fluorophore requires a deeper understanding of the photophysics of an aromatic sulfoxide first and, therefore, the next Chapter will specifically shed some light on this problem.

3.8 Experimental procedure

3.8.1 Synthetic details and tabulated spectroscopic data

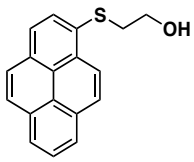

59:[103] To KOH (195.0 mg, 3.475 mmol, 2.0 eq) in dry DMF (6 mL) under N_2, 2-thioethanol (273.6 mg, 3.501 mmol, 2.0 eq) was added. The resulting mixture was stirred at rt until KOH disappeared which was followed by dropwise addition of **52** (493.0 mg, 1.753 mmol, 1 eq) in dry DMF (7 mL). The resulting solution was stirred at 110 ^oC for 1 h. The reaction mixture was cooled to rt, diluted with diethyl ether (50 mL) and washed with brine (2x40 mL). The organic layers were dried over $MgSO_4$ and evaporated. Purification by column chromatography (silica gel; DCM) gave **59** (437.1 mg, 90%).

R_f: 0.43 (silica gel TLC; 5% EtOAc:DCM)

^{1}H-NMR (300 MHz; $CDCl_3$), δ: 8.74 (d, *J* = 9.3 Hz, 1H), 8.24-8.10 (m, 5H), 8.07-8.01 (m, 3H), 3.72 (t, *J* = 5.9 Hz, 2H), 3.27 (t, *J* = 5.9 Hz, 2H).

^{13}C-NMR (125 MHz; $CDCl_3$), δ: 132.2, 131.5, 131.2, 131.1, 130.8, 129.1, 128.6, 128.1, 127.4, 126.5, 125.7, 125.7, 125.5, 125.1, 124.7, 124.7, 60.8, 39.2.

IR(neat), cm^{-1}: 3356 (s), 3039 (m), 2922 (w), 1593 (m), 1046 (s), 1029 (s), 841 (vs).

HRMS-ESI(+): Calculated for $C_{18}H_{14}NaOS$ $[M+Na]^+$ 301.06576; found 301.06579.

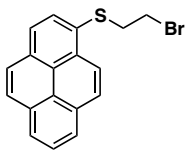

60: To a solution of **59** (437.1 mg, 1.572 mmol, 1 eq) and CBr_4 (627.4 mg, 1.891 mmol, 1.2 eq) in dry DCM (10 mL), PPh_3 (494.1 g, 1.884 mmol, 1.2 eq) was added. The resulting solution was stirred for 3 h at rt. The solvent was evaporated and the crude residue was purified by column chromatography (silica gel; hexane) to give **60** (396.0 mg, 74%).

R_f: 0.14 (silica gel TLC; hexane).

^{1}H-NMR (500 MHz; Aceton-d_6), δ: 8.74 (d, *J* = 9.2 Hz, 1H), 8.35-8.27 (m, 5H), 8.19 (q, *J* = 9.7 Hz, 2H), 8.11 (t, *J* = 7.6 Hz, 1H), 3.62-3.55 (m, 4H).

^{13}C-NMR (125 MHz; Acetone-d_6), δ: 132.72, 132.34, 132.11, 131.93, 131.53, 129.62, 129.32, 128.9, 128.22, 127.52, 126.66, 126.61, 126.18, 126.04, 125.23, 125.22, 38.32, 31.38.

IR(neat), cm^{-1}: 3039 (w), 2918 (w), 1504 (m), 1190 (w), 842 (vs).

HRMS-EI(+): Calculated for $C_{18}H_{13}BrS$ $[M]^+$ 339.99158; found 339.99172.

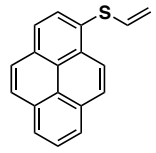

61: To a solution of **60** (205.3 mg, 601.6 μmol, 1 eq) in THF:EtOH (2:3; 3 mL), KOH (38.1 mg, 0.679 mmol, 1.1eq) was added. The resulting mixture was refluxed for 1 h, cooled to rt, diluted with DCM (20 mL) and washed with brine (2x10 mL). The combined aq. layers were washed with DCM (20 mL). The combined organic layers were dried over $MgSO_4$, evaporated and purified by column chromatography (silica gel; hexane) to give **61** (136.0 mg, 87%).

R_f: 0.25 (silica gel TLC; hexane).

^{1}H-NMR (400 MHz; $CDCl_3$), δ: 8.59 (d, *J* = 9.2 Hz, 1H), 8.23-8.02 (m, 8H), 6.64 (dd, *J* = 16.5, 9.6 Hz, 1H), 5.32 (d, *J* = 9.6 Hz, 1H), 5.10 (d, *J* = 16.5 Hz, 1H).

^{13}C-NMR (100 MHz; $CDCl_3$), δ: 132.8, 132.1, 131.7, 131.5, 131.5, 131.2, 128.6, 128.3, 127.5, 127.4, 126.5, 125.8, 125.8, 125.5, 125.3, 124.9, 124.7, 114.2.

IR(neat), cm^{-1}: 3040 (m), 1583 (s), 1178 (w), 1027 (w), 954 (m), 841 (vs).

HRMS-EI(+): Calculated for $C_{18}H_{12}S$ $[M]^+$ 260.06542; found 260.06518.

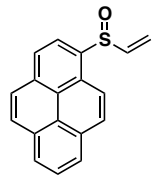

58: To a solution of **61** (223.1 mg, 856.5 μmol, 1 eq) in DCM (40 mL), mCPBA (190.0 mg, 70% assay, 770.7 μmol, 0.9 eq) was added at 0 ^oC. The resulting solution was stirred for 40 min and then washed with saturated aq. $NaHCO_3$ (20 mL). The organic layer was dried over $MgSO_4$ and evaporated. Purification by column chromatography (silica gel; 10% EtOAc:DCM) gave **58** (223.6 mg, 97%).

R_f: 0.28 (Silica gel TLC; 10% EtOAc: DCM).

^{1}H-NMR (400 MHz; $CDCl_3$), δ: 8.49 (d, *J* = 8.1 Hz, 1H), 8.43 (d, *J* = 9.2 Hz, 1H), 8.33 (d, *J* = 8.1 Hz, 1H), 8.28 (d, *J* = 7.6 Hz, 2H), 8.23-8.06 (m, 4H), 6.78 (dd, *J* = 16.4, 9.6 Hz, 1H), 6.35 (dd, *J* = 16.4, 0.4 Hz, 1H), 5.89 (dd, *J* = 9.6, 0.4 Hz, 1H).

^{13}C-NMR (125 MHz; $CDCl_3$), δ: 142.5, 135.6, 133.5, 131.4, 130.6, 129.6, 129.5, 128.3, 127.5, 126.9, 126.7, 126.6, 125.9, 124.8, 124.5, 121.9, 121.0, 120.3.
IR(neat), cm^{-1}: 3043 (m), 1591 (m), 1191 (m), 1061 (vs), 952 (m), 846 (vs).
HRMS-ESI(+): Calculated for $C_{18}H_{12}NaOS$ $[M+Na]^+$ 299.05011; found 299.04999.

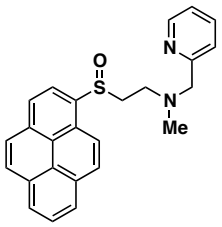

MePic: To a solution of **58** (26.7 mg, 9.67 μmol, 1 eq) in MeOH (1.2 mL), methylpicolylamine (27.9 mg, 0.228 mmol, 2.0 eq) was added. The resulting reaction mixture was stirred at 60 °C for 1 day. After cooling to rt and evaporating solvent, the crude residue was dissolved in DCM (2 mL) and Boc_2O (42.7 mg, 0.196 mmol, 2.0 eq) added. The resulting mixture was stirred for 3 h. The solvent was evaporated and the crude residue purified by column chromatography (silica gel; 5% MeOH:DCM) to give **MePic** (34.4 mg, 89 %).
R_f: 0.18 (silica gel TLC; 5% MeOH:DCM).
^{1}H-NMR (400 MHz; $CDCl_3$), δ: 8.62 (d, *J* = 8.1 Hz, 1H), 8.45 (d, *J* = 4.2 Hz, 1H), 8.34 (d, *J* = 8.1 Hz, 1H), 8.28-8.24 (m, 3H), 8.18-8.05 (m, 4H), 7.54 (td, *J* = 7.6, 1.7 Hz, 1H), 7.41 (d, *J* = 7.8 Hz, 1H), 7.06 (dd, *J* = 6.6, 5.3 Hz, 1H), 3.74-3.66 (m, 2H), 3.32-3.23 (m, 1H), 3.16-3.08 (m, 2H), 2.74 (t, *J* = 7.7 Hz, 1H), 2.32 (s, 3H).
^{13}C-NMR (100 MHz; $CDCl_3$), δ: 158.9, 149.2, 136.79, 136.61, 133.2, 131.3, 130.6, 129.29, 129.13, 127.65, 127.50, 126.77, 126.60, 126.43, 125.6, 124.59, 124.55, 123.1, 122.2, 121.5, 120.7, 63.7, 55.5, 50.8, 42.6.
IR(neat), cm^{-1}: 3046 (m), 2795 (m), 1589 (s), 1569 (m), 1458 (s), 1433 (s), 1190 (m), 1049 (vs), 849 (vs), 758 (s).
HRMS-ESI(+): Calculated for $C_{25}H_{23}N_2OS$ $[M+H]^+$ 399.15256; found 399.15231.

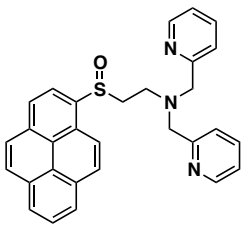

DiPic: To a solution of **58** (54.4 mg, 0.197 mmol, 1 eq) in MeOH (2 mL), 2,2'-dipicolylamine (0.147 g, 0.737 mmol, 3.8 eq) was added. The resulting reaction mixture was stirred at 60 °C for 3 days. After cooling to rt and evaporating solvent, the crude residue was dissolved in DCM (2 mL) and Fmoc-Cl (0.205 mg, 0.795 mmol, 4.0 eq) added. The resulting mixture was stirred for 3 h. The solvent was evaporated and the crude residue purified by column

chromatography (silica gel; 1:2:97 MeOH:TFA:DCM) to give **DiPic** (68.9 mg, 73.6 %).

R_f: 0.18 (silica gel TLC; 1:2:97 MeOH:TEA:DCM).

^{1}H-NMR (300 MHz; CD_2Cl_2), δ: 8.52 (d, *J* = 8.1 Hz, 1H), 8.38 (ddd, *J* = 4.9, 1.7, 0.9 Hz, 2H), 8.31 (dd, *J* = 16.2, 7.6 Hz, 3H), 8.21-8.07 (m, 5H), 7.55 (td, *J* = 7.6, 1.8 Hz, 2H), 7.47 (d, *J* = 7.8 Hz, 2H), 7.05 (ddd, *J* = 7.3, 4.9, 1.3 Hz, 2H), 3.89-3.78 (m, 4H), 3.31 (dt, *J* = 12.6, 7.4 Hz, 1H), 3.18 (dt, *J* = 13.4, 7.1 Hz, 1H), 3.07-2.99 (m, 1H), 2.91-2.83 (m, 1H).

^{13}C-NMR (100 MHz; CD_2Cl_2), δ: 159.5, 149.5, 137.8, 136.8, 133.5, 131.8, 131.0, 129.5, 129.4, 127.9, 127.2, 126.9, 126.8, 125.8, 124.9, 124.9, 123.56, 122.5, 121.9, 121.3, 60.7, 55.5, 48.0.

IR(neat), cm^{-1}: 3047 (w), 2918 (w), 2824 (w), 1589 (s), 1474 (m), 1432 (m), 1190 (w), 1048 (s), 849 (vs).

HRMS-ESI(+): Calculated for $C_{30}H_{26}N_3OS$ $[M+H]^+$ 476.17911; found 476.17863.

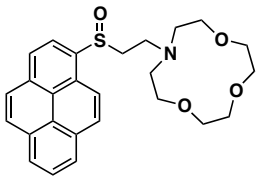

AC-NO_3: To solution of **58** (10.6 mg, 38.4 μmol, 1 eq) in MeOH (1.2 mL), 1-aza-12-crown-4 (75.8 mg, 0.432 mmol, 11.4 eq) was added. The resulting reaction mixture was stirred at 70 °C for 3 days. After cooling to rt and evaporating solvent, the crude residue was dissolved in DCM (3 mL) and Fmoc-Cl (0.118 g, 0.457 mmol, 12.0 eq) was added. The resulting solution was stirred for 3 h. The solvent was evaporated and purified by column chromatography (silica gel; 5% MeOH:DCM) to give **AC-NO_3** (15.9 mg, 92%).

R_f: 0.11 (silica gel TLC; 5% MeOH:DCM).

^{1}H-NMR (400 MHz; $CDCl_3$), δ: 8.64 (d, *J* = 8.1 Hz, 1H), 8.39 (d, *J* = 3.1 Hz, 1H), 8.37 (d, *J* = 2.0 Hz, 1H), 8.29-8.26 (m, 2H), 8.21-8.06 (m, 4H), 3.81-3.65 (m, 12H), 3.29-3.20 (m, 2H), 2.97-2.77 (m, 4H), 2.70-2.64 (m, 2H).

^{13}C-NMR (125 MHz; $CDCl_3$), δ: 137.2, 133.2, 131.4, 130.7, 129.3, 129.1, 127.6, 127.6, 126.8, 126.6, 126.4, 125.7, 124.7, 124.6, 121.4, 121.1, 71.7, 70.8, 70.3, 56.0, 55.9, 49.8.

IR(neat), cm^{-1}: 3045 (w), 2918 (m), 2815 (m), 1588 (m) 1359 (m), 1131 (s), 1045 (s), 850 (vs).

HRMS-ESI(+): Calculated for $C_{26}H_{30}NO_4S$ $[M+H]^+$ 452.18901; found 452.18950 .

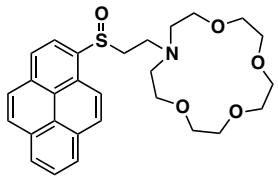

AC-NO$_4$: To solution of **58** (15.5 mg, 56.1 μmol, 1 eq) in MeOH (1.2 mL), 1-aza-15-crown-5 (80.1 mg, 0.365 mmol, 6.5 eq) was added. The resulting reaction mixture was stirred at 70 °C for 3 days. After cooling to rt and evaporating solvent, the crude residue was dissolved in DCM (2 mL) and Fmoc-Cl (0.110 g, 0.427 mmol, 7.0 eq) was added. The resulting solution was stirred for 3 h. The solvent was evaporated and purified by column chromatography (5% deactivated alumina; 2% MeOH:DCM) to give **AC-NO$_4$** (25.6 mg, 92%).

R$_f$: 0.19 (alumina TLC; 2% MeOH:DCM).

^{1}H-NMR (500 MHz; $CDCl_3$), δ: 8.62 (d, *J* = 8.1 Hz, 1H), 8.36 (d, *J* = 8.1 Hz, 1H), 8.30 (d, *J* = 9.1 Hz, 1H), 8.27 (dd, *J* = 7.6, 2.8 Hz, 2H), 8.20-8.06 (m, 4H), 3.69-3.60 (m, 16H), 3.25-3.17 (m, 2H), 3.04-2.99 (m, 1H), 2.89-2.72 (m, 5H).

^{13}C-NMR (126 MHz; $CDCl_3$), δ: 13-C NMR (126 MHz; CDCl3): δ 137.0, 133.2, 131.4, 130.6, 129.3, 129.1, 127.63, 127.53, 126.8, 126.57, 126.44, 125.6, 124.63, 124.58, 121.5, 121.0, 71.2, 70.6, 70.4, 70.2, 55.9, 55.0, 49.9.

IR(neat), cm^{-1}: 3046 (m), 2956 (m), 2855 (s), 1588 (m), 1455 (s), 1353 (s), 1123 (vs), 1046 (s), 935 (m), 851 (vs), 716 (s).

HRMS-ESI(+): Calculated for $C_{28}H_{33}NNaO_5S$ $[M+Na]^+$ 518.19716 found 518.19715.

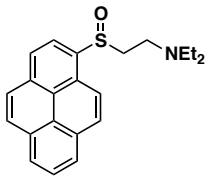

EtNEt$_2$: To solution of **58** (17.0 mg, 61.5 μmol, 1 eq) in MeOH (1.2 mL), diethyl amine (20.0 μL, 0.193 mmol, 3.1 eq) was added. The resulting reaction mixture was stirred at 60 °C for 1 day. After cooling to rt, reaction mixture was diluted with 15 mL DCM and washed with brine. The organic layer collected, evaporated and purified by column chromatography (silica gel; 5% MeOH:DCM) to give **EtNEt$_2$** (18.0 mg, 84%).

R$_f$: 0.19 (silica gel TLC; 5% MeOH:DCM).

^{1}H-NMR (500 MHz; $CDCl_3$), δ: 8.63 (d, *J* = 8.1 Hz, 1H), 8.36 (d, *J* = 8.1 Hz, 1H), 8.29-8.25 (m, 3H), 8.19-8.06 (m, 4H), 3.21-3.11 (m, 2H), 3.05-3.01 (m, 1H), 2.78-2.71 (m, 1H), 2.62-2.49 (m, 4H), 1.02 (t, *J* = 7.1 Hz, 6H).

^{13}C-NMR (125 MHz; $CDCl_3$), δ: 137.1, 133.2, 131.4, 130.6, 129.24, 129.12, 127.61, 127.54, 126.78, 126.59, 126.43, 125.6, 124.63, 124.58, 121.5, 120.9, 55.9, 47.1, 46.5.

IR(KBr), cm^{-1}: 2969 (s), 2813 (m), 1590 (s), 1382 (m), 1301 (s), 1195 (s), 1154 (s), 1127 (vs), 1028 (s), 849 (vs), 712 (s).

HRMS-ESI(+): Calculated for $C_{22}H_{24}NOS$ $[M+H]^+$ 350.15731; found 350.15727.

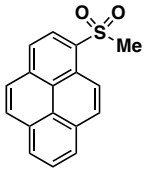

Me-SO$_2$: To a solution of **53** (59.5 mg, 0.239 mmol, 1 eq) in DCM (5 mL), mCPBA (129.9 mg, 70% assay, 526.9 μmol, 2.2 eq) was added at 0 °C. The resulting solution was stirred for 40 min at rt, diluted with DCM (20 mL) and then washed with saturated aq. $NaHCO_3$ (10 mL). The organic layer was dried over $MgSO_4$ and evaporated. Purification by column chromatography (silica gel; 25% EtOAc:DCM) gave **Me-SO$_2$** (57.9 mg, 86%).

R_f: 0.36 (silica gel TLC; 25% EtOAc:DCM)

^{1}H-NMR (500 MHz; $CDCl_3$), δ: 9.05 (d, *J* = 9.4 Hz, 1H), 8.74 (d, *J* = 8.2 Hz, 1H), 8.35-8.31 (m, 3H), 8.25 (dd, *J* = 11.7, 8.6 Hz, 2H), 8.14-8.10 (m, 2H), 3.31 (s, 3H).

^{13}C-NMR (125 MHz; $CDCl_3$), δ: 135.7, 131.9, 131.1, 130.9, 130.2, 129.0, 127.49, 127.34, 127.25, 127.15, 127.05, 125.3, 124.4, 124.2, 122.7, 45.1.

IR(KBr), cm^{-1}: 2927 (w), 1587 (s), 1296 (vs), 1192 (s), 1154 (s), 1129 (vs), 948 (m), 848 (vs), 759 (s), 714 (s).

HRMS-ESI(+): Calculated for $C_{17}H_{12}NaO_2S$ $[M+Na]^+$ 303.04502; found 303.04498.

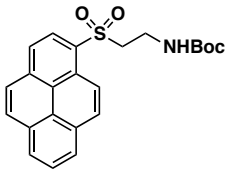

62: To a solution of **56** (21.0 mg, 53.4 μmol, 1 eq) in DCM (1 mL), mCPBA (13.9 mg, 70% assay, 56.4 μmol, 1.05 eq) was added at 0 °C. The resulting solution was stirred for 40 min, diluted with DCM (20 mL) and then washed with saturated aq. $NaHCO_3$ (10 mL).

The organic layer was dried over $MgSO_4$ and evaporated. Purification by column chromatography (silica gel; 5% EtOAc:DCM) gave **62** (18.7 mg, 86%).

R_f: 0.18 (silica gel TLC; 5% EtOAc:DCM).

^{1}H-NMR (500 MHz; $CDCl_3$), δ: 8.99 (d, *J* = 9.4 Hz, 1H), 8.69 (d, *J* = 8.2 Hz, 1H), 8.34-8.31 (m, 3H), 8.24 (t, *J* = 8.2 Hz, 2H), 8.14-8.09 (m, 2H), 5.07 (s, 1H), 3.61-3.57 (m, 4H), 1.24 (s, 9H).

^{13}C-NMR (125 MHz; $CDCl_3$), δ: 155.6, 135.9, 131.13, 131.10, 131.08, 130.27, 130.22, 129.3, 127.63, 127.51, 127.23, 127.21, 125.4, 124.4, 124.2, 122.5, 79.9, 56.5, 35.2, 28.3.

IR(KBr), cm^{-1}: 3382 (s), 2977 (m), 1711 (vs), 1590 (s), 1511 (s), 1366 (s), 1296 (s), 1249 (s), 1165 (s), 1124 (s), 850 (vs), 704 (s).

HRMS-ESI(+): Calculated for $C_{23}H_{23}NNaO_4S$ $[M+Na]^+$ 432.12400; found 432.12417.

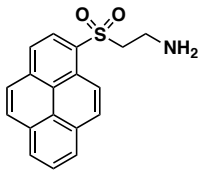

<u>$EtNH_2$-SO_2</u>: To a solution of **62** (18.7 mg, 45.6 μmol, 1 eq) in DCM (0.9 mL), TFA (0.09 mL, 11.7 mmol, 25.0 eq) was added at rt and stirred for 4 h. The reaction mixture was diluted with DCM (20 mL) and washed with aq. NaOH (pH 12; 10 mL). The aq. layer was again washed with DCM (10 mL) and the combined organic layers were dried over Na_2SO_4 and evaporated. Purification by column chromatography (silica gel; 10% MeOH:DCM) gave **$EtNH_2$-SO_2** (11.2 mg, 79%).

R_f: 0.38 (silica gel TLC; 10% MeOH:DCM).

^{1}H-NMR (500 MHz; $CDCl_3$), δ: 9.07 (d, *J* = 9.4 Hz, 1H), 8.73 (d, *J* = 8.2 Hz, 1H), 8.35 (dt, *J* = 8.3, 3.6 Hz, 3H), 8.28 (t, *J* = 8.5 Hz, 2H), 8.16-8.13 (m, 2H), 3.55 (t, *J* = 6.2 Hz, 2H), 3.15 (t, *J* = 6.2 Hz, 2H).

^{13}C-NMR (100 MHz; CD_2Cl_2), δ: 136.1, 131.5, 131.4, 131.2, 131.1, 130.6, 129.6, 128.1, 127.9, 127.7, 127.62, 127.56, 125.7, 124.8, 124.5, 123.2, 60.4, 37.1.

IR(KBr), cm^{-1}: 3378 (m), 3047 (m), 2918 (s) 1589 (s), 1381 (s), 1297 (vs), 1195 (s), 1124 (vs), 1027 (s), 847(vs) 708 (s).

HRMS-ESI(+): Calculated for $C_{18}H_{16}NO_2S$ $[M+H]^+$ 310.08963; found 310.08976.

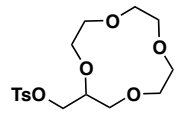

64: To a solution of 2-hydroxymethyl-12-crown-4 (**63**, 297.3 mg, 1.442 mmol, 1 eq) and pyridine (0.60 mL, 7.4 mmol, 5.0 eq) in DCM (50 mL) at 0 ^{o}C under N_2, 4-toluenesulfonyl chloride (552.3 mg, 2.896 mmol, 2.0 eq) was added. The resulting reaction mixture was stirred for 4 h at 0 ^{o}C and washed with 10% aq. HCl (20 mL) followed by 10% aq. NaOH (20 mL). The organic layer was dried over Na_2SO_4, evaporated and the crude residue was purified by column chromatography (silica gel: 5% MeOH: DCM) to give **64** (403.3 mg, 78%).

R_f: 0.42 (silica gel TLC; 5% MeOH:DCM).

^{1}H-NMR (500 MHz; $CDCl_3$), δ: 7.80-7.78 (m, 2H), 7.35-7.33 (m, 2H), 4.05-3.99 (m, 2H), 3.85 (m, 1H), 3.72-3.50 (m, 15H), 2.45 (s, 3H).

^{13}C-NMR (125 MHz; $CDCl_3$), δ: 145.0, 133.6, 130.0, 128.2, 77.4, 71.2, 70.8, 70.7, 70.6, 70.5, 69.9, 21.9.

IR(neat), cm^{-1}: 3062 (w), 2956 (m), 2920 (m), 2867 (m), 1725 (m), 1597 (s), 1448 (s), 1189 (vs),1176 (vs), 1096 (vs), 916 (s).

HRMS-ESI(+): Calculated for $C_{16}H_{24}NaO_7S$ $[M+Na]^+$ 383.11349; found 383.11366

.

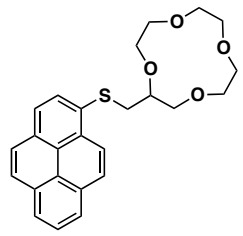

65: To a solution of **52** (384.0 mg, 1.365 mmol, 1.2 eq) in dry THF (3 mL) at -78 ^{o}C under N_2, *t*-BuLi (0.94 mL, 1.5 M in pentane, 1.4 mmol, 1.25 eq) was added dropwise and stirred for 45 min. To the reaction mixture, S_8 (43.7 mg, 1.36 mmol, 1.2 eq) was added and after 15 min the dry ice-acetone bath was removed. The reaction mixture was stirred for another 45 min, followed by addition of solution of **64** (403.2 mg, 1.126 mmol, 1 eq) in dry THF (4 mL). The reaction mixture was stirred overnight at rt, diluted with DCM (20 mL) and washed with brine (2x15 mL). The aq. layers were washed with DCM (2x20 mL). The combined organic layers were dried over Na_2SO_4 and evaporated. Purification by column chromatography (silica gel; 3% MeOH:DCM) gave **65** (252.0 g, 67%).

R_f: 0.20 (silica gel TLC; 3%MeOH:DCM).

^{1}H-NMR (500 MHz; $CDCl_3$), δ: 8.70 (d, *J* = 9.2 Hz, 1H), 8.21-8.00 (m, 8H), 3.87 (dd, *J* = 11.0, 2.6 Hz, 1H), 3.79-3.53 (m, 14H), 3.26 (dd, *J* = 13.5, 6.3 Hz, 1H), 3.15 (dd, *J* = 13.5, 6.4 Hz, 1H).

^{13}C-NMR (125 MHz; $CDCl_3$), δ: 131.6, 131.5, 131.2, 131.0, 129.7, 128.2, 127.8, 127.5, 126.4, 125.5, 125.4, 125.1, 124.7, 78.9, 72.9, 71.1, 71.0, 70.9, 70.8, 70.5, 70.4, 37.5.

IR(neat), cm^{-1}: 3042 (m), 2914 (vs), 2859 (vs), 1592 (s), 1358 (s), 1135 (s), 1028 (m), 918 (m), 845 (vs).

HRMS-ESI(+): Calculated for $C_{25}H_{26}NaO_4S$ $[M+Na]^+$ 445.14440; found 445.14435.

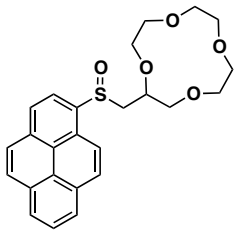

Crown-O_4: To a solution of **65** (252.0 mg, 596.4 μmol, 1.0 eq) in DCM (30 mL), mCPBA (124.3 mg, 77% assay, 720.3 μmol, 0.9 eq) was added at 0 °C. The resulting solution was stirred for 40 min and then washed with saturated aq. $NaHCO_3$ (20 mL). The organic layer was dried over $MgSO_4$ and evaporated. Purification by column chromatography (silica gel; 1% MeOH:DCM) gave **Crown-O_4** (261.5 mg, 87%).

R_f: 0.20 (silica gel TLC; 1% MeOH:DCM).

^{1}H-NMR (400 MHz; diastereomeric mixture; $CDCl_3$), δ: 8.63 (dd, *J* = 8.1, 3.1 Hz), 8.35 (dd, *J* = 8.1, 2.2 Hz), 8.28-8.25 (m), 8.20-8.06 (m), 4.32-4.28 (m), 4.12-3.25 (m), 2.88 (dd, *J* = 13.4, 2.4 Hz).

^{13}C-NMR (100 MHz; diastereomeric mixture; $CDCl_3$), δ: 137.1, 136.4, 133.3, 131.4, 130.7, 130.6, 129.5, 129.4, 129.3, 129.2, 127.8, 127.5, 127.4, 126.8, 126.8, 126.7, 126.6, 126.5, 125.7, 125.6, 124.7, 124.6, 124.5, 121.6, 121.1, 121.0, 120.9, 74.5, 74.1, 72.3, 71.3, 71.2, 71.1, 71.0, 70.9, 70.8, 70.8, 70.7, 70.6, 70.5, 70.5, 69.5, 61.4, 59.2.

IR(KBr), cm^{-1}: 3043 (w), 2917 (m), 2850 (m), 1589 (m), 1299 (w), 1131 (s), 848 (vs).

HRMS-ESI(+): Calculated for $C_{25}H_{26}NaO_5S$ $[M+Na]^+$ 461.13932 ; found 461.13956 .

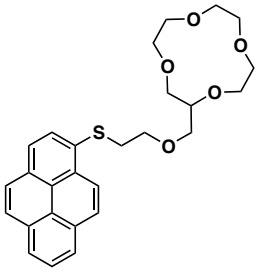

66: A solution of **59** (89.1 mg, 0.320 mmol, 1.5 eq) in dry THF (2 mL), was added to NaH (9.52 mg, 60% dispersion in oil, 0.240 mmol, 1.1 eq) at rt under N_2 atmosphere. The resulting suspension was stirred for 30 min, and followed by the addition of a solution of **64** (78.2 mg, 0.217 mmol, 1 eq) in dry THF (2 mL) at rt. The resulting reaction mixture was stirred at rt for overnight. After dilution with DCM (20 mL), the solution was washed with 20 mL brine. The aqueous layer was washed with DCM (20 mL). The combined organic layer was dried over Na_2SO_4 and evaporated. Purification by column chromatography (silica gel; 70% EtOAc:DCM) gave **66** (35.4 mg, 40%).

R_f: 0.16 (silica gel TLC; 70% EtOAc:DCM).

^{1}H-NMR (500 MHz; $CDCl_3$), δ: 8.72 (d, *J* = 9.2 Hz, 1H), 8.21-8.00 (m, 8H), 3.75-3.73 (m, 1H), 3.67-3.53 (m, 15H), 3.41 (m, 3H), 3.26 (t, *J* = 6.7 Hz, 2H).

^{13}C-NMR (126 MHz; $CDCl_3$), δ: 131.9, 131.5, 131.2, 130.9, 130.5, 130.2, 128.2, 127.8, 127.4, 126.4, 125.54, 125.40, 125.05, 124.89, 124.70, 78.7, 71.7, 71.3, 71.06, 70.86, 70.83, 70.78, 70.55, 70.53, 70.38, 35.4.

IR(KBr), cm^{-1}: 3040 (m), 2956 (m), 2857 (s), 1646 (m), 1592 (s), 1456(s), 1360 (m), 1292 (m), 1135 (s), 1096 (s), 1027 (s), 914 (s), 847 (vs), 714 (s).

HRMS-ESI(+): Calculated for $C_{27}H_{30}NaO_5S$ $[M+Na]^+$ 489.17062; found 489.17130.

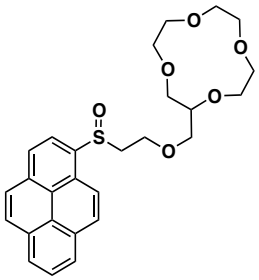

Crown-O_5: To a solution of **66** (35.4 mg, 75.9 μmol, 1 eq) in DCM (3 mL), mCPBA (15.7 mg, 77% assay, 70.0 μmol, 0.9 eq) was added at 0 °C. The resulting solution was stirred for 40 min, diluted with DCM (20 mL) and then washed with saturated aq. $NaHCO_3$ (15 mL). The organic layer was dried over $MgSO_4$ and evaporated. Purification by column chromatography (silica gel; 4% MeOH:DCM) gave **Crown-O_5** (28.6 mg, 78%).

R_f: 0.18 (silica gel TLC; 4% MeOH:DCM).

^{1}H-NMR (300 MHz; diastereomeric mixture; $CDCl_3$), δ: 8.62 (td, *J* = 8.0, 1.2 Hz), 8.39-8.07 (m), 4.07-3.98 (m), 3.85-3.44 (m), 3.34-3.26 (m), 3.22-3.13 (m).

^{13}C-NMR (125 MHz; diastereomeric mixture; $CDCl_3$), δ: 136.4, 136.3, 133.3, 133.3, 131.3, 130.6, 130.5, 129.4, 129.4, 129.2, 129.2, 127.8, 127.7, 127.5, 126.8, 126.6, 126.5, 125.7, 125.6, 124.5, 121.3, 120.8, 120.7, 78.6, 78.5, 71.8, 71.7, 71.6, 71.1, 71.0, 70.9, 70.8, 70.8, 70.5, 70.5, 70.5, 70.3, 64.6, 64.5, 58.1, 57.9.

IR(KBr), cm^{-1}: 3046 (m), 2917 (s), 2856 (s), 1589 (m), 1480 (s), 1306 (m), 1191 (s), 1134 (s), 852 (vs), 715 (s).

HRMS-ESI(+): Calculated for $C_{27}H_{30}NaO_6S$ $[M+Na]^+$ 505.16553; found 505.16486.

Chapter 4

Towards Understanding the Nature of Excited States in Sulfoxide

4.1 Introduction

In the previous Chapters, 2 and 3, we learned that the addition of metal ions enhances Φ_F of alkyl pyrenyl sulfoxide based fluorophores. It was proposed that enhancement in the Φ_F results from the metal coordination assisted suppression of sulfoxide's deactivation/non-radiative decay pathway. Moreover, luminescent properties of aromatic sulfoxides were discussed in ***Section 2.2***, and it was learned that photostereomutation predominantly contributes to the deactivation of aromatic sulfoxides' excited states. However, direct evidence for Φ_F enhancement and concurrent effect on photostereomutation is required to establish the relationship of these ideas. It also needs to be understood how metal coordination leads to higher Φ_F in our sulfoxide-based fluorophores. The present chapter is an effort towards addressing these specific problems.

4.2 Effect of metal coordination on photostereomutation

In order to understand whether photostereomutation is influenced by the metal ion coordination, photoracemization[§] of optically active methyl pyrenyl sulfoxide **(*S*)-Me**, as illustrated in ***Figure 4.1***, was investigated.

Figure 4.1: *Optically active methylpyrenyl sulfoxide.*[a]

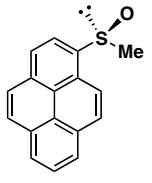

(*S*)-Me

[a] *SO bond depicted as single bond without any polarization for convenience.*

4.2.1 Synthesis of (*S*)-Me

[§] *The use of term photoracemization in place of photostereomutation is appropriate as we deal with enantiomerically enriched* ***(S)-Me****.*

The synthesis of chiral sulfoxide **(*S*)-Me** was accomplished by both vanadium-catalyzed asymmetric oxidation of the corresponding prochiral sulfide and kinetic resolution of a racemic sulfoxide mixture.[114] Both asymmetric transformations required imine based chiral ligand **68**.

Ligand **68** (***Scheme 4.1***) was synthesized from commercially available 3,5-diiodosalicaldehyde **67** and (*S*)-*tert*-leucinol, using the procedure reported by Legros *et al.*[115] 3,5-Diiodosalicaldehyde **67** was mixed with (*S*)-*tert*-leucinol in ethanol and the resulting bright yellow solution was stirred at rt for 16 h. The yellow coloured imine **68** was obtained in 62% yield after recrystallization from cyclohexane.

Scheme 4.1: *Synthesis of chiral ligand* ***68****.*

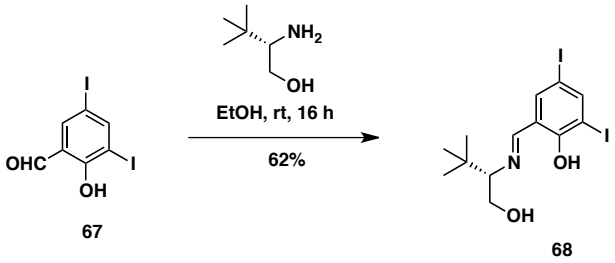

Synthesis of chiral sulfoxide **(*S*)-Me** was accomplished as outlined in ***Scheme 4.2***.[114] The sulfide **53** was oxidized by H_2O_2 in the presence of a chiral catalyst, generated *in situ* from $VO(acac)_2$ and ligand **68**.

Scheme 4.2: *Synthesis of* **(*S*)-Me**.

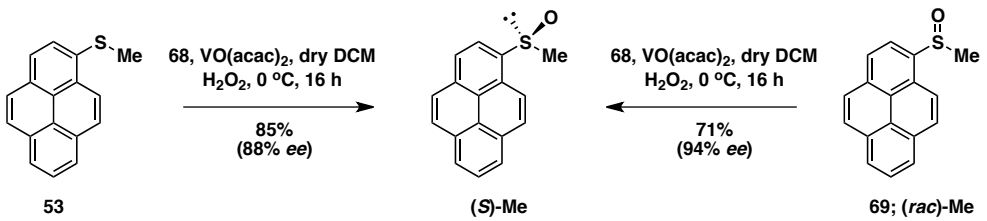

(*S*)-Me was obtained in 85% yield with an enantiomeric excess (*ee*) of 88%. The absolute configuration of sulfoxide was confirmed to be *S* by single crystal XRD (***Appendix IV***). **(*S*)-Me** was also synthesized by kinetic resolution of **69** with H_2O_2

in the presence of the same chiral catalyst. This method furnished **(*S*)-Me** in lower yield (*ca.* 71%), however, better *ee* (*ca.* 94%) was achieved.

4.2.2 Photoracemization of (*S*)-Me -/+ $Mg(ClO_4)_2$

Irradiation of 2.5 mM **(*S*)-Me** in ACN was carried out, with and without $Mg(ClO_4)_2$, in quartz cuvettes. At different time intervals, a small sample was taken out and the enantiomeric composition was determined by HPLC on a chiral column (***Section 4.6.1***). The two enantiomers of **Me** were found to be the major products by HPLC, confirming the absence of any significant side reactions on irradiation.

Figure 4.2: *Photoracemization of* **(*S*)-Me**. *Enantiomeric excess (ee) vs. time plot.*

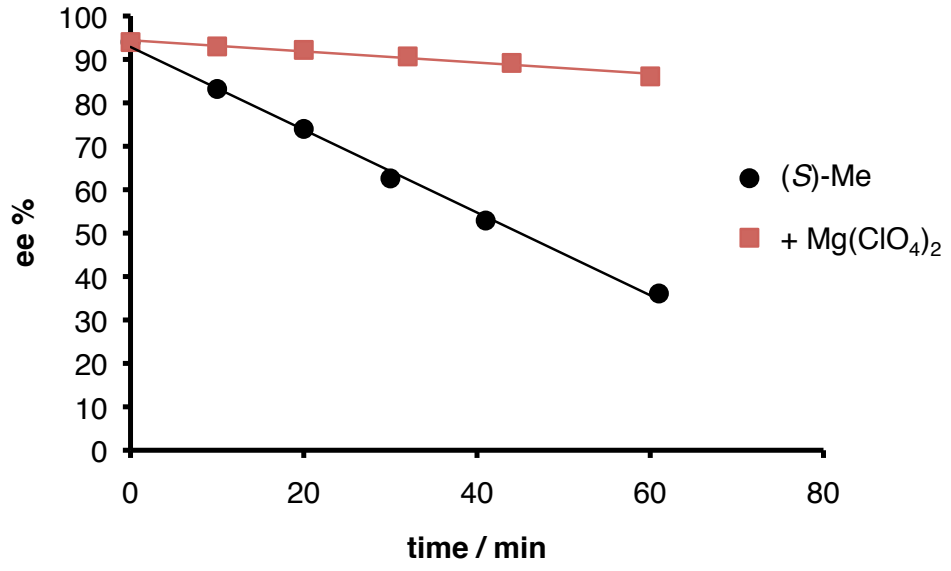

In the absence of Mg^{2+}, the plot (***Figure 4.2***) demonstrates a steep decline in the optical purity of **(*S*)-Me** by irradiation in the time period of 1 h. The addition of Mg^{2+} slows down the photoracemization process, as *ee* does not change significantly over the same period. This experiment explicitly connects the Φ_F enhancement in metal coordination to the suppression of photoracemization (*i.e.*, non-radiative deactivation pathway) in our sulfoxide-based fluorophores.

Having established the connection between Φ_F enhancement and photoracemization's suppression, the next step is to explore how these changes are brought about by metal ion coordination. To answer *'how'*, we first need to understand the nature of excited state in our sulfoxides. Therefore, the next section will focus on sulfoxide excited states.

4.3 Nature of excited state in sulfoxides

The thorough understanding of the excited state can be accomplished by investigating the role of electronic effects on the sulfoxides' spectroscopic properties. To study electronic effects two approaches were followed. The first approach was to make substitution on the pyrene ring of **Me**, as illustrated (**70;** ***Figure 4.3***). For the second approach methyl group was first replaced by phenyl (**71a**; ***Figure 4.3***). This approach was pursued for following reasons: first, electronic variation among alkyl groups is expected to be minimal and second, sulfoxide with phenyl (*i.e.*, **PyS(O)Ph**; ***Section 2.1.5***) also exhibited Φ_F enhancement with metal ion coordination. Then, "the *para* position" of phenyl was substituted with electron withdrawing and donating groups (**71b-c**; ***Figure 4.3***).

Figure 4.3: *Targets for studying electronic effects.*

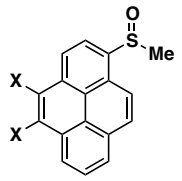

70 ; X = OC_6H_{13}

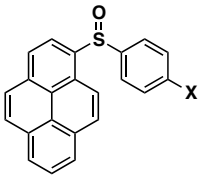

71a; X = H

71b; X = CF_3

71c; X = OCH_3

4.3.1 Synthesis of target 70

The synthesis of **70**, for studying the influence of electron rich pyrene ring on the spectroscopic properties of **Me**, was accomplished in three steps as outlined in ***Scheme 4.3.*** The synthesis of compound **70** began with mono lithium-

halogen exchange on compound **72**[**] by *n*-Buli. The carbanion thus generated was quenched with dimethyl disulfide to give sulfide intermediate **73** in 83% yield. Another lithium-halogen exchange on compound **73** followed by quenching with MeOH provided compound **74** in 93% yield. Partial oxidation of sulfide **74** was carried out with 0.9 eq. mCPBA at 0 °C in DCM, which furnished sulfoxide **70** in 86% yield.

Scheme 4.3: *Synthesis of target **70**.*

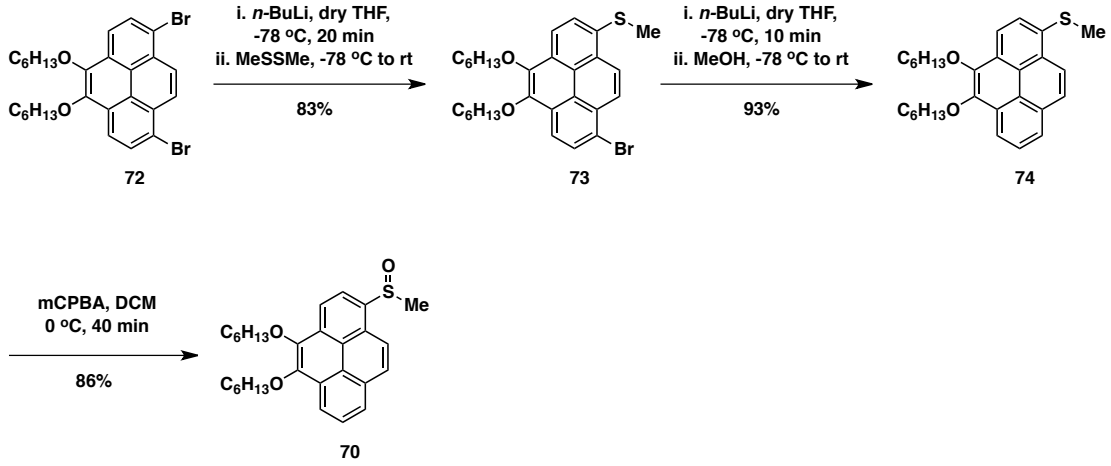

Table 4.1: *Spectroscopic properties of **70** vs. **Me**.*

Compound	λ_{ex} [a,b]	λ_{em} [a,b]	Φ_F [c]
70; X = OC_6H_{13}	356	408	0.429
Me	349	377	0.012

Measurements done in ACN. [a]Excitation/emission spectra acquired at 10^{-5} M or O.D~0.3. [b]Longest λ excitation/emission maxima. [c]Absolute quantum yields.

4.3.2 Photophysical properties of target 70

Fluorophore **70** exhibits a small red shift (*ca.* 7 nm) in longest excitation wavelength in comparison to **Me** (***Table 4.1***). Additionally, a bigger red shift (*ca.* 30 nm) was observed for the longest emission wavelength (***Table 4.1; Appendix***

[**] *We would like to thank Prof. Dr. Graham J. Bodwell, Memorial University of Newfoundland for kindly giving us a gram of compound **72**.*

V). The most dramatic variation was observed in Φ_F of fluorophore **70** (*ca.* 43% vs. 1.2% for **Me**). The implication of this startling enhancement in Φ_F of **70** will be discussed in ***Section 4.4***.

4.3.3 Synthesis of targets 71a-c

The synthesis of various *p*-substituted phenyl pyrenyl sulfoxides **71a-c** (***Figure 4.3***) required appropriate *p*-substituted diphenyl disulfides. Diphenyl disulfide was commercially available, whereas the *p*-OCH_3 and *p*-CF_3 disulfides **76a-b** (***Scheme 4.4***) were synthesized by a procedure reported by Ternay *et al*.[116]

Scheme 4.4: *Synthesis of disulfide precursors* ***76a-b****.*

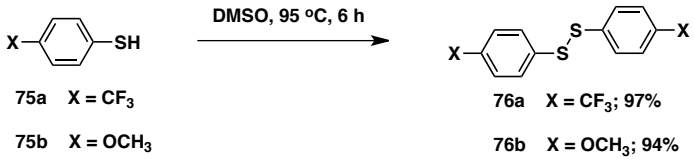

With various *para*-substituted phenyl disulfides now accessible, sulfoxides **71a-c** (***Figure 4.3***) were synthesized as outlined in ***Scheme 4.5***.

Scheme 4.5: *Synthesis of targets* ***71a-c****.*

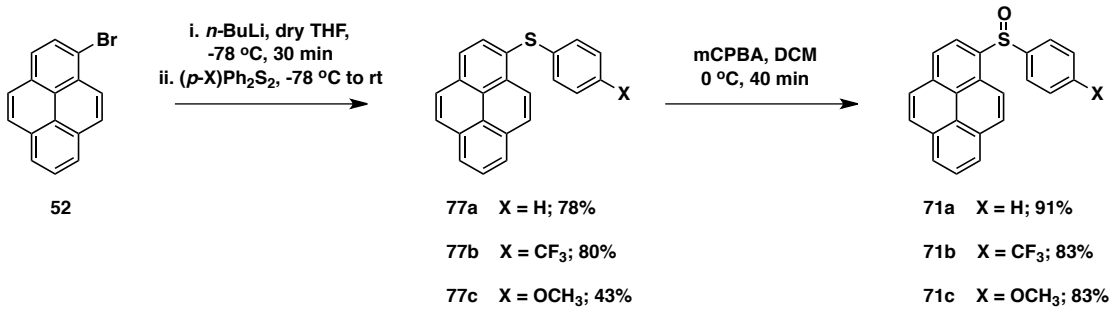

The synthesis began with lithium-halogen exchange on 1-bromopyrene **5** at -78 °C under N_2. The carbanion thus generated was quenched with various *para*-substituted disulfides to give the corresponding phenyl pyrenyl sulfides **77a-c**.

Sulfides **77a-b** were synthesized in good overall yield (*ca.* 80%), whereas only 43% of **77c** was isolated as pure material. Sulfides **77a-c** were oxidized to the corresponding sulfoxides **71a-c** with 0.9 equiv. mCPBA in 80-90% yield.

4.3.4 Spectroscopic properties of 71a-c *vs.* Me

The extinction coefficients remain similar for **71a-c** (***Table 4.2***). Only a few nm (*ca.* < 5nm) of bathochromic shift was observed in the longest λ excitation/emission maxima for **71a-c** in comparison to **Me** (***Table 4.2***; ***Appendix V-VI***). The Φ_F did not change much by replacing methyl with phenyl (**71a** *vs.* **Me**). However, a dramatic variation in Φ_F was observed with changing substituent at *para* in phenylpyrenyl sulfoxides **71a-c**. The Φ_F decreased *ca.* 10 fold when an electron withdrawing *p*-CF_3 group in **71b** was replaced by electron donating *p*-OCH_3 in **71c** (***Table 4.2***).

Table 4.2: *Spectroscopic data of* ***71a-c*** *and* ***Me****.*

Compound	λ_{ex} [a,b]	λ_{em} [a,b]	ε [c]	Φ_F [d]	τ [e]/ns
71a; *p*-H	351	380	35.5	0.011	0.46
71b; *p*-CF_3	352	381	35.9	0.053	1.84
71c; *p*-OCH_3	352	379	39.7	0.006	0.19
Me	349	377	34.2	0.012	1.18

Measurements done in ACN. [a]Excitation/emission spectra acquired at 10^{-5} M. [b]Longest λ excitation/emission maxima. [c]10^3 M^{-1} cm^{-1}. [d]Absolute quantum yields. [e]χ^2 = 0.6-1.3.

The lifetimes, τ, of sulfoxides **71a-c** were measured (***Table 4.2***) and an interesting trend was observed. As seen with Φ_F, τ was observed to have decreased *ca.* 10 fold, when *p*-CF_3 group in **71b** replaced by *p*-OCH_3 group in **71c** (***Table 4.2***) More conclusive information could be acquired from τ by extracting the rate of radiative k_r and all non-radiative processes together k_{nr}. k_r and k_{nr} for a molecule in excited state are related to Φ_F and τ by equations (i) and (ii).

$$(i) \qquad k_r = \Phi_F \times \frac{1}{\tau}$$

$$(ii) \qquad k_{nr} = \frac{1-\tau}{\tau}$$

Sulfoxide **71a** with *p*-H**,** as control, points out that k_{nr} is two orders of magnitude greater than k_r (***Table 4.3***). In sulfoxides **71a-c**, k_r remains almost invariant with change in electronic behavior of the *p*-substituent. However, a striking trend was observed for k_{nr} of sulfoxides **71a-c**. Switching from *p*-CF_3 in **71b** to *p*-OCH_3 in **71c** raises the rate of non-radiative processes nearly by 10 fold. This suggests that on going from electron releasing *p*-OCH_3 to withdrawing *p*-CF_3 substituent, *ca.* 10 fold enhancement in Φ_F is predominantly due to *ca.*10 fold suppression of k_{nr}.

Table 4.3: *k_r and k_{nr} for **71a-c**.*

Compound	Φ_F	τ/ns	$k_r/10^8$ s^{-1}	$k_{nr}/10^8$ s^{-1}
71a; *p*-H	0.011	0.46	0.24	21.5
71b; *p*-CF_3	0.053	1.84	0.29	5.15
71c; *p*-OCH_3	0.006	0.19	0.32	53.7

4.3.5 Proposed model for photostereomutation in 71a-c

Based on fluorescence quantum yield Φ_F and lifetime τ of a series of molecules **71a-c**, a viable model can be proposed for the photostereomutation in these sulfoxides. The proposed qualitative model for photostereomutation in sulfoxide **71a**, with no *p*-substituent, as our control, is illustrated in ***Figure 4.4***. The proposed model relies on the internal charge transfer (ICT) from sulfoxide to the pyrene ring in the excited state. As a result, the sulfur center assumes a radical cationic character. This will be termed "sulfoxide radical cation" for rest of the discussion, although the molecule as a whole remains neutral.

The involvement of a true sulfoxide radical cation, as an intermediate, has been established by Aurisicchio *et al.* for efficient photochemical racemization of optically active methyl aryl sulfoxides.[117,118] DFT calculations, on the optimized pyramidal and planar sulfoxide radical cation, estimated a very low energy barrier (E_a ~ 11 kcal·mol^{-1}) for the pyramidal inversion relative to that for neutral sulfoxide (E_a ~ 40 kcal·mol^{-1}).

Figure 4.4: *Proposed model for* photostereomutation *in* ***71a****.*

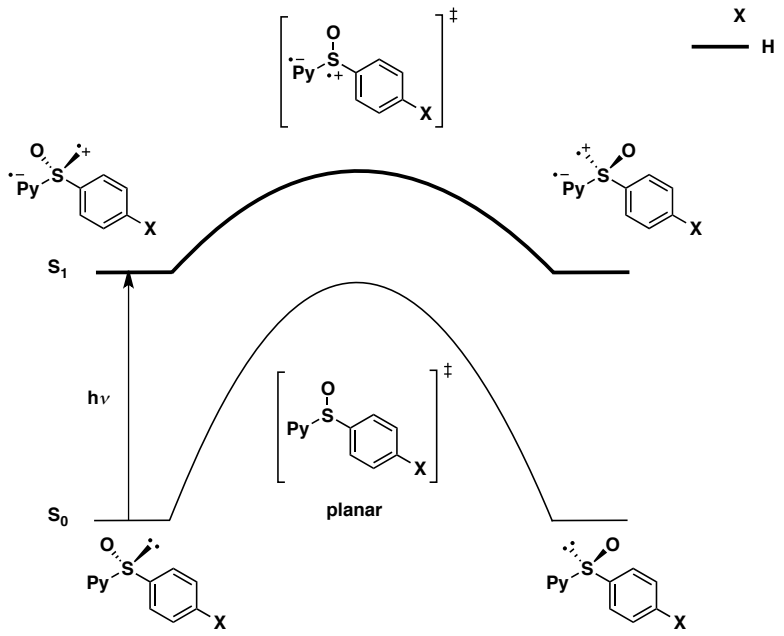

4.3.5.1 Description of excited state in the proposed model for 71a

Firstly, the light black curve in ***Figure 4.4*** qualitatively represents the ground electronic state (S_0) for sulfoxide **71a** with a planar transition state and the high barrier for thermal pyramidal inversion in sulfoxide. We presume that a saddle point with planar geometry lies, as well, on the excited electronic state (S_1) of sulfoxide **71a** (**bold curve**; ***Figure 4.4***). However, because of the sulfoxide radical cationic character in S_1, the requisite energy barrier to reach to the planar geometry in S_1 is much lower than in S_0. As a result, the S_1-S_0 energy gap for planar geometry will be lower than that for pyramidal geometry. Consequently, in accord with energy gap rule, S_1-S_0 rate of internal conversion (IC) would be

higher at planar geometry. Fast IC to S_0 at planar geometry would be followed by the non-radiative return to either of the enantiomers, resulting in fast stereomutation/pyramidal inversion[††].

4.3.5.2 Substituent effect on pyramidal inversion in 71a

The rate of thermal racemization (*i.e.*, racemization from S_0 state), in a related series of optically pure *p*-substituted sulfoxides (**78a-c**; ***Figure 4.5***), varied by a factor less than two.[81] It suggests that the energy barrier for thermal racemization is only slightly altered by electronic effects. However, a significant variation (*ca.* 10 fold) in Φ_F of our sulfoxides **71b-c** (*p*-OCH_3 vs. *p*-CF_3**;** ***Section 4.3.4***) suggests stronger electronic effects dependence of pyramidal inversion in the excited state.

Figure 4.5: *Thermal racemization in series of sulfoxides* ***78a-c*** *studied by Mislow et al.*

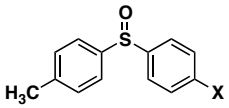

78a; X = H

78b; X = CF_3

78c; X = OCH_3

The best way to perceive the role of electronic effects on the excited state is to understand the extent of their influence on the sulfoxide radical cation in the pyramidal and planar geometries. In the pyramidal geometry, the orbital of sulfur which holds radical cation character would be sp^3 hybridized (**79a; *Figure 4.6***)

Figure 4.6: *Pyramidal and planar sulfoxide radical cation of* ***71a****.*

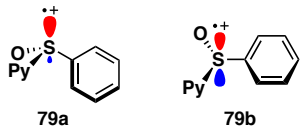

79a **79b**

†† *Pyramidal inversion is more appropriate since it indicates stereomutation without bond breaking/making, and which is in accord with our proposed model. Henceforth, the term pyramidal inversion will be used in place of photostereomutaion as the non-radiative deactivation pathway.*

whereas, in planar geometry this orbital will have a pure p character (**79b; *Figure 4.6***). Because of the p character in **79b**, the interaction of the radical cationic sulfur centre with the π-ring on neighboring phenyl ring would be more efficient. As a result, the substituent on phenyl ring is expected to more strongly influence the planar excited state in comparison to the pyramidal excited state.

Exchanging *p*-H in **71a** with electron withdrawing *p*-CF_3 group in **71b** would destabilize the sulfoxide radical cation (***red curve; Figure 4.7***), whereas replacing *p*-H with electron donating *p*-OCH_3 group in **71c** would lead to stabilization (***green curve; Figure 4.7***). Therefore, the S_1-S_0 energy gap at planar geometry would increase with *p*-substituent as follows:

$$OCH_3 < H < CF_3$$

Figure 4.7: *Proposed model exhibiting electronic effects in* ***71a-c****.*

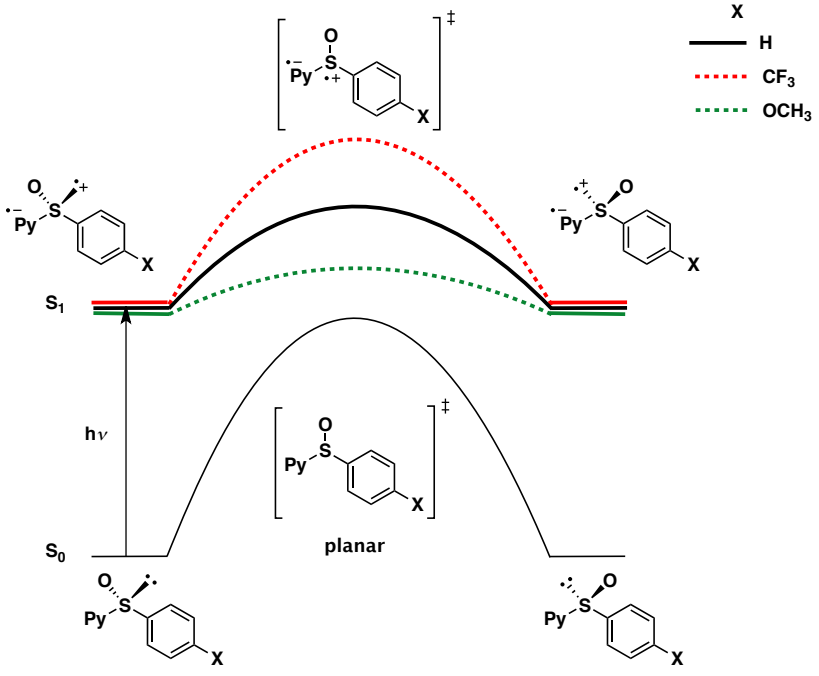

This qualitative trend in S_1-S_0 energy gap at planar geometry suggests that in **71b** (X = CF_3) the rate of internal conversion (IC) and hence, pyramidal inversion will be lower than **71c** (X = OCH_3). Consequently, the Φ_F increases in

71b (X = CF_3) at the expense of suppressed pyramidal inversion (*i.e*, non-radiative deactivation).

4.3.6 Effect of electron rich pyrene in 70 *vs.* Me

In **70** (X = OC_6H_{13}; ***Figure 4.3***), remarkably high Φ_F of 0.43 was observed *vs.* Φ_F of 0.012 for **Me** (***Table 4.1***). The observation can be rationalized by considering that the pyrene ring in **70**, containing two electron donating OC_6H_{13} groups, is very electron rich. The high electron density on pyrene would be resistant to ICT from sulfoxide and hence preclude sulfoxide radical cation formation in the excited state. The energy barrier, as a consequence, to reach planar geometry in the excited state will be higher. This will result in a high S_1-S_0 energy gap at planar geometry, lower rate of IC and pyramidal inversion, and therefore high Φ_F.

The high Φ_F in **70**, thus provides further evidence for the involvement of ICT and sulfoxide radical cation formation in the excited state.

4.4 Origin of connection between metal coordination, Φ_F and photostereomutation

The key points which we derive from our various experiments and analysis of the results are as follows:

- Metal coordination enhances the fluorescence emission and suppresses the photostereomutation in sulfoxides.

- Rate of non-radiative deactivation (*i.e.,* pyramidal inversion) is dependent on the S_1-S_0 energy gap at the planar geometey, which in turn is a function of stability of sulfoxide radical cation in the excited state.

Based on these two key points we can pronounce that metal ion, on coordination to sulfoxide, withdraws the electron density and destabilizes the sulfoxide radical cation (***red curve***; ***Figure 4.8***). The S_1-S_0 energy gap at the planar geometry is raised with destabilization of the sulfoxide radical cation. High S_1-S_0 gap manifests in suppression of the pyramidal inversion of the sulfoxide and consequently enhancement of Φ_F.

Figure 4.8: *Alteration of excited state by metal ion coordination.*

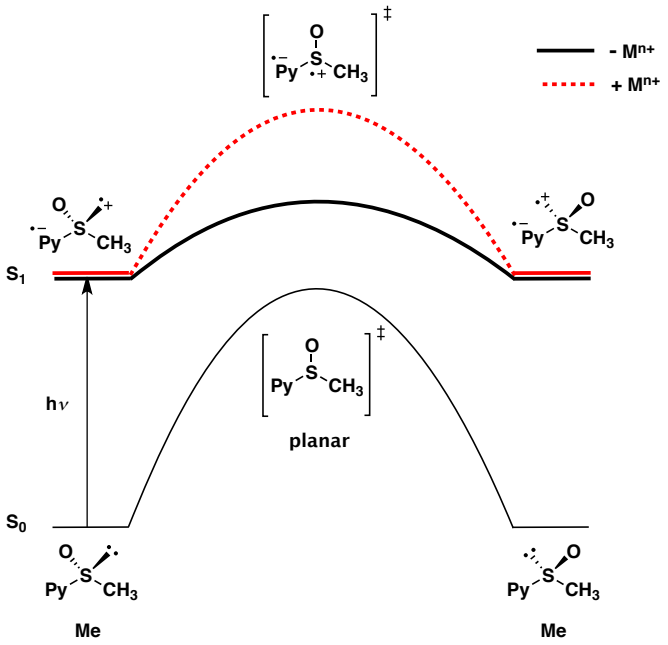

4.5 Conclusion

In the begining of this chapter, it was successfully proved that metal coordination suppresses the photoracemization of **(*S*)-Me** - an enantiomer of control sulfoxide **Me**. The result elegantly underlines the qualitative relation between enhancement of fluorescence emission and suppression in pyramidal inversion - the prominent non-radiative pathway present in 1°-alkyl pyrenyl sulfoxides.

Later, a viable model for nature of excited state of our sulfoxides was proposed. The model assumes the formation of "sulfoxide radical cation" in the

excited state by ICT, which was proved by investigating substituent effect on the spectroscopic properties of control molecule **Me** or its phenyl analog. The proposed model enabled us to explain how exactly metal coordination facilitated fluorescence enhancement is related to the suppresion of pyramidal inversion.

Our investigations of substituent effect, on spectroscopic properties of sulfoxides, certainly empowers us with the knowledge that electron deficient fluorophores with longer excitation/emission wavelengths are the requisite for future fluorescent chemosensor development.

4.6 Experimental part

4.6.1 Photoracemization of (*S*)-Me

In two quartz cuvettes each, 2 mL of 2.5×10^{-3} M **(*S*)-Me** in spectroscopic grade ACN was taken. In one of them, 105 mg (~100 eq.) $Mg(ClO_4)_2$ was added. Both cuvettes were irradiated with 125 W medium pressure UV lamp for 60 min. 150 μL of sample was taken out from the cuvettes at regular intervals of time. The ACN was evaporated and the sample was diluted with isopropyl alcohol (IPA) before injecting into analytical HPLC. For the samples with Mg(II) salt, a small scale extraction was performed thrice with H_2O-EtOAc. The combined EtOAc phase was evaporated and the residue diluted with IPA for HPLC analysis.

HPLC conditions: CHIRALPAK AD-H column (4.6 mm ϕ x 250 mm *l*), 7% IPA:hexane solvent mixture, 1 mL/min flow rate and retention time of two enantiomers are 19.06 and 21.95.

4.6.2 Synthetic details and tabulated spectroscopic data

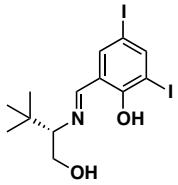

(S)-(-)-2-(*N*-3,5-Diiodosalicyliden) amino-3,3-dimethyl-1-butanol 68:[115] To a solution of (S)-*tert*-leucinol (343.7 mg, 2.933 mmol, 1.0 eq) in EtOH (6 mL), 3,5-diiodosalicylaldehyde (**67**; 1.095 g, 2.928 mmol, 1 eq) was added. The resulting mixture was stirred for 16 h and then solvent evaporated. The residue was recrystallized from cyclohexane to give yellow needle shaped crystals of **68** (853.4 mg, 62 %)

^{1}H-NMR (300 MHz; $CDCl_3$), δ: 14.79-14.73 (m, 1H), 8.13 (s, 1H), 8.05 (d, *J* = 2.1 Hz, 1H), 7.56 (d, *J* = 2.1 Hz, 1H), 4.00 (dd, *J* = 11.2, 2.9 Hz, 1H), 3.71 (dd, *J* = 11.2, 9.5 Hz, 1H), 3.08 (dd, *J* = 9.5, 2.9 Hz, 1H), 1.00 (s, 9H).

$[\alpha]_d$ = -14.3 (c 1.0, acetone).

ESI-MS(+): Calculated for $C_{13}H_{17}I_2NNaO_2$ $[M+Na]^+$; 495.92 found 495.90.

^{1}H-NMR data were in accord with those previously reported.[115]

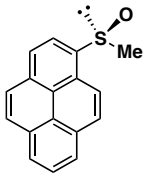

(*S*)-Me:[114]

Method 1: To a solution of $VO(acac)_2$ (3.016 mg, 11.37 μmol, 0.1 eq) in dry DCM (0.6 mL), **68** (8.072 mg, 17.06 μmol, 0.15 eq) was added. The resulting reaction mixture was then stirred for 2 h at rt. A solution of **3** (28.8 mg, 0.116 mmol, 1 eq) in dry DCM (1 mL) was added and the reaction mixture was stirred for 30 min at rt before cooling it down to 0 °C. After 30 min, 30% H_2O_2 (15.0 μL, 0.145 mmol, 1.2 eq) was added and the resulting mixture stirred for 16 h at 0 °C. The reaction mixture was then quenched by 10% $Na_2S_2O_3$ (6 mL) and extracted with DCM (2x20 mL). The combined organic phase was dried over Na_2SO_4 and evaporated. Purification by column chromatography (silica gel; 40% EtOAc:DCM) gave **(*S*)-Me** (88% *ee*, 26.0 mg, 85%).

Method 2: To a solution of $VO(acac)_2$ (1.59 mg, 5.98 μmol, 0.02 eq) in dry DCM (0.6 mL), **68** (4.68 mg, 9.89 μmol, 0.04 eq) was added. The resulting reaction mixture was then stirred for 2 h at rt. A solution of **(*rac*)-Me** (73.3 mg, 0.277 mmol, 1 eq) in dry DCM (1 mL) was added and the reaction mixture was stirred

for 30 min at rt before cooling it down to 0 °C. After 30 min, 30% H_2O_2 (17.0 μL, 0.165 mmol, 0.6 eq) was added and the resulting mixture stirred for 16 h at 0 °C. The reaction mixture was then quenched by 10% $Na_2S_2O_3$ (3 mL) and extracted with DCM (2x25 mL). The combined organic phase was dried over Na_2SO_4 and evaporated. Purification by column chromatography (silica gel; 40% EtOAc:DCM) gave **(*S*)-Me** (94% *ee*, 25.9 mg, 71%).

R_f: 0.36 (silica gel TLC; 40% EtOAc:DCM).

^{1}H-NMR (400 MHz; $CDCl_3$), δ: 8.65 (d, *J* = 8.1 Hz, 1H), 8.34 (d, *J* = 8.0 Hz, 1H), 8.25-8.03 (m, 7H), 2.89 (s, 3H).

^{13}C-NMR (100 MHz; $CDCl_3$), δ: 138.2, 133.3, 131.3, 130.5, 129.4, 129.2, 127.4, 127.2, 126.78, 126.65, 126.47, 125.8, 124.56, 124.50, 120.7, 120.4, 43.6.

IR(neat), cm^{-1}: 3044 (m), 2912 (w), 1592 (s), 1415 (s), 1189 (s), 1057 (vs), 951 (s), 847 (vs), 713 (s).

HRMS-ESI(+): Calculated for $C_{17}H_{12}NaOS$ $[M+Na]^+$ 287.05011; found 287.04975.

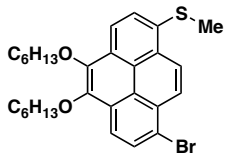

73: *n*-BuLi (0.08 mL, 1.4 M in hexane, 0.112 mmol, 1.05 eq) was added dropwise to a solution of **72** (59.7 mg, 0.107 mmol, 1 eq) in dry THF (3 mL) at -78 °C under N_2. The solution was stirred for 20 min and methyl disulfide (15.0 μL, 0.169 mmol, 1.1 eq) was added. After 15 min, the dry ice-acetone bath was removed and the reaction mixture was allowed to reach rt**.** The solvent was evaporated and the crude residue dissolved in DCM (20 mL) and washed with brine (15 mL). The aq. layer was washed with DCM (20 mL) and the combined organic layers were dried over Na_2SO_4 and evaporated. Purification by column chromatography (silica gel; 10% DCM:hexane) gave **73** (46.9 mg, 83%).

R_f: 0.24 (silica gel TLC; 10% DCM:hexane).

^{1}H-NMR (400 MHz; $CDCl_3$), δ: 8.65 (d, *J* = 9.5 Hz, 1H), 8.47 (d, *J* = 9.2 Hz, 2H), 8.31 (d, *J* = 8.4 Hz, 1H), 8.24 (d, *J* = 8.4 Hz, 1H), 8.04 (d, *J* = 8.3 Hz, 1H), 4.31 (q, *J* = 6.7 Hz, 4H), 2.70 (s, 3H), 1.99-1.93 (m, 4H), 1.63-1.58 (m, 4H), 1.41-1.39 (m, 8H), 0.94 (t, *J* = 6.9 Hz, 6H).

^{13}C-NMR (101 MHz; $CDCl_3$), δ: 144.2, 143.5, 133.5, 130.6, 129.7, 129.5, 129.0, 127.5, 126.43, 126.31, 125.5, 124.2, 123.0, 120.4, 119.7, 74.1, 32.0, 30.75, 30.73, 26.2, 22.9, 17.6, 14.3.

IR(neat), cm^{-1}: 2953 (vs), 2926 (vs), 2859 (s), 1595 (s), 1454 (m), 1378 (m), 1297 (s), 1220 (m), 1098 (s), 817 (vs) 723 (vs).

HRMS-ESI(+): Calculated for $C_{29}H_{35}BrNaO_2S$ $[M+Na]^+$ 549.14333; found 549.14340.

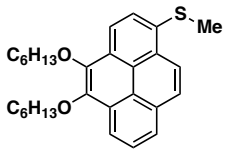

74: *n*-BuLi (0.06 mL, 1.4 M in hexane, 0.084 mmol, 1.0 eq) was added dropwise to a solution of **73** (46.9 mg, 88.9 μmol, 1 eq) in dry THF (2.5 mL) at -78 °C under N_2. The solution was stirred for 10 min and MeOH (1.0 mL) was added. After 15 min, the dry ice-acetone bath was removed and the reaction mixture was allowed to reach rt**.** The solvent was evaporated and the crude residue dissolved in DCM (20 mL) and washed with brine (15 mL). The aq. layer was washed with DCM (20 mL) and the combined organic layers were dried over Na_2SO_4 and evaporated. Purification by column chromatography (silica gel; 20% DCM:hexane) gave **74** (37.2 mg, 93%).

R_f: 0.33 (silica gel TLC; 20% DCM:hexane).

^{1}H-NMR (400 MHz; $CDCl_3$), δ: 8.57 (d, *J* = 9.2 Hz, 1H), 8.50-8.44 (m, 2H), 8.13 (t, *J* = 8.0 Hz, 2H), 8.05-8.01 (m, 2H), 4.34 (t, *J* = 6.7 Hz, 4H), 2.70 (s, 3H), 2.02-1.95 (m, 4H), 1.67-1.60 (m, 4H), 1.45-1.40 (m, 8H), 0.97-0.94 (m, 6H).

^{13}C-NMR (101 MHz; $CDCl_3$), δ: 144.1, 143.9, 132.5, 131.2, 129.7, 129.4, 127.8, 127.5, 126.4, 126.2, 124.7, 124.0, 123.5, 123.0, 119.81, 119.74, 74.0, 32.0, 30.8, 26.2, 22.9, 17.8, 14.3.

IR(neat), cm^{-1}: 3045 (w), 2954 (vs), 2929 (vs), 2856 (m), 1597 (s), 1470 (m) 1299 (vs), 1218 (m), 1099 (vs), 1066 (s), 825 (s), 726 (m).

HRMS-ESI(+):Calculated for $C_{29}H_{36}NaO_2S$ $[M+Na]^+$ 471.23282; found 471.23305.

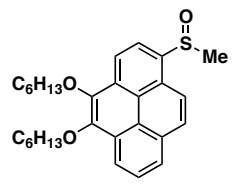

70: To a solution of **74** (26.3 mg, 58.7 μmol, 1 eq) in DCM (3 mL), mCPBA (11.8 mg, 77% assay, 52.7 μmol, 0.9 eq) was added at 0 °C. The resulting solution was stirred for 40 min. The reaction mixture was diluted with DCM (15 mL) and

washed with saturated aq. $NaHCO_3$ (15 mL). The aq. layer was washed once again with DCM (15 mL). The combined organic layers were dried over Na_2SO_4 and evaporated. Purification by column chromatography (silica gel; 10% EtOAc:DCM) gave **70** (21.1 mg, 86%).

R_f: 0.23 (silica gel TLC; 10% EtOAc:DCM).

^{1}H-NMR (400 MHz; $CDCl_3$), δ: 8.68 (d, *J* = 1.1 Hz, 2H), 8.60 (dd, *J* = 7.8, 1.1 Hz, 1H), 8.24-8.17 (m, 3H), 8.09 (t, *J* = 7.7 Hz, 1H), 4.36 (dt, *J* = 15.3, 6.7 Hz, 4H), 2.91 (s, 3H), 2.02-1.95 (m, 4H), 1.66-1.59 (m, 4H), 1.46-1.36 (m, 8H), 0.94 (tt, *J* = 6.3, 1.5 Hz, 6H).

^{13}C-NMR (101 MHz; $CDCl_3$), δ: 145.6, 144.0, 137.4, 131.5, 130.5, 129.40, 129.26, 127.2, 126.9, 125.8, 122.76, 122.74, 121.2, 120.9, 120.43, 120.28, 74.21, 74.17, 43.7, 31.9, 30.75, 30.72, 26.2, 22.9, 14.3.

IR(neat), cm^{-1}: 2954 (s), 2930 (s), 1597 (s), 1584 (m), 1456 (m), 1414 (m), 1307 (vs), 1220 (m), 1099 (s), 1060 (vs), 843 (s) 729 (m).

HRMS-ESI(+):Calculated for $C_{29}H_{36}NaO_3S$ $[M+Na]^+$ 487.22774; found 487.22816.

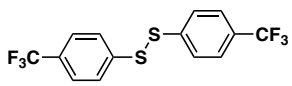

76a:[116] 4-trifluoromethylbenzenethiol (**75a**, 500.0 μL, 3.648 mmol, 1 eq) was added to DMSO (3.0 mL) at 95 °C. The resulting solution was stirred at 95 °C for 6 hours. The reaction mixture was cooled down to rt, diluted with DCM (30 mL) and washed twice with brine (15 mL). The combined aq. layer was washed with DCM (20 mL). The combined organic layer was dried over $MgSO_4$ and evaporated. Purification by column chromatography (silica gel; hexane) gave **76a** (627.4 mg, 97%).

R_f: 0.32 (silica gel TLC; hexane).

^{1}H-NMR (300 MHz; $CDCl_3$), δ: 7.58 (s, 4H).

HRMS-EI(+): Calculated for $C_{14}H_8F_6S_2$ $[M]^+$; 353.99661 found 353.99663.

^{1}H-NMR data were in accord with those previously reported.[119]

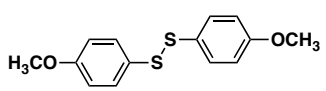

76b:[116] 4-methoxybenzenethiol (**75b**, 200.0 μL, 1.626 mmol, 1 eq) was added to DMSO (1.0 mL) at 95 °C. The resulting solution was stirred at 95 °C for 6 hours. The reaction mixture was cooled down to rt, diluted with DCM (20 mL) and washed twice with brine (15

mL). The combined aq. layer was washed with DCM (20 mL). The combined organic layer was dried over $MgSO_4$ and evaporated. Purification by column chromatography (silica gel; 5% EtOAc:hexane) gave **76b** (213.4 mg, 94%).

R_f: 0.15 (silica gel TLC; 5% EtOAc:hexane).

^{1}H-NMR (400 MHz; $CDCl_3$), δ: 7.42-7.38 (m, 4H), 6.85-6.82 (m, 4H), 3.80 (s, 6H).

EI-MS(+): Calculated for $C_{14}H_{14}O_2S_2$ $[M]^+$; 278.04 found 278.0.

^{1}H-NMR data were in accord with those previously reported. [120]

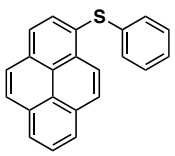

77a:[73] *n*-BuLi (0.74 mL, 1.6 M in hexane, 1.2 mmol, 1.2 eq) was added dropwise to a solution of **52** (276.5 mg, 983.5 μmol, 1 eq) in dry THF (9 mL) at -78 °C under N_2. The solution was stirred for 30 min and phenyl disulfide (257.6 mg, 1.179 mmol, 1.2 eq) sas added. After 15 min, the dry ice-acetone bath was removed and the reaction mixture was allowed to reach rt**.** The solvent was evaporated and the crude residue dissolved in DCM (30 mL) and washed with brine (20 mL). The aq. layer was washed with DCM (20 mL) and the combined organic layers were dried over $MgSO_4$ and evaporated. Purification by column chromatography (deactivated alumina; hexane) gave **77a** (0.238 g, 78%).

R_f: 0.19 (alumina TLC; 100% hexane).

^{1}H-NMR (400 MHz; $CDCl_3$), δ: 8.67 (d, *J* = 9.2 Hz, 1H), 8.23-8.02 (m, 8H), 7.24-7.12 (m, 5H).

EI-MS(+): Calculated for $C_{22}H_{14}S$ $[M]^+$ 310.08; found 310.0

^{1}H-NMR data were in accord with those previously reported.[73]

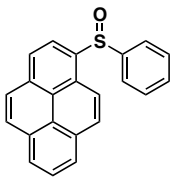

71a:[73] To a solution of **77a** (32.2 mg, 0.103 mmol, 1 eq) in DCM (5.3 mL), mCPBA (22.7 mg, 70% assay, 92.0 μmol, 0.9 eq) was added at 0 °C. The resulting solution was stirred for 40 min. The reaction mixture was diluted with DCM (15 mL) and washed with saturated aq. $NaHCO_3$ (15 mL). The organic layer was dried over $MgSO_4$ and evaporated. Purification by column chromatography (deactivated alumina; 20% hexane:DCM) gave **71a** (30.8 mg, 91%).

R_f: 0.27 (alumina TLC; 20% hexane:DCM).

^{1}H-NMR (300 MHz; $CDCl_3$), δ: 8.60 (dd, *J* = 8.7, 4.2 Hz, 2H), 8.31-8.03 (m, 7H), 7.71 (dd, *J* = 7.6, 1.9 Hz, 2H), 7.41-7.34 (m, 3H).

HRMS-ESI(+): Calculated for $C_{22}H_{14}NaOS$ $[M+Na]^+$ 349.06631; found 349.06597.

^{1}H-NMR data were in accord with those previously reported.[73]

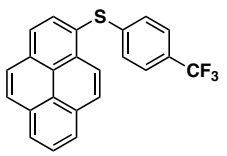

77b: n-BuLi (0.72 mL, 1.22 M in hexane, 0.88 mmol, 1.05 eq) was added dropwise to a solution of **52** (235.1 mg, 836.2 μmol, 1 eq) in dry THF (9 mL) at -78 °C under N_2. The resulting solution was stirred for 30 min and 4-trifluoromethylphenyl disulfide (**76a**; 325.2 mg, 917.7 μmol, 1.1 eq) in dry THF (3 mL) was added. After 15 min, the dry ice-acetone bath was removed and reaction mixture was allowed to reach rt. The solvent was evaporated and the crude residue dissolved in DCM (30 mL) and washed with brine (20 mL). The aq. layer was washed with DCM (20 mL) and the combined organic layers were dried over $MgSO_4$ and evaporated. Purification by column chromatography (silica gel; hexane) gave **77b** (253.1 mg, 80%).

R_f: 0.19 (silica gel TLC; hexane).

^{1}H-NMR (400 MHz; $CDCl_3$), δ: 8.59 (d, *J* = 9.2 Hz, 1H), 8.28-8.05 (m, 8H), 7.38 (d, *J* = 8.5 Hz, 2H), 7.10 (d, *J* = 8.4 Hz, 2H).

^{13}C-NMR (100 MHz; $CDCl_3$), δ: 144.3, 144.2, 144.2, 134.7, 133.6, 132.9, 131.3, 131.1, 129.4, 129.1, 127.4, 127.4, 126.8, 126.7, 126.3, 126.2, 126.0, 126.0, 125.9, 125.9, 125.8, 125.7, 125.6, 125.1, 125.0,124.6, 123.0.

IR(neat), cm^{-1}: 3044 (w), 1604 (m), 1325 (vs), 1164 (m), 1121 (s), 1062 (m), 1013 (m), 845 (s).

HRMS-EI(+): Calculated for $C_{23}H_{13}F_3S$ $[M]^+$ 378.06846; found 378.06822.

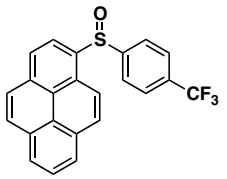

71b: To a solution of **77b** (41.4 mg, 0.109 mmol, 1 eq) in DCM (6 mL) mCPBA (24.7 mg, 70% assay, 0.100 mmol, 0.9 eq) was added at 0 °C. The resulting solution was stirred for 40 min. The reaction mixture was diluted with DCM (15 mL) and washed with saturated aq. $NaHCO_3$ (15 mL). Organic layer was dried over $MgSO_4$ and evaporated. Purification by column chromatography (deactivated alumina; 50% DCM:hexane) gave **71b** (32.7 mg, 83%).

R_f: 0.31 (alumina TLC; 50% DCM:hexane).

^{1}H-NMR (300 MHz; $CDCl_3$), δ: 8.68 (d, *J* = 9.2 Hz, 1H), 8.51 (d, *J* = 8.2 Hz, 1H), 8.32-8.19 (m, 5H), 8.13-8.08 (m, 2H), 7.83 (d, *J* = 8.2 Hz, 2H), 7.64 (d, *J* = 8.2 Hz, 2H).

^{13}C-NMR (125 MHz; $CDCl_3$), δ: 150.6, 137.0, 133.9, 133.2, 132.9, 132.6, 132.4, 131.4, 130.6, 130.1, 129.9, 129.1, 127.4, 127.4, 127.0, 126.8, 126.5, 126.5, 126.4, 126.4, 125.9, 125.1, 125.0, 124.7, 124.5, 122.8, 12.6, 121.3.

IR(neat), cm^{-1}: 3046 (w), 1604 (m), 1400 (m), 1323 (vs), 1127 (s), 1059 (vs), 1013 (s), 845 (vs).

HRMS-APCI(+): Calculated for $C_{23}H_{14}F_3OS$ $[M+H]^+$ 395.07120; found 395.07153.

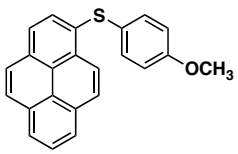

77c: *n*-BuLi (0.89 mL, 1.22 M in hexane, 1.1 mmol, 1.0 eq) was added dropwise to the solution of **52** (306.2 mg, 1.089 mmol, 1 eq) in dry THF (9 mL) at -78 °C under N_2. The solution was stirred for 30 min and solution of 4-methoxyphenyl disulfide (**76b**; 330.9 mg, 1.188 mmol, 1.1 eq) in THF (3 mL) was added. After 15 min of stirring, the dry ice-acetone bath was removed and reaction mixture was allowed to reach rt**.** The solvent was evaporated and the crude residue dissolved in DCM (30 mL) and washed with brine (20 mL). The aq. layer was washed with DCM (20 mL) and the combined organic layers were dried over $MgSO_4$ and evaporated. Purification by column chromatography (silica gel; 5% EtOAc:hexane) gave **77c** (158.8 mg, 43%).

R_f: 0.18 (silica gel TLC; 5% EtOAc:hexane).

^{1}H-NMR (300 MHz; $CDCl_3$), δ: 8.67 (d, *J* = 9.2 Hz, 1H), 8.21-8.17 (m, 2H), 8.14 (d, *J* = 9.3 Hz, 1H), 8.03 (m, 4H), 7.91 (d, *J* = 8.1 Hz, 1H), 7.38-7.33 (m, 2H), 6.89-6.84 (m, 2H), 3.79 (s, 3H).

^{13}C-NMR (75 MHz; $CDCl_3$), δ: 159.4, 133.5, 131.7, 131.6, 131.2, 130.7, 130.7, 129.6, 128.3, 127.7, 127.5, 126.6, 126.4, 125.6, 125.5, 125.5, 125.3, 124.7, 124.5, 115.3, 55.6.

IR(neat), cm^{-1}: 3040 (m), 2958 (w), 1591 (s), 1492 (vs), 1245 (vs), 1173 (m), 1029 (m), 843 (vs).

HRMS-EI(+): Calculated for $C_{23}H_{16}OS$ $[M]^+$ 340.09164; found 340.09148.

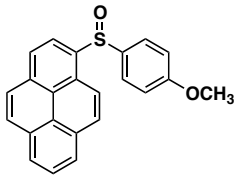

71c: To a solution of **77c** (33.8 mg, 99.3 μmol, 1 eq) in DCM (5 mL), mCPBA (22.4 mg, 70% assay, 90.8 μmol, 0.9 eq) was added at 0 °C. The resulting solution was stirred for 40 min. The reaction mixture was diluted with DCM (15 mL) and washed with saturated aq. $NaHCO_3$ (15 mL). The organic layer was dried over $MgSO_4$ and evaporated. Purification by column chromatography (alumina; DCM) gave **71c** (26.9 mg, 83%).

R_f: 0.3 (alumina TLC; DCM).

^{1}H-NMR (300 MHz; $CDCl_3$), δ: 8.67 (d, *J* = 8.2 Hz, 1H), 8.47 (d, *J* = 9.2 Hz, 1H), 8.33 (d, *J* = 8.2 Hz, 1H), 8.26-8.22 (m, 2H), 8.15 (d, *J* = 9.4 Hz, 2H), 8.10-8.02 (m, 2H), 7.65-7.60 (m, 2H), 6.89-6.84 (m, 2H), 3.74 (s, 3H).

^{13}C-NMR (125 MHz; $CDCl_3$), δ: 162.0, 137.7, 137.1, 133.5, 131.4, 130.6, 129.4, 129.4, 128.3, 127.6, 127.5, 126.8, 126.7, 126.5, 125.7, 124.9, 124.6, 122.2, 121.5, 115.0, 55.6.

IR(neat), cm^{-1}: 3046 (w), 2938 (w), 1591 (s), 1494 (s), 1303 (m), 1253 (vs), 1172 (m), 1046 (vs), 849 (s).

HRMS-APCI(+): Calculated for $C_{23}H_{17}O_2S$ $[M+H]^+$ 357.09438; found 340.09454.

References

(1) Vallee, B. L.; Falchuk, K. H. *Physiological reviews* **1993**, *73*, 79–118.

(2) CAMPBELL, A. K. *Proceedings of the Nutrition Society* **1990**, *49*, 51-56.

(3) Berridge, M. J.; Bootman, M. D.; Lipp, P. *Nature* **1998**, *395*, 645–648.

(4) Minta, A.; Tsien, R. Y. *J. Biol. Chem.* **1989**, *264*, 19449–19457.

(5) Kang, J.; Kang, H. K.; Kim, H.; Lee, J.; Song, E. J.; Jeong, K.-D.; Kim, C.; Kim, J. *Supramol. Chem.* **2013**, *25*, 65–68.

(6) Berg, J. M.; Tymoczko, J. L.; Stryer, L. *Biochemistry*, 5th ed.; W. H. Freeman and Co.:New York, 2001; pp 541-545.

(7) Berg, J. M.; Tymoczko, J. L.; Stryer, L. *Biochemistry*, 5th ed.; W. H. Freeman and Co.: New York, 2001; pp 792-812.

(8) Berg, J. M.; Tymoczko, J. L.; Stryer, L. *Biochemistry*, 5th ed.; W. H. Freeman and Co.: New York, 2001; pp 413-416.

(9) Margoshes, M. *Anal. Chem.* **1962**, *34*, 221R–224R.

(10) Bühlmann, P.; Pretsch, E.; Bakker, E. *Chem. Rev.* **1998**, *98*, 1593–1688.

(11) Bakker, E.; Bühlmann, P.; Pretsch, E. *Chem. Rev.* **1997**, *97*, 3083–3132.

(12) Bryan, A. J.; De Silva, A. P.; de Silva, S. A.; Rupasinghe, R.; Sandanayake, K. *Biosensors* **1989**, *4*, 169–179.

(13) Bissell, R. A.; De Silva, A. P.; Gunaratne, H. Q. N.; Lynch, P. L. M.; Maguire, G. E. M.; Sandanayake, K. R. A. S. *Chem. Soc. Rev.* **1992**, *21*, 187-195.

(14) Goodwin, P. M.; Ambrose, W. P.; Keller, R. A. *Acc. Chem. Res.* **1996**, *29*, 607–613.

(15) Orrit, M.; Bernard, J. *Phys. Rev. Lett.* **1990**, *65*, 2716–2719.

(16) Lakowicz, J. R. *Principles of Fluorescence spectroscopy*, 3rd ed.; Springer: New York, 2006.

(17) Fabbrizzi, L.; Poggi, A. *Chem. Soc. Rev.* **1995**, *24*, 197-202.

(18) Demchenko, A. P. *Intoduction to Fluorescence Sensing*; Springer Science: London, 2009.

(19) Valeur, B.; Leray, I. *Coord. Chem. Rev.* **2000**, *205*, 3–40.

(20) De Silva, A. P.; Gunaratne, H. N.; Gunnlaugsson, T.; Huxley, A. J.; McCoy, C. P.; Rademacher, J. T.; Rice, T. E. *Chem. Rev.* **1997**, *97*, 1515–1566.

(21) Formica, M.; Fusi, V.; Giorgi, L.; Micheloni, M. *Coord. Chem. Rev.* **2012**, *256*, 170–192.

(22) Tsukanov, A. V.; Dubonosov, A. D.; Bren, V. A.; Minkin, V. I. *Chem. Heterocycl. Compd.* **2008**, *44*, 899–923.

(23) Bell, T. W.; Hext, N. M. *Chem. Soc. Rev.* **2004**, *33*, 589-598.

(24) Callan, J. F.; De Silva, A. P.; Magri, D. C. *Tetrahedron* **2005**, *61*, 8551–8588.

(25) Franck, J.; Dymond, E. G. *Trans. Faraday Soc.* **1926**, *21*, 536-542.

(26) Condon, E. U. *Phys. Rev.* **1926**, *28*, 1182-1201.

(27) Condon, E. U. *Phys. Rev.* **1928**, *32*, 858-872.

(28) Herschel, J. F. W. *Phil. Trans. R. Soc. Lond.* **1845**, *135*, 143–145.

(29) Kasha, M. *Discuss. Faraday Soc.* **1950**, *9*, 14-19.

(30) Stokes, G. G. *Phil. Trans. R. Soc. Lond.* **1852**, *142*, 463–562.

(31) Rurack, K.; Resch-Genger, U. *Chem. Soc. Rev.* **2002**, *31*, 116–127.

(32) Shin, Y. K.; Yongseog, C. *Bull. Korean Chem. Soc.* **1999**, *20*, 796-800.

(33) Adams, S. R.; Harootunian, A. T.; Buechler, Y. J.; Taylor, S. S.; Tsien, R. Y. *Nature* **1991**, *349*, 694–697.

(34) Bourson, J.; Pouget, J.; Valeur, B. *J. Phys. Chem.* **1993**, *97*, 4552–4557.

(35) Gunnlaugsson, T.; Nieuwenhuyzen, M.; Richard, L.; Thoss, V. *J. Chem. Soc., Perkin Trans. 2*, **2002**, 141–150.

(36) Wasielewski, M. R. *Chem. Rev.* **1992**, *92*, 435–461.

(37) Kavarnos, G. J.; Turro, N. J. *Chem. Rev.* **1986**, *86*, 401–449.

(38) Weller, A. *Pure Appl. Chem.* **1968**, *16*, 115–124.

(39) Rehm, D.; Weller, A. *Isr. J. Chem.* **1970**, *8*, 259-271.

(40) Closs, G. L.; Miller, J. R. *Science* **1988**, *240*, 440–447.

(41) Bissell, R. A.; de Silva, A. P.; Gunaratne, H. Q. N.; Lynch, P. L. M.; Maguire, G. E. M.; McCoy, C. P.; Sandanayake, K. R. A. S. *Top. Curr. Chem.* **1993**, 168, 223-264.

(42) De Silva, A. P.; de Silva, S. A. *J. Chem. Soc., Chem. Commun.* **1986**, 1709-1710.

(43) Akkaya, E. U.; Huston, M. E.; Czarnik, A. W. *J. Am. Chem. Soc.* **1990**, *112*, 3590–3593.

(44) Golchini, K.; Mackovic-Basic, M.; Gharib, S. A.; Masilamani,D.; Lucas, M. E.; Kurtz, I. *Am. J. Physiol.* **1990**, *258*, F438.

(45) De Silva, A. P.; Nimal Gunaratne, H. Q.; Samankumara Sandanayake, K. *Tetrahedron Lett.* **1990**, *31*, 5193–5196.

(46) Burdette, S. C.; Walkup, G. K.; Spingler, B.; Tsien, R. Y.; Lippard, S. J. *J. Am. Chem. Soc.* **2001**, *123*, 7831–7841.

(47) De Silva, A. P.; Gunaratne, H. Q. N.; Lynch, P. L. M. *J. Chem. Soc., Perkin Trans. 2* **1995**, 685-690.

(48) Krasovitskii, B. M.; Bolotin, B. M. *Organic Luminescent Materials*; VCH: Weinheim, 1989.

(49) Jones, G.; Jackson, W. R.; Kanoktanaporn, S.; Bergmark, W. R. *Photochem. Photobiol.* **1985**, *42*, 477–483.

(50) Kessler, M. A.; Wolfbeis, O. S. *Spectrochim. Acta* **1991**, *47A*, 187.

(51) Martin, M. M.; Plaza, P.; Meyer, Y. H.; Badaoui, F.; Bourson, J.; Lefevre, J.-P.; Valeur, B. *J. Phys. Chem* **1996**, *100*, 6879–6888.

(52) Martin, M. M.; Plaza, P.; Dai Hung, N.; Meyer, Y. H.; Bourson, J.; Valeur, B. *Chem. Phys. Lett.* **1993**, *202*, 425–430.

(53) Dumon, P.; Jonusauskas, G.; Dupuy, F.; Pée, P.; Rulliere, C.; Létard, J.-F.; Lapouyade, R. *J. Phys. Chem.* **1994**, *98*, 10391–10396.

(54) Letard, J.-F.; Lapouyade, R.; Rettig, W. *Mol. Cryst. Liq. Cryst.* **1993**, *236*, 41–46.

(55) Grynkiewicz, G.; Poenie, M.; Tsien, R. Y. *J. Biol. Chem.* **1985**, *260*, 3440–3450.

(56) Delmond, S.; Létard, J. F.; Lapouyade, R.; Mathevet, R.; Jonusauskas, G.; Rullière, C. *New J. Chem.* **1996**, *20*, 861.

(57) Soh, N.; Sakawaki, O.; Makihara, K.; Odo, Y.; Fukaminato, T.; Kawai, T.; Irie, M.; Imato, T. *Bioorg. Med. Chem.* **2005**, *13*, 1131–1139.

(58) Lemieux, G. A.; de Graffenried, C. L.; Bertozzi, C. R. *J. Am. Chem. Soc.* **2003**, *125*, 4708–4709.

(59) Griffin, B. A. *Science* **1998**, *281*, 269–272.

(60) Murray, S. G.; Hartley, F. R. *Chem. Rev.* **1981**, *81*, 365–414.

(61) Cooper, S. R. *Acc. Chem. Res.* **1988**, *21*, 141–146.

(62) Griesbeck, A. G.; Schieffer, S. *Photochem. Photobiol. Sci.* **2003**, *2*, 113–117.

(63) Vonlanthen, M. Fluorescent Chemosensors for Metal Ions Based on Photoinduced Electron Transfer (PET) from Sulfur. Ph.D. Thesis, University of Zurich, Zurich, 2013.

(64) Gunnlaugsson, T.; Ali, H. D. P.; Glynn, M.; Kruger, P. E.; Hussey, G. M.; Pfeffer, F. M.; Santos, C. M. G.; Tierney, J. *J. Fluoresc.* **2005**, *15*, 287–299.

(65) Gunnlaugsson, T.; Glynn, M.; Tocci née Hussey, G. M.; Kruger, P. E.; Pfeffer, F. M. *Coord. Chem. Rev.* **2006**, *250*, 3094–3117.

(66) Tolpygin, I. E.; Shepelenko, E. N.; Revinskii, Y. V.; Tsukanov, A. V.; Dubonosov, A. D.; Bren, V. A.; Minkin, V. I. *Russ. J. Gen. Chem.* **2010**, *80*, 765–770.

(67) Finney, N. S.; Vonlanthen, M. *Unpublished Results*.

(68) Vonlanthen, M.; Finney, N. S. *J. Org. Chem.* **2013**, *78*, 3980-3988.

(69) Malashikhin, S. A.; Baldridge, K. K.; Finney, N. S. *Org. Lett.* **2010**, *12*, 940–943.

(70) Mello, J. V.; Finney, N. S. *J. Am. Chem. Soc.* **2005**, *127*, 10124–10125.

(71) Lee, W.; Jenks, W. S. *J. Org. Chem.* **2001**, *66*, 474–480.

(72) Exceptions to this trend that sulfoxide are the least emissive in corresponding sulfide/sulfoxide/sulfone series: (a) Christensen, P. R.; Nagle, J. K.; Bhatti, A.; Wolf, M. O. *J. Am. Chem. Soc.* **2013**, *135*, 8109-8112. (b) Dane, E. L.; King, S. B.; Swager, T. B. *J. Am. Chem. Soc.* **2010**, *132*, 7758-7768.

(73) Malashikhin, S.; Finney, N. S. *J. Am. Chem. Soc.* **2008**, *130*, 12846–12847.

(74) Calligaris, M.; Carugo, O. *Coord. Chem. Rev.* **1996**, *153*, 83–154.

(75) Calligaris, M. *Coord. Chem. Rev.* **2004**, *248*, 351–375.

(76) Malashikhin, S. I. Efficient Discovery of Fluorescent Chemosensors Based on a Biarylpyridine Scaffold II. Visual Detection of the Explosive TATP The Origins of Sulfoxides “non-emission”. Ph.D. Thesis, University of Zurich, Zurich, 2010.

(77) Jenks, W. S.; Lee, W.; Shutters, D. *J. Phys. Chem.* **1994**, *98*, 2282–2289.

(78) Mislow, K.; Simmons, T.; Melillo, J. T.; Ternay, A. L. *J. Am. Chem. Soc.* **1964**, *86*, 1452–1453.

(79) Solladié, G. *Synthesis* **1981**, 185–196.

(80) Fernández, I.; Khiar, N. *Chem. Rev.* **2003**, *103*, 3651–3706.

(81) Rayner, D. R.; Gordon, A. J.; Mislow, K. *J. Am. Chem. Soc.* **1968**, *90*, 4854–4860.

(82) Rauk, A.; Allen, L. C.; Mislow, K. *Angew. Chem. Int. Ed. Engl.* **1970**, *9*, 400–414.

(83) Archer, R. A.; Kitchell, B. S. *J. Am. Chem. Soc.* **1966**, *88*, 3462–3463.

(84) Spry, D. O. *J. Am. Chem. Soc.* **1970**, *92*, 5006–5008.

(85) Still, I. W. J. In *The Chemistry of Sulfones and Sulfoxides*; Patai, S., Rappaport, Z., Stirling, C. J. M., Eds.; John Wiley & Sons Ltd.: New York, 1988; pp 873–887.

(86) Ganter, C.; Moser, J. F. *Helv. Chim. Acta* **1971**, *54*, 2228–2251.

(87) Schenck, G. O.; Krauch, C. H. *Chem. Ber.* **1963**, *96*, 517–519.

(88) Mislow, K.; Axelrod, M.; Rayner, D. R.; Gotthardt, H.; Coyne, I. M.; Hammond, G. S. *J. Am. Chem. Soc.* **1965**, *87*, 4958–4959.

(89) Hammond, G. S.; Gotthardt, H.; Coyne, L. M.; Axelrod, M.; Rayner, D. R.; Mislow, K. *J. Am. Chem. Soc.* **1965**, *87*, 4959–4960.

(90) Cooke, R. S.; Hammond, G. S. *J. Am. Chem. Soc.* **1970**, *92*, 2739–2745.

(91) Cooke, R. S.; Hammond, G. S. *J. Am. Chem. Soc.* **1968**, *90*, 2958–2959.

(92) Guo, Y.; Jenks, W. S. *J. Org. Chem.* **1995**, *60*, 5480–5486.

(93) Guo, Y.; Jenks, W. S. *J. Org. Chem.* **1997**, *62*, 857–864.

(94) Darmanyan, A. P.; Gregory, D. D.; Guo, Y.; Jenks, W. S. *J. Phys. Chem. A* **1997**, *101*, 6855–6863.

(95) Darmanyan, A. P.; Gregory, D. D.; Guo, Y.; Jenks, W. S.; Burel, L.; Eloy, D.; Jardon, P. *J. Am. Chem. Soc.* **1998**, *120*, 396–403.

(96) Guo, Y.; Darmanyan, A. P.; Jenks, W. S. *Tetrahedron Lett.* **1997**, *38*, 8619–8622.

(97) Vos, B. W.; Jenks, W. S. *J. Am. Chem. Soc.* **2002**, *124*, 2544–2547.

(98) Bunce, N. J.; Lamarre, J.; Vaish, S. P. *Photochem. Photobiol.* **1984**, *39*, 531–533.

(99) Cubbage, J. W.; Jenks, W. S. *J. Phys. Chem. A* **2001**, *105*, 10588–10595.

(100) Xu, Q.; (null); Yip, H.; Jen, A. K.-Y. *Nanotechnology* **2008**, *19*, 135605.

(101) Hill, Z. D.; MacCarthy, P. *J. Chem. Educ.* **1986**, *63*, 162.

(102) Baliah, V.; Pillay, M. K. *Indian J. Chem.* **1971**, *9*, 815-817.

(103) Sipilä, K.; Hase, T. *Synth. Commun.* **1997**, *27*, 1391–1393.

(104) Kruppa, M.; König, B. *Chem. Rev.* **2006**, *106*, 3520–3560.

(105) Izatt, R. M.; Pawlak, K.; Bradshaw, J. S.; Bruening, R. L. *Chem. Rev.* **1991**, *91*, 1721–2085.

(106) Poon, T.; Mundy, B. P.; Shattuck, T. W. *J. Chem. Educ.* **2002**, *79*, 264.

(107) Baughman, T. W.; Sworen, J. C.; Wagener, K. B. *Tetrahedron* **2004**, *60*, 10943–10948.

(108) van der Schaaf, P. A.; Kolly, R.; Kirner, H.-J.; Rime, F.; Mühlebach, A.; Hafner, A. *J. Organomet. Chem.* **2000**, *606*, 65–74.

(109) Mann, C. K. *Anal. Chem.* **1964**, *36*, 2424–2426.

(110) Acid-induced fluorescence enhancement as a probe for PET. For early examples, see: (a) Cox, G. S.; Turro, N. J.; Yang, N. C.; Chen, M.-J. *J. Am. Chem. Soc.* **1984**, *106*, 422-424. (b) Konopelski, J. P.; Kotzyba- Hibert, F.; Lehn, J.-M.; Desvergne, J.-P.; Fagés, F.; Castellan, A.; Bouas- , H. *J. Chem. Soc., Chem. Commun.* **1985**, 433-436.

(111) Czech, B.; Son, B.; Bartsch, R. A. *Tetrahedron Lett.* **1983**, *24*, 2923–2926.

(112) Kato, E.; Iwano, N.; Yamada, A.; Kawabata, J. *Tetrahedron* **2011**, *67*, 7692–7702.

(113) Kathayat, R. S.; Finney, N. S. *J. Am. Chem. Soc.* **2013**, *135*, 12612–12614.

(114) Drago, C.; Caggiano, L.; Jackson, R. F. W. *Angew. Chem. Int. Ed. Engl.* **2005**, *44*, 7221–7223.

(115) Legros, J.; Bolm, C. *Chem. Eur. J.* **2005**, *11*, 1086–1092.

(116) Ternay, A. L.; Brzezinska, E.; Sorokin, V.; Cook, C.; Lyaschenko, Y. E. *J. Appl. Toxicol.* **2000**, *20*, S31–34.

(117) Aurisicchio, C.; Baciocchi, E.; Gerini, M. F.; Lanzalunga, O. *Org. Lett.* **2007**, *9*, 1939–1942.

(118) Baciocchi, E.; Del Giacco, T.; Gerini, M. F.; Lanzalunga, O. *J. Phys. Chem. A* **2006**, *110*, 9940–9948.

(119) Tang, R.; Mislow, K. *J. Am. Chem. Soc.* **1970**, *92*, 2100–2104.

(120) Boerzel, H.; Koeckert, M.; Bu, W.; Spingler, B.; Lippard, S. J. *Inorg. Chem.* **2003**, *42*, 1604–1615.

Appendix

Appendix I: *Crystallographic Data for* ***Pyr:ZnCl$_2$.***

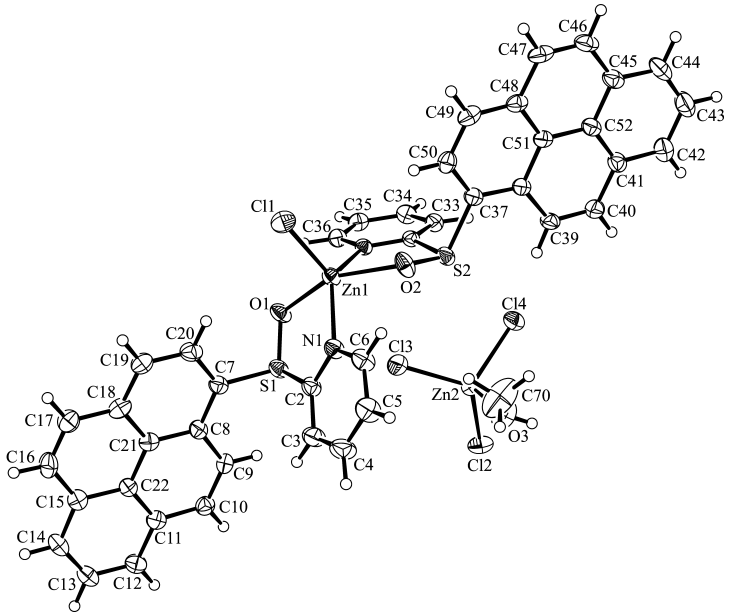

Crystallised from	CH_2Cl_2/ MeOH
Empirical formula	$C_{44}H_{32}Cl_6N_2O_3S_2Zn_2$
Formula weight [g mol^{-1}]	1044.35
Crystal colour, habit	colourless, prism
Crystal dimensions [mm]	0.15 ´ 0.17 ´ 0.25
Temperature [K]	160(1)
Crystal system	triclinic
Space group	$P\bar{1}$ (#2)
Z	2
Reflections for cell determination	34243
2*q* range for cell determination [°]	4 – 55
Unit cell parameters *a* [Å]	9.0445(2)
b [Å]	14.1554(3)
c [Å]	18.2190(3)
a [°]	70.410(1)
b [°]	81.092(1)

g [°]	89.690(1)
V [Å^3]	2168.32(8)
F(000)	1056
D_x [g cm^{-3}]	1.599
m(Mo Ka) [mm^{-1}]	1.615
Scan type	f and w
2q(max) [°]	55
Transmission factors (min; max)	0.714; 0.804
Total reflections measured	44755
Symmetry independent reflections	9921
R_{int}	0.050
Reflections with $I > 2s(I)$	7930
Reflections used in refinement	9919
Parameters refined; restraints	565; 24
Final $R(F)$ [$I > 2s(I)$ reflections]	0.0452
$wR(F^2)$ (all data)	0.1206
Weights: $w = [s^2(F_O^2) + (0.0561P)^2 + 3.2116P]^{-1}$ where $P = (F_O^2 + 2F_C^2)/3$	
Goodness of fit	1.024
Final D_{max}/s	0.002
Dr (max; min) [e Å^{-3}]	1.65; -0.90
$s(d_{(C-C)})$ [Å]	0.004 – 0.006

Appendix II: *Job plot* ***AC-NO$_4$*** *in ACN vs. (a) $LiClO_4$ (b)$MgClO_4$ (c) $Ca(ClO_4)_2$. (For details see* ***Section 2.6.2.3****)*

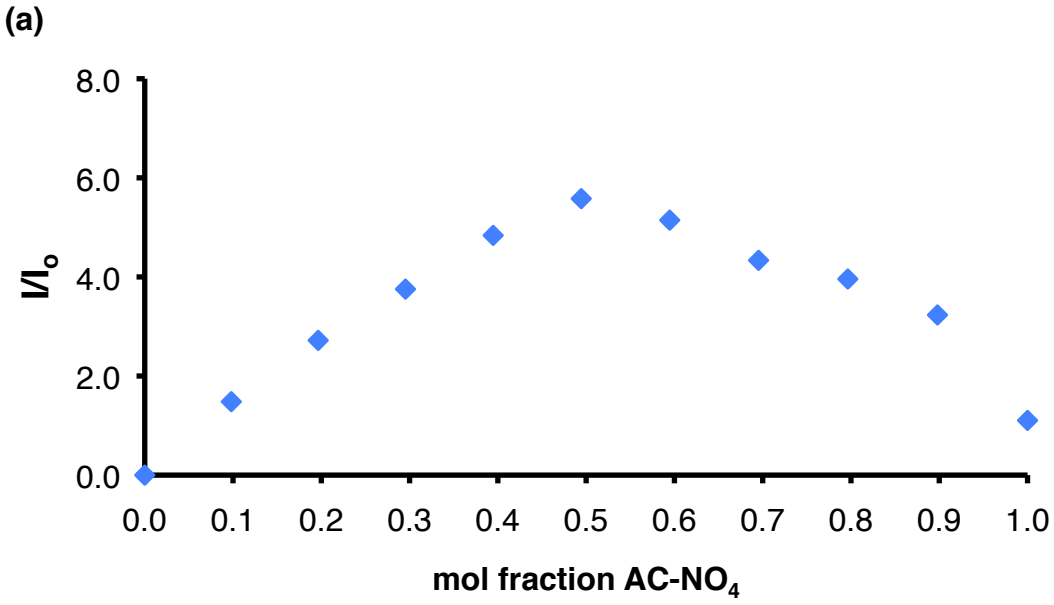

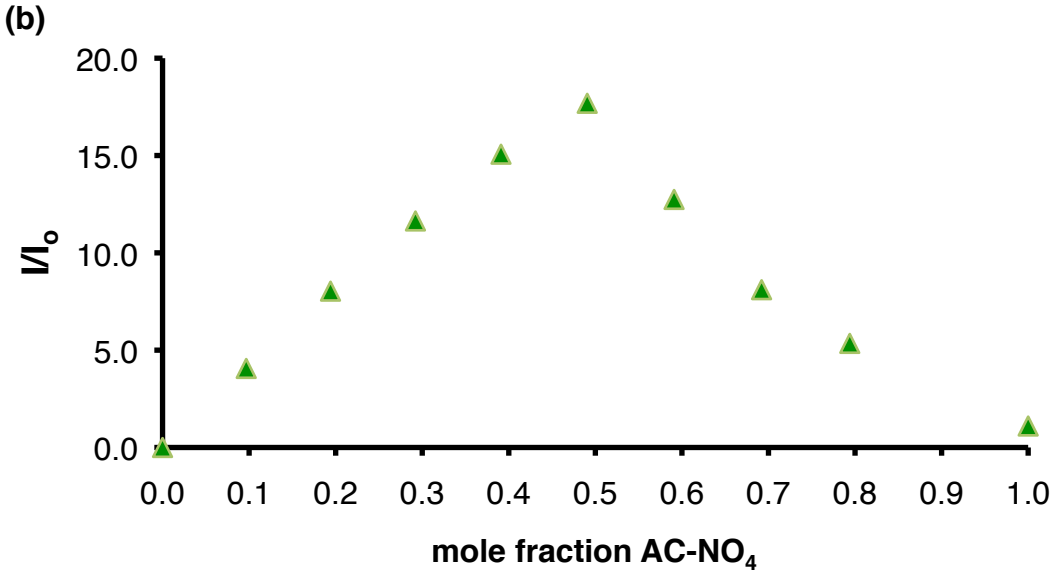

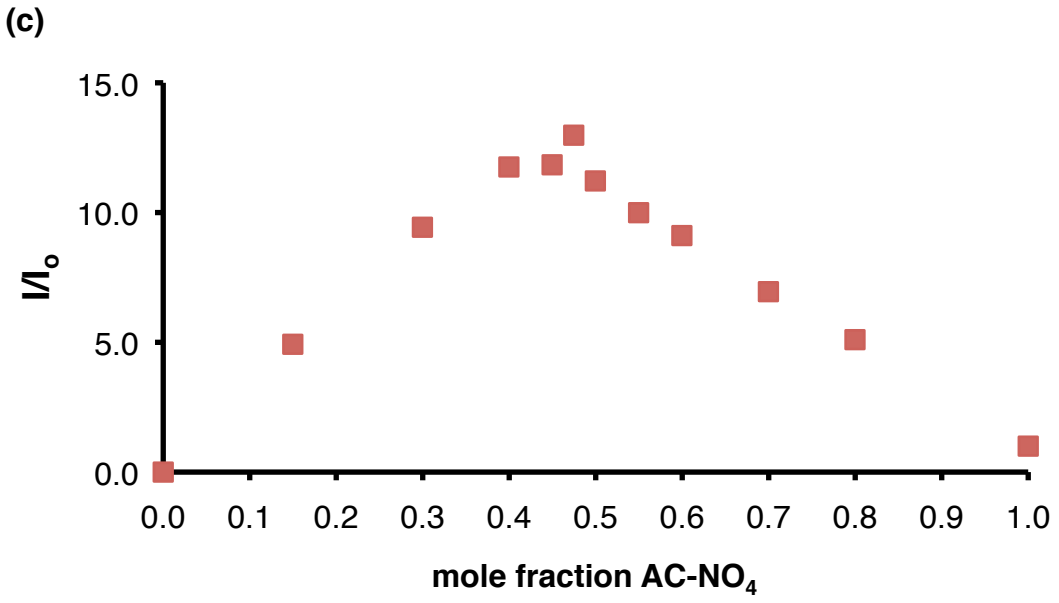

Appendix III: *Job plot* ***Crown-O$_4$*** *vs. Ca(ClO$_4$)$_2$ in ACN. (For details see* ***Section 2.6.2.3****)*

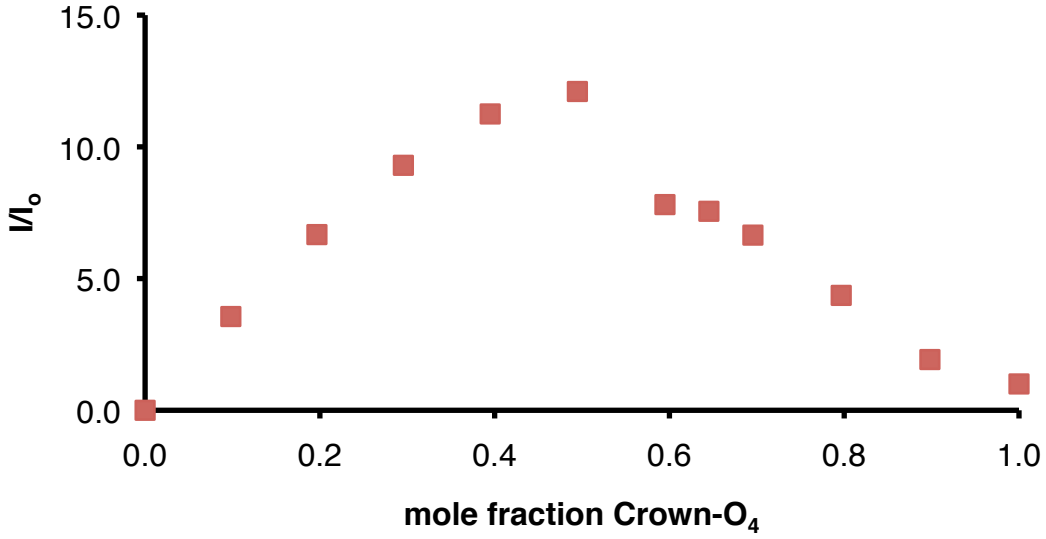

Appendix IV: *Crystallographic Data for* ***(S)-Me****.*

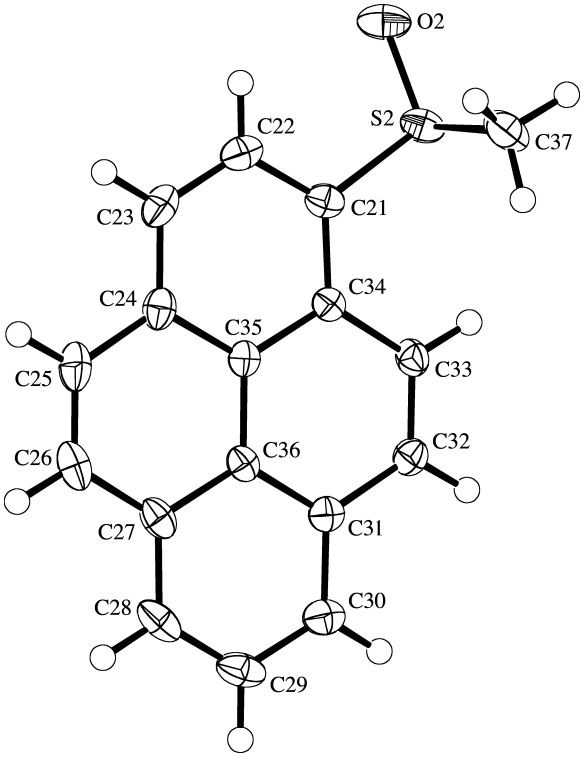

Crystallised from	CH_2Cl_2
Empirical formula	$C_{17}H_{12}OS$
Formula weight [g mol^{-1}]	264.34
Crystal colour, habit	colourless, prism
Crystal dimensions [mm]	0.15 ´ 0.15 ´ 0.19
Temperature [K]	160(1)
Crystal system	orthorhombic
Space group	$P2_12_12_1$ (#19)
Z	8
Reflections for cell determination	19618
2*q* range for cell determination [°]	5 – 61
Unit cell parameters *a* [Å]	10.28646(11)
b [Å]	13.11062(16)
c [Å]	18.6124(2)
a [°]	90
b [°]	90

g [°]	90
V [Å^3]	2510.10(5)
F(000)	1104
D_x [g cm^{-3}]	1.399
m(Mo Ka) [mm^{-1}]	0.244
Scan type	w
2q(max) [°]	61.0
Transmission factors (min; max)	0.894; 1.000
Total reflections measured	31593
Symmetry independent reflections	6936
R_{int}	0.026
Reflections with $I > 2s(I)$	6539
Reflections used in refinement	6936
Parameters refined	345
Final $R(F)$ [$I > 2s(I)$ reflections]	0.0315
$wR(F^2)$ (all data)	0.0832
Weights: $w = [s^2(F_O^2) + (0.0462P)^2 + 0.4553P]^{-1}$ where $P = (F_O^2 + 2F_C^2)/3$	
Goodness of fit	1.036
Final D_{max}/s	0.001
Dr (max; min) [e Å^{-3}]	0.24; -0.27
$s(d_{(C-C)})$ [Å]	0.002 – 0.003

***Appendix V: 70** vs. **Me** in ACN (a) UV-Vis spectra (b) Normalized fluorescence emission.*

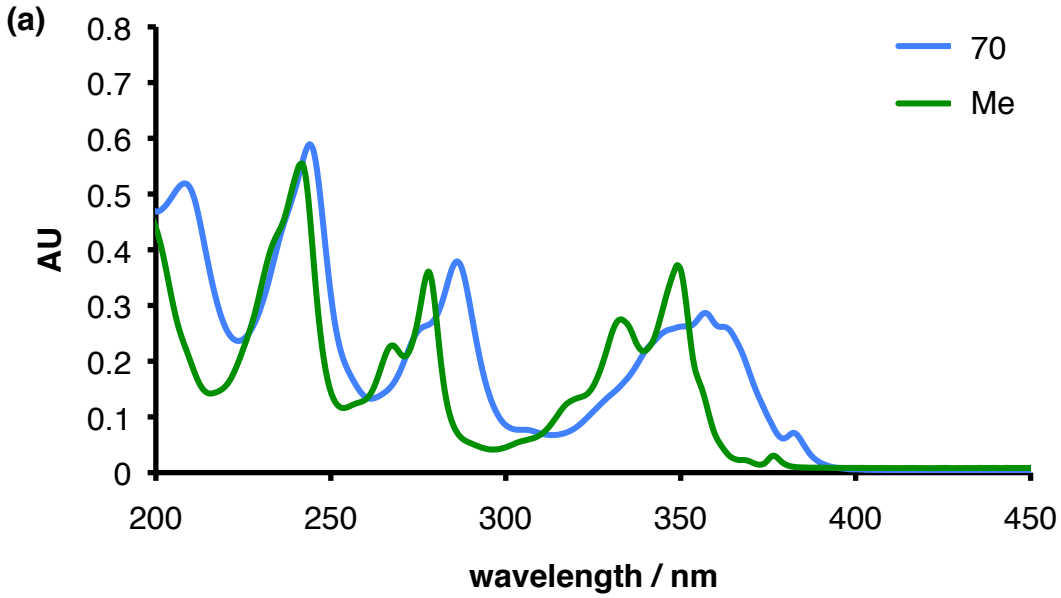

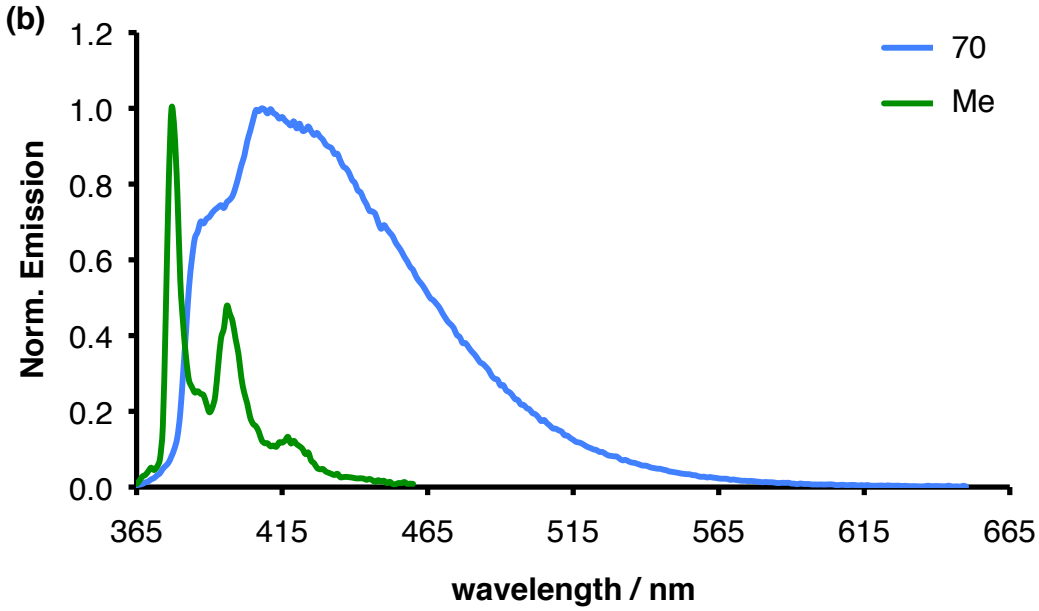

Appendix VI*:** 10^{-5} *M* ***71a-c *in ACN (a) UV-Vis spectra (2) Fluorescence spectra.*

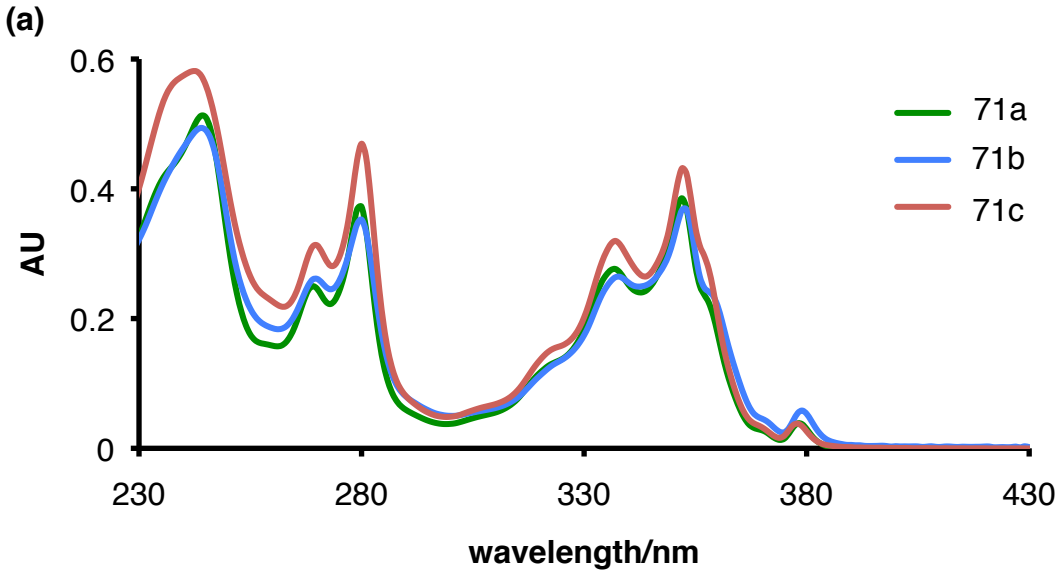

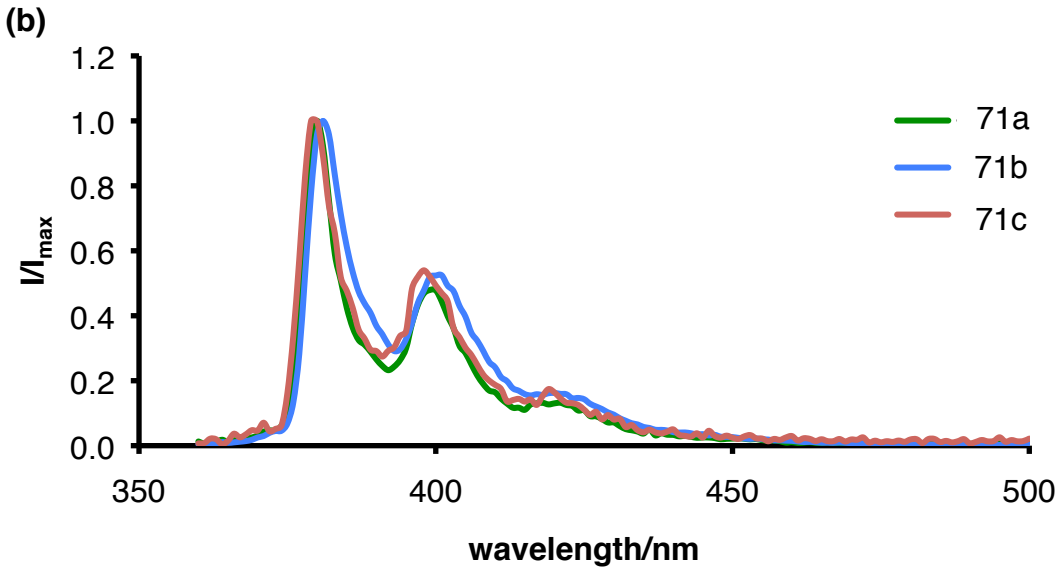

Curriculum Vitae

Surname: KATHAYAT

First Name: Rahul Singh

Date of Birth: 15. 01. 1987

Nationality: Indian

Marital Status: Married

Present address: Brüggliäcker 36
8050 Zurich, Switzerland.

Ph. no.: +41787957187

email: singh@oci.uzh.ch
rskphychemist2007@gmail.com

Education:

Sep 2009 -Present:	Ph.D. studies under the supervision of PD Dr. Nathaniel S. Finney at University of Zurich, Switzerland. Doctoral Thesis “Sulfoxides As a New Reporting Element for Metal Ion Responsive Fluorescent Chemosensor Development.”
Jul 2007 - May 2009:	M.Sc. Chemistry at Indian Institute of Technology (IIT) Bombay, India. Master's Thesis “Design and Synthesis of Amplified Fluorescent Polymer Based on 3,4-alkylenedioxy thiophene” under the supervision of Prof. Dr. Anil Kumar.
Jul 2004 - Apr 2009:	B.Sc. Chemistry at Hindu College, Delhi University, India.
Apr 2002 - Mar 2004:	10 + 2 at Sarvodaya Girls SSS, Sect 5, Rohini, Delhi-85, India.
Apr 2001 - Mar 2002:	10 (High School) at Sarvodaya Girls SSS, Sect 5,

Rohini, Delhi-85, India.

Scientific Participation:

GRC-Physical Organic Chemistry 2013: Poster presentation titled “Fluorescence Based Metal Ion Detection by Alkyl/Aryl Pyrenyl Sulfoxides”.

CMSZH Retreat 2013: Oral presentation titled “Fluorescence Based Metal Ion Detection by Alkyl Pyrenyl Sulfoxides”.

4th EuCheMS Chemistry Congress 2012: Poster presentation titled “Fluorescence Based Metal Ion Detection by Alkyl/Aryl Pyrenyl Sulfoxides”.

SCS (Swiss Chemical Society) 2011: Oral presentation titled “Fluorescence Based Metal Ion Detection: Binding-induced Conformational Restriction Mechanism”.

SCS (Swiss Chemical Society) 2010: Poster presentation titled “Fluorescence Based Metal Ion detection of Hg(II) and Ag(I) Ions”.

Teaching Experience:

4 semesters of Organic Chemistry practicals to under graduates in University of Zurich.

Supervised an undergraduate for 2 months summer internship in University of Zurich.

Scholastic Achievement:

Secured All India Rank 11th in Graduate Aptitude Test in Engineering (GATE) 2009 for chemistry.

Merit Cum Means (MCM) scholarship 2007-2008 in Indian Institute of Technology (IIT, bombay), Mumbai, India.

Secured All India Rank 52nd in Indian Institute of Tech. Joint Admission Test M.Sc. (IIT-JAM) 2007.

Qualified, Council of Scientific and Industrial Research - National Eligibility Test (CSIR-NET) for lectureship in India.

List of Publications:

Kathayat, R. S.; Finney, N. S. *“Sulfoxides as Response Elements for Fluorescent Chemosensors”*, *J. Am. Chem. Soc.*, **2013**, *135*, 12612-12614.